ATLAS Note

ATL-COM-PHYS-2019-962

11th June 2021

Draft version 0.1

WZ + Heavy Flavor Production in pp collisions at $\sqrt{s}$ = 13 TeV

The ATLAS Collaboration[1], Aaron Webb[a], Peter Onyisi[a]

[a] *Univ. of Texas at Austin*

A measurement of the cross-section for production of WZ with an associated heavy flavor jet is performed using 140 fb^{-1} of proton-proton collision data at $\sqrt{s} = 13$ TeV from the ATLAS experiment at the LHC. A measurement of the fully leptonic decay mode, $WZ \to l\nu ll$, is performed. The cross-section of WZ + b and WZ + charm in various fiducial regions is measured.

Contents

List of contributions

Aaron Webb	Main analyser. Responsible for ntuple production, fits, and note writing.
Peter Onyisi	Advisor to Aaron Webb. Analysis design and implementation strategy.

1 Changes and outstanding items

1.1 Changelog

This is version 11

1.1.1 Changes relative to v10

- Included Zjets plots with lep Pt, eta split by flavor
- Clarified the text on a few points regarding systematics, results
- Fixed an outdated yield table, combined rare top with ttbar
- resolved a high Vgamma uncertainty caused by a single large weight event
- included correlation plots for the tZ BDT inputs

1.1.2 Changes relative to v9

- Reordered note to put fiducial region definition in the intro, tZ BDT before the event selection
- moved alternative fit strategies from the appendix into the main text of the note
- removed correlation matrix plot from results
- added c/light rejection rates for each DL1r WP
- updated OR procedure - previously had an outdated algorithm
- Updated results section to include latest fits, table summarizing results
- Replaced correlation table with a plot

1.1.3 Changes relative to v8

- Included more references to appendices in the text
- Expanded explanation of fiducial region definition
- Previous draft claimed that both standard and custom PLVs were used. Text is fixed to state that a custom PLV is used for lepton iso, but standard lepton id is used
- Included plots of PLV output, included WPs used
- specified that non-prompt CR plots are post correction

- changed title of results section

1.1.4 Changes relative to v7

- Moved from LO to NLO tZ sample
- Add additional plots of Z+jets and ttbar CRs in Section A.2
- Clarified CDI file used, MC ptag, PFlow jet algorithm
- Included overlap removal procedure
- Included details on PLV
- Added plots of missing tZ BDT input features for each fit region
- Changed reference on PLV to recent ttH/ttW note
- Included alternate fits with WZ+1-2 jet inclusive, tZ floating

1.1.5 Changes relative to v5

- added list of DSIDs to an appendix
- included systematics on jet migrations
- Updated results section to include simultaneous fit over 1-jet and 2-jet bins, describe unfolding procedure
- Updated other sections to account for this change
- Included info about migrations in Section 5.2

1.1.6 Changes relative to v4

- Fixed various typos, clarified wording
- Expanded info about JER uncertainties, electron systematics, theory uncertainties
- removed a table on lepton selection, included information in the text instead
- Plotted lepton Pt Z and W for Zjet CR, rather than lep 1 and 2
- fixed binning in kinematic plots
- Included prefit and postfit yield tables
- added signal modelling systematics
- included alternate fit studies with tZ included in signal

1.1.7 Changes relative to v3

- Merged introduction into executive summary, including unblinding details and list of SRs/CRs used
- listed ptag used (p4133), and release (AB 21.2.127)
- Included table reftab:xsecUnc listing x-sec uncertainties used
- Removed selection criteria listed in table **??** (QMisID, AmbiguityType) that were removed from the analysis
- specified variable used to make truth jet flavor determination (HadronConeExclTruthLabelID)
- fixed bug in MtLepMet calculation, updated selection/fits to account for this
- Included plots of MtLepMet and PtZ, swapped lep 1 and 2 p_T plots for lep W and lep Z plots
- updated tZ BDT training to reduce overfitting, updated plots to include error bars, feature importance
- updated table 8 to clarify selection, fix the tZ_BDT cut used
- replace a few broken ntuples which included large weight events
- include DL1r distribution for Z+jets and $t\bar{t}$ VRs
- Expanded section on fakes, included information on derived scale factors from VRs.
- Changed the kinematic plots to include $p_T(Z)$ and $m_T(W)$, list lepton p_T based on W and Z candidates.

1.1.8 Changes relative to v2

- Added alternate VBS samples to include missing b-jet diagrams
- Included a section on tZ interference effects, **??**.
- Updated to reflect changes for 2018, including the move to PFlow jets, DL1r, updated trigger, and updated AnalysisBase version (now 21.2.127)
- Revised fit regions, using seperate 1-jet and 2-jet fits, with all 2-j regions included
- updated plots for tZ BDT, added details about the model
- Included truth jet information

1.1.9 Changes relative to v1

- Added GRL list
- Fixed latex issue in line 92, typo in line 172
- Added tables 6 and **??**, summarizing the event and object selection
- Added table 2, which includes the DSID of samples used
- Included reference to WZ inclusive paper in introduction

1.2 Outstanding Items

- Unblind, update plots and fits to include data
- Add cross-section, significance once unblinded

2 Executive Summary

The production of WZ in association with a heavy flavor jet represents an important background for many major analyses. This includes any process with multiple leptons and b-jets in the final state, such as $t\bar{t}H$, $t\bar{t}W$, and $t\bar{t}Z$. While precise measurements have been made of inclusive WZ production [1], WZ + heavy flavor remains poorly understood. This is largely because the QCD processes involved in the production of the b-jet make it difficult to simulate accurately. This introduces a large uncertainty for analyses that include this process as a background.

We perform a study of the fully leptonic decay mode of this channel; that is, events where both the W and Z decay leptonically. Because WZ has no associated jets at leading order, while the major backgrounds for this channel tend to have high jet multiplicity, events with more than two jets are rejected. This gives a final state signature of three leptons and one or two jets.

Events that meet a preselection criteria are sorted into regions based on the b-taggin score of their associated jets. This is done to separate WZ + b-jet events from WZ + charm and WZ + light jets. These regions are fit to data in order make a more accurate estimate of the contribution of WZ + heavy-flavor, where heavy-flavor jets include b-jets and charm jets. The full Run-2 dataset collected by the ATLAS detector, representing 139 fb^{-1} of data from pp collisions at $\sqrt{s} = 13$ TeV, is used for this study.

The fiducial volume at particle level is defined based on the number of stable leptons and jets in each event. Three light leptons with total charge ±1 and one or two associated jets are required. Only leptons which do not originate from hadron or τ decays are considered. The phase space definitions use dressed kinematics of the final state particles. Leptons are dressed by summing the momentum of photons within a cone of $\Delta R < 0.1$ of the lepton to correct the leptons energy. Particle level jets are reconstructed using the anti-k_t algorithm with a radius of $R = 0.4$. The kinematic selection applied to these objects is summarized below:

- Three light leptons with total charge ±1, $|\eta| < 2.5$
- OS lepton with p_T >10 GeV, SS leptons with p_T >20 GeV
- One OSSF lepton pair with $|M(ll) - 91.2\ \mathrm{GeV}| < 10\ \mathrm{GeV}$
- One or two associated truth jets with p_T >25 GeV, $|\eta| < 2.5$, $R < 0.4$

The result of the fit is used to extract the cross-section in this fiducial region for WZ + b and WZ + c with one associated jet, and WZ + b and WZ + c with two associated jets, where the number and flavor of the jets is determined at particle level. Events with both charm and b-jets are counted as WZ + b. The analysis reports a cross-section measurement of WZ + b and WZ + c, along with their correlations, for both 1-jet and 2-jet exclusive regions. Normalization factors, representing how the MC prediction differs from the observed result, are also reported.

Section 3 details the data and Monte Carlo (MC) samples used in the analysis. The reconstruction of various physics objects is described in Section 4. Section 6 describes the event selection applied to these samples, along the definitions of the various regions used in the fit. The multivariate analysis techniques used to separate the tZ background from WZ + heavy flavor are described in Section 5. Section 7 describes the various sources of systematic uncertainties considered in the fit. Finally, the results of the analysis are summarized in Section 8, followed by a brief conclusion in Section 9.

3 Data and Monte Carlo Samples

Both data and Monte Carlo samples used in this analysis were prepared in the `xAOD` format, which was used to produce a `DxAOD` sample in the `HIGG8D1` derivation framework. The `HIGG8D1` framework is designed for the $t\bar{t}H$ multi-lepton analysis, which targets events with multiple leptons as well as tau hadrons. This framework reduces the size of the dataset by removing events based on event topology and only keeping useful information for each event. Events are removed from the derivations that do not meet one of the following selections:

- at least two light leptons within a range $|\eta|<2.6$, with leading lepton $p_T > 15$ GeV and subleading lepton $p_T > 5$ GeV
- OR at least one light lepton with $p_T > 15$ GeV within a range $|\eta|<2.6$, and at least two hadronic taus with $p_T > 15$ GeV.

Samples were then generated from these `HIGG8D1` derivations with p-tag of p4134 for data and p4133 for Monte Carlo using AnalysisBase version 21.2.127 modified to include custom variables.

3.1 Data Samples

The study uses a sample of proton-proton collision data collected by the ATLAS detector from 2015 through 2018 at an energy of $\sqrt{s} = 13$ TeV, which represents an integrated luminosity of 139 fb^{-1} [2]. This data set was collected with a bunch-crossing rate of 25 ns. All data used in this analysis was verified by data quality checks [3], having been included in the following Good Run Lists:

- data15_13TeV.periodAllYear_DetStatus-v79-repro20-02_DQDefects-00-02-02 _PHYS_StandardGRL_All_Good_25ns.xml
- data16_13TeV.periodAllYear_DetStatus-v88-pro20-21_DQDefects-00-02-04 _PHYS_StandardGRL_All_Good_25ns.xml
- data17_13TeV.periodAllYear_DetStatus-v97-pro21-13_Unknown_PHYS_StandardGRL _All_Good_25ns_Triggerno17e33prim.xml
- data18_13TeV.periodAllYear_DetStatus-v102-pro22-04_Unknown_PHYS_StandardGRL _All_Good_25ns_Triggerno17e33prim.xml

Runs included from the AllYear period containers are included.

3.2 Monte Carlo Samples

Several different generators were used to produce Monte Carlo simulations of the signal and background processes. For all samples, the response of the ATLAS detector is simulated using GEANT4 [4]. The WZ signal samples are simulated using Sherpa 2.2.2 [5]. Signal events are generated using NNPDF30NNLO PDF set with up to one parton at NLO and 2 to 3 partons at LO [6].

The tZ background is simulated at NLO with MADGRAPH5_aMC@NLO, with PYTHIA8 used to perform parton showering and fragmentation. The NNPDF30NNLO PDF set is used.

Specific information about the Monte Carlo samples being used can be found in Table 1. A list of the specific samples used by data set ID is shown in Table 2.

Table 1: The configurations used for event generation of signal and background processes, including the event generator, matrix element (ME) order, parton shower algorithm, and parton distribution function (PDF).

Process	Event generator	ME order	Parton Shower	PDF
WZ, VV	SHERPA 2.2.2	MEPS NLO	SHERPA	CT10 [7]
tZ	MG5_aMC [8]	NLO	PYTHIA 8	CTEQ6L1
$t\bar{t}W$	MG5_aMC	NLO	PYTHIA 8	NNPDF 3.0 NLO
	(SHERPA 2.1.1)	(LO multileg)	(SHERPA)	(NNPDF 3.0 NLO)
$t\bar{t}(Z/\gamma^* \to ll)$	MG5_aMC	NLO	PYTHIA 8	NNPDF 3.0 NLO
$t\bar{t}H$	MG5_aMC	NLO	PYTHIA 8	NNPDF 3.0 NLO [6]
	(MG5_aMC)	(NLO)	(HERWIG++) [9]	(CT10 [7])
$tHqb$	MG5_aMC	LO	PYTHIA 8	CT10
tHW	MG5_aMC	NLO	HERWIG++	CT10
	(SHERPA 2.1.1)	(LO multileg)	(SHERPA)	(NNPDF 3.0 NLO)
tWZ	MG5_aMC	NLO	PYTHIA 8	NNPDF 2.3 LO
$t\bar{t}t$, $t\bar{t}t\bar{t}$	MG5_aMC	LO	PYTHIA 8	NNPDF 2.3 LO [10]
$t\bar{t}W^+W^-$	MG5_aMC	LO	PYTHIA 8	NNPDF 2.3 LO
$t\bar{t}$	POWHEG-BOX v2 [11]	NLO	PYTHIA 8	NNPDF 3.0 NLO
$t\bar{t}\gamma$	MG5_aMC	LO	PYTHIA 8	NNPDF 2.3 LO
s-, t-channel, Wt single top	POWHEG-BOX v1 [12]	NLO	PYTHIA 6	CT10
$qqVV$, VVV				
$Z \to l^+l^-$	SHERPA 2.2.1	MEPS NLO	SHERPA	NNPDF 3.0 NLO

Sample	DSID
WZ	364253, 364739-42
VV	364250, 364254, 364255, 363355-60, 364890
$t\bar{t}W$	410155
$t\bar{t}Z$	410156, 410157, 410218-20
low mass $t\bar{t}Z$	410276-8
Rare Top	410397, 410398, 410399
single Top	410658-9, 410644-5
three Top	304014
four Top	410080
$t\bar{t}WW$	410081
Z + jets	364100-41
low mass Z + jets	364198-215
W + jets	364156-97
$V\gamma$	364500-35
tZ	412063-5
tW	410013-4
WtZ	410408
VVV	364242-9
VH	342284-5
WtH	341998
$t\bar{t}\gamma$	410389
$t\bar{t}$	410470
$t\bar{t}H$	345873-5, 346343-5

Table 2: List of Monte Carlo samples by data set ID used in the analysis.

4 Object Reconstruction

All regions defined in this analysis share a common lepton, jet, and overall event preselection. The selection applied to each physics object is detailed here; the event preselection, and the selection used to define the various fit regions, is described in Section 6.

4.1 Trigger

Events are required to be selected by dilepton triggers, as summarized in Table 3.

	Dilepton triggers (2015)
$\mu\mu$ (asymm.)	HLT_mu18_mu8noL1
ee (symm.)	HLT_2e12_lhloose_L12EM10VH
$e\mu$, μe ($\sim$symm.)	HLT_e17_lhloose_mu14
	Dilepton triggers (2016)
$\mu\mu$ (asymm.)	HLT_mu22_mu8noL1
ee (symm.)	HLT_2e17_lhvloose_nod0
$e\mu$, μe ($\sim$symm.)	HLT_e17_lhloose_nod0_mu14
	Dilepton triggers (2017)
$\mu\mu$ (asymm.)	HLT_mu22_mu8noL1
ee (symm.)	HLT_2e24_lhvloose_nod0
$e\mu$, μe ($\sim$symm.)	HLT_e17_lhloose_nod0_mu14
	Dilepton triggers (2018)
$\mu\mu$ (asymm.)	HLT_mu22_mu8noL1
ee (symm.)	HLT_2e24_lhvloose_nod0
$e\mu$, μe ($\sim$symm.)	HLT_e17_lhloose_nod0_mu14

Table 3: List of lowest p_T-threshold, un-prescaled dilepton triggers used for 2015-2018 data taking.

4.2 Light leptons

Electron candidates are reconstructed from energy clusters in the electromagnetic calorimeter that are associated with charged particle tracks reconstructed in the inner detector [13]. Electron candidates are required to have $p_T > 10$ GeV and $|\eta_{\text{cluster}}| < 2.47$. Muon candidates are reconstructed by combining inner detector tracks with track segments or full tracks in the muon spectrometer [14]. Muon candidates are required to have $p_T > 10$ GeV and $|\eta| < 2.5$. Candidates in the transition region between different electromagnetic calorimeter components, $1.37 < |\eta_{\text{cluster}}| < 1.52$, are rejected. A multivariate likelihood discriminant combining shower shape and track information is used to distinguish real electrons from hadronic showers (fake electrons). To further reduce the non-prompt electron contribution, the track is required to be consistent with originating from the primary vertex; requirements are imposed on the transverse impact parameter significance ($|d_0|/\sigma_{d_0} < 5$) and the longitudinal impact parameter ($|\Delta z_0 \sin\theta_\ell| < 0.5$ mm). Electron candidates are required to pass TightLH identification.

Muon candidates are reconstructed by combining inner detector tracks with track segments or full tracks in the muon spectrometer [14]. Muon candidates are required to have $p_T > 10$ GeV and $|\eta| < 2.5$. The longitutinal impact parameter is the same for both electrons and muons, while muons are required to pass a slightly tighter transverse imapact parameter, $|d_0|/\sigma_{d_0} < 3$. Muons are also required to pass Medium ID requirements.

Leptons are additionally required to pass a non-prompt BDT selection developed by the $t\bar{t}H$ multilepton/$t\bar{t}W$ analysis group. This BDT and the WPs used are summarized in Appendix A.1, and described in detail in [15]. Optimized working points and scale factors for this BDT are taken from that analysis.

4.3 Jets

Jets are reconstructed from calibrated topological clusters built from energy deposits in the calorimeters [16], as well as information from the inner tracking detector, using the anti-k_t algorithm with a radius parameter $R = 0.4$. Particle Flow, or PFlow, jets are used in the analysis. Jets with energy contributions likely arising from noise or detector effects are removed from consideration [17], and only jets satisfying $p_T > 25$ GeV and $|\eta| < 2.5$ are used in this analysis. For jets with $p_T < 60$ GeV and $|\eta| < 2.4$, a jet-track association algorithm is used to confirm that the jet originates from the selected primary vertex, in order to reject jets arising from pileup collisions [18].

4.4 B-tagged Jets

In order to make a measurement of WZ + heavy flavor it is necessary to distinguish these events from WZ + light jets. For this purpose, the DL1r b-tagging algorithm is used to distinguish heavy flavor jets from lighter ones. The DL1r algorithm [19] uses jet kinematics, particularly jet vertex information, as input for a neural network which assigns each jet a score designed to reflect how likely that jet is to have originated from a b-quark.

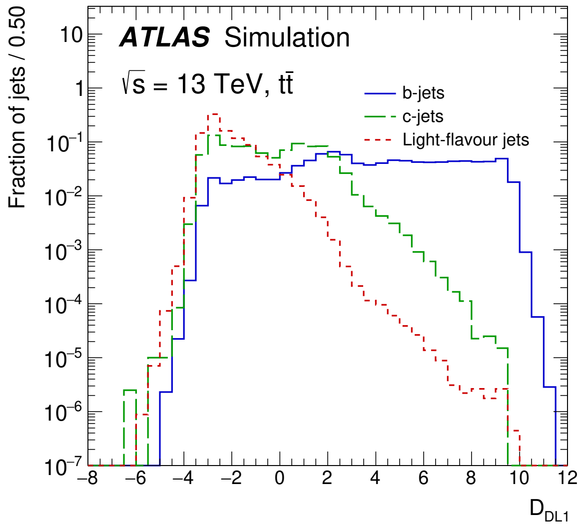

Figure 1: Output distribution of the DL1r algorithm for pure samples of b-jets, charm jets, and light jets, with each normalized to unity [19]

From the output of the BDT, working points (WPs) are developed based on the efficiency of truth b-jets at particular values of the DL1r algorithm. These WPs are taken from the March 2020 CDI file, 2020-21-13TeV-MC16-CDI-2020-03-11_v2.root. The working points used in this analysis are summarized in Table 4.

WP	Rejection	
b-jet eff.	c-jet	light jet
85%	2.6	29
77%	4.9	130
70%	9.4	390
60%	27	1300

Table 4: c-jet and light-flavor jet rejections corresponding to each b-tagging Working Point by b-jet efficiency, evaluated on $t\bar{t}$ events.

As shown in table 4, a tighter WP will accept fewer b-jets, but reject a higher fraction of charm and light jets. Generally, analyses that include b-jets will use a fixed working point, for example, requiring that a jet pass the 70% threshold. By instead treating these working points as bins, e.g. events with jets that fall between the 85% and 77% WPs fall into one bin, while events with jets passing the 60% WP fall into another, additional information can be gained. This analysis uses each of these working points to form orthogonal regions in order to provide separation between WZ + b, WZ + c, and WZ + light.

4.5 Missing transverse energy

Missing transverse momentum (E_T^{miss}) is used as part of the event selection. The missing transverse momentum vector is defined as the negative of the vector sum of the transverse momenta of all reconstructed physics objects as well as remaining unclustered energy, the latter of which is estimated from low-p_T tracks associated with the primary vertex but not assigned to a hard object, with object definitions taken from [20]. Light leptons considered in the E_T^{miss} reconstruction are required to have p_T>10 GeV, while jets are required to have p_T>20 GeV.

4.6 Overlap removal

To avoid double counting objects and remove leptons originating from decays of hadrons, overlap removal is performed in the following order: any electron candidate within $\Delta R = 0.1$ of another electron candidate with higher p_T is removed; any electron candidate within $\Delta R = 0.1$ of a muon candidate is removed; any jet within $\Delta R = 0.2$ of an electron candidate is removed; if a muon candidate and a jet lie within $\Delta R = min(0.4{,}0.04{+}10[GeV]/p_T(muon))$ of each other, the jet is kept and the muon is removed if the jet has at least three associated tracks, otherwise the jet is removed and the muon is kept.

This algorithm is applied to the preselected objects. The overlap removal procedure is summarized in Table 5.

Keep	**Remove**	**Cone size (Δ R)**
electron	electron (low p_T)	0.1
muon	electron	0.1
electron	jet	0.2
jet	muon	min(0.4, 0.04 + 10[GeV]/p_T (muon)), $n_t rack$ >3
muon	jet	min(0.4, 0.04 + 10[GeV]/p_T (muon)), $n_t rack$ <3

Table 5: Summary of the overlap removal procedure between electrons, muons, and jets.

5 tZ Separation Multivariate Analysis

Because tZ produces a final state identical to signal, it represents a predominant background in the most signal enriched regions. That is, the region with one jet passing the 60% DL1r WP. Therefore, a boosted decision tree (BDT) algorithm is trained to separate *WZ* + heavy flavor from tZ.

Separation between tZ and *WZ* + heavy flavor is achieved in part by reconstructing the invariant mass of the top candidate, which clusters more closely to the top mass for tZ than WZ + heavy flavor. The result of this BDT is used to create a tZ enriched region in the fit, reducing its impact on the measurement of WZ + heavy flavor.

5.1 Top Mass Reconstruction

The reconstruction of the top mass follows the procedure described in detail in section 6.1 of [21]. The mass of the top quark candidate is reconstructed from the jet, the lepton not included in the Z-candidate, and a reconstructed neutrino. In the case that there is one jet in the event, there is only possible b-jet candidate. For events with two jets, the jet with the highest DL1r score is used.

The neutrino from the W decay is expected to be the only source of E_T^{miss}. Therefore, the E_T and ϕ of the neutrino are taken from the E_T^{miss} measurement. This leaves the z-component of the neutrino momentum, $p_{\nu z}$ as the only unknown.

This unknown is solved for by taking the combined invariant mass of the lepton and neutrino to give the invariant mass of the W boson:

$$(p_l + p_\nu)^2 = m_W^2$$

Expanding this out into components, this equation gives:

$$\sqrt{p_{T\nu}^2 + p_{z\nu}^2} E_l = \frac{m_w^2 - m_l^2}{2} + p_{T\nu}(p_{lx} cos\phi_\nu + p_{ly} sin\phi_\nu) + p_{lz} p_{\nu z}$$

This equation gives two solutions for $p_{\nu z}$. For cases where only one of these solutions is real, that is taken as the value of $p_{\nu z}$. For instances with two real solutions, the one which is shown to be correct in the largest fraction of simulations is taken. For cases when no real solution is found, often because of detector effects, the value of E_T^{miss} is varied in decreasing increments of 100 MeV until a real solution is found.

The reconstructed top mass distribution for tZ and WZ + b can be seen in figure 2.

5.2 tZ BDT

A Boosted Decision Tree (BDT), specifically XGBoost [22], is used to provide separation between tZ and WZ+b. The following kinematic variables are used as inputs:

- The invariant mass of the reconstructed top candidate
- p_T of each of the leptons, jet
- The invariant mass of each combination of lepton pairs, $M(ll)$

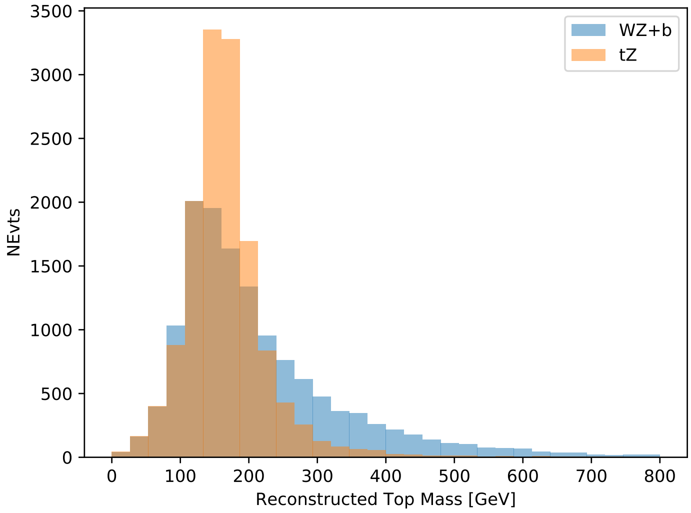

Figure 2: Reconstructed top mass distributions for tZ and WZ + b, measured in MeV.

- E_T^{miss}
- Distance between each combination of leptons, $\Delta R(ll)$
- Distance between each lepton and the jet, $\Delta R(lj)$

The training samples included only events meeting the requirements of the 1-jet, 60% b-tag region, i.e. passing all the selection described in section 6 and having exactly one jet which passes the tightest (60%) DL1r working point.

The distributions of a few of these features for both signal and background is shown in figure 3.

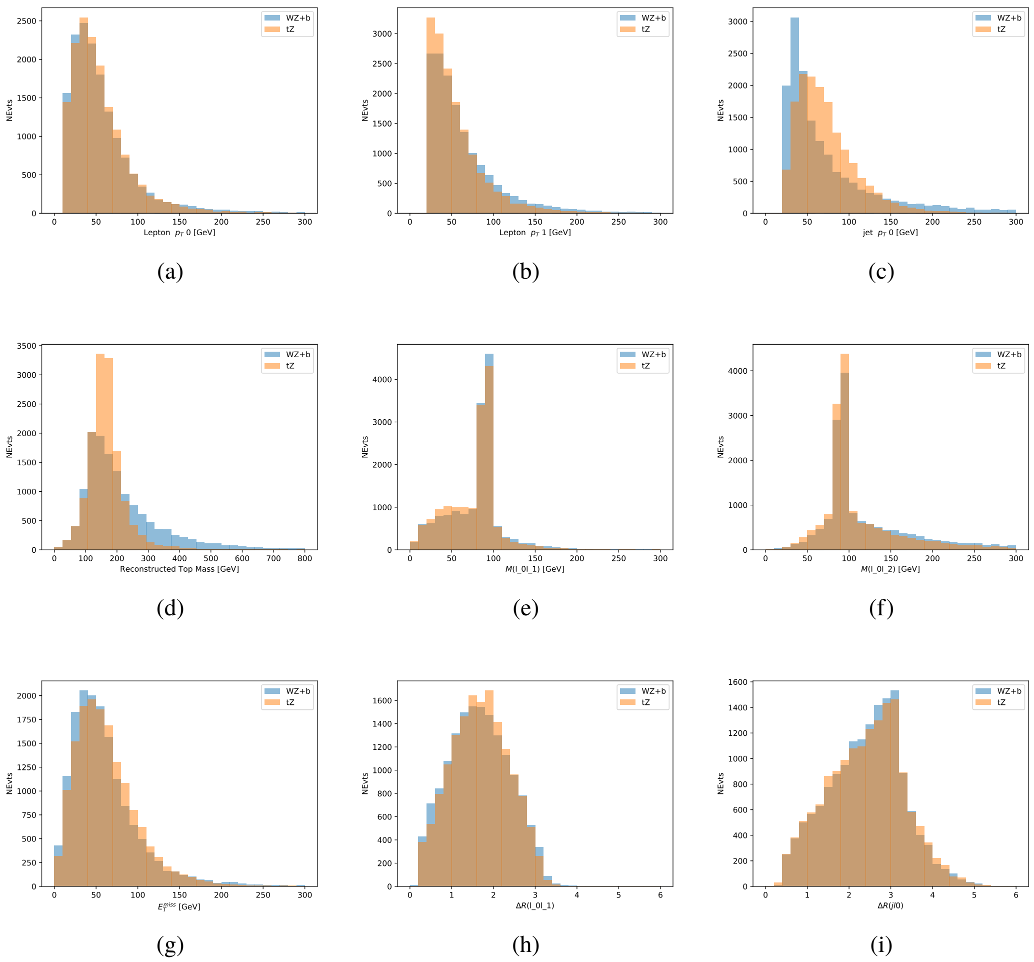

Figure 3: Distribution of input features of the BDT for signal (WZ) and background (tZ). Both are scaled to an equal number of events. (a), (b) and (c) show the p_{T} of lepton 0, lepton 1, and the jet, (d) show the reconstructed top mass, (e) and (f) show the invariant mass of leptons 0 and 1, leptons 0 and 2. (g) shows the E_{T}^{m}iss of each event. (h) and (i) show the ΔR between lepton 0 and lepton 1, and the jet.

Correlations between the input features are shown in figure 4.

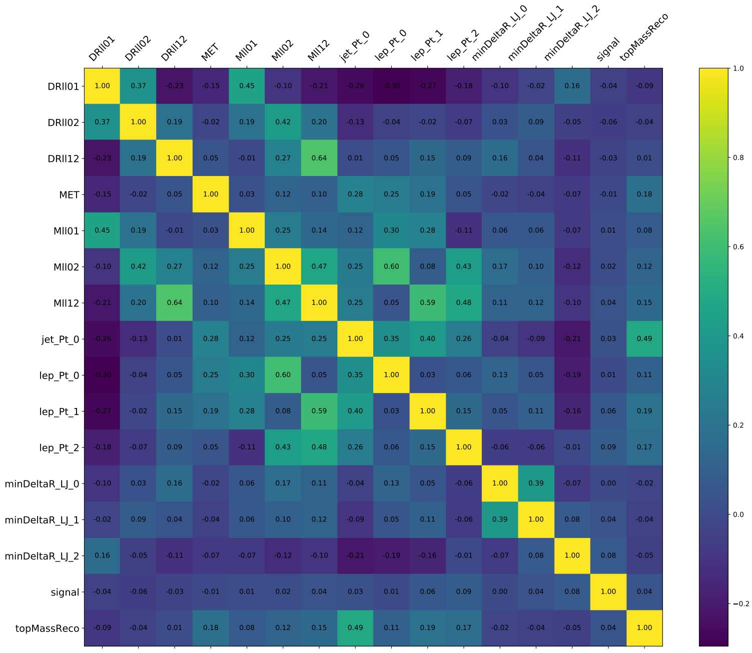

Figure 4: Correlation matrix of the input features of the tZ separation BDT.

A sample of 20,000 background (tZ) and signal (WZ+b) Monte Carlo events are used to train the BDT. And additional 5,000 events are reserved for testing the model, in order to prevent over-fitting. A total of 750 decision trees with a maximum depth of 6 branches are used to build the model. These parameters are chosen empirically, by training several models with different parameters and selecting the one that gave the best separation for the test sample.

The results of the BDT training are shown in figure 5. The output scores for both signal and background events is shown on the left. The right shows the receiving operating characteristic (ROC) curve that results from the MVA. The ROC curve represents the background rejection as a function of signal efficiency, where each point on the curve represents a different response score.

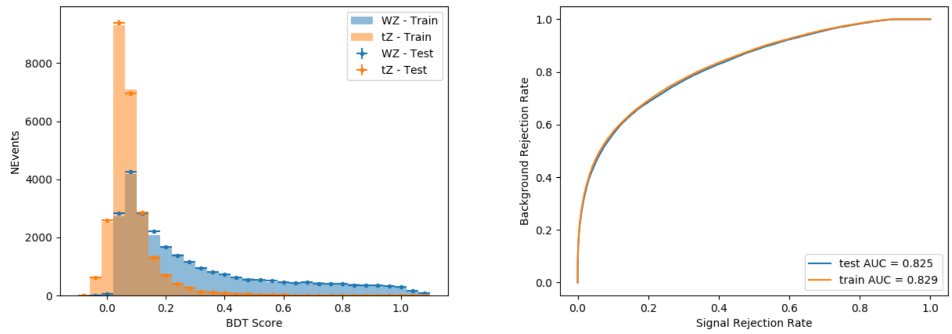

(a) (b)

Figure 5: Distribution of the BDT response for signal and background events on the left, the ROC curve for the BDT on the right.

The relative important of each input feature in the model, measured by how often they appeared in the decision trees, is shown in figure 6.

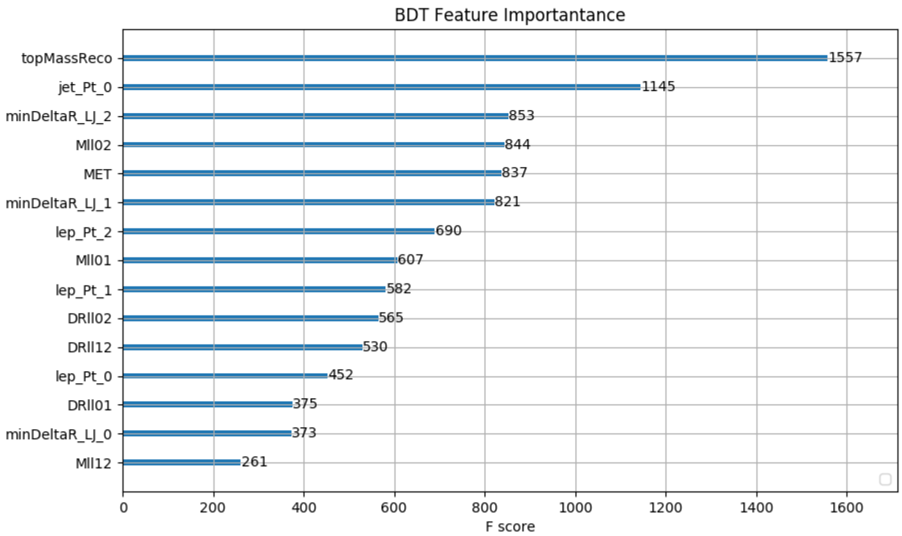

Figure 6: Relative importance of each input feature in the model.

These results suggest that some amount of separation can be achieved between these two processes, with a high BDT score selecting a set of events that is pure in WZ + b. A BDT score of 0.12 is selected as a cutoff, where events with scores higher than this form a signal enriched region, and events with scores lower than this form a tZ control region. This cutoff is selected by varying the value of this cutoff in stat-only Asimov fits, and selecting the value that minimizes the statistical uncertainty on WZ + b. A working point of 0.12 produces a background rejection rate of 74%, compared to a signal acceptance of 78%.

The possibility of using solely the reconstructed top mass shown in Figure 2 to separate tZ and WZ + b was considered, and produced the ROC curve shown in Figure 7. This shows significantly reduced separation compared to the BDT, justifying the use of the more complex BDT in the analysis.

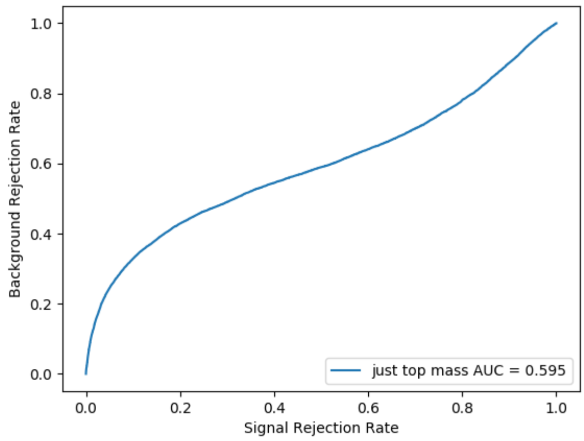

Figure 7: ROC for the separation of tZ and WZ + b produced from the distribution of the reconstructed top mass.

5.3 tZ Interference Studies

Because it includes an on-shell Z boson as well as a b-jet and W from the top decay, tZ production represents an identical final state to WZ + b-jet. This implies the possibility of matrix level interference between these two processes not accounted for in the Monte Carlo simulations, which consider the two processes independently. Truth level studies are performed in order to estimate the impact of these interference effects.

In order to estimate the matrix level interference effects between tZ and WZ + b-jet, two different sets of simulations are produced using MadGraph 5 [23] - one which simulates these two processes independently, and another where they are produced simultaneously, such that interference effects are present. These two sets of samples are then compared, and the difference between them can be taken to represent any interference effects.

MadGraph simulations of 10,000 tZ and 10,000 WZ + b-jet events are produced, along with 20,000 events where both are present, in the fiducial region where three leptons and at least one jet are produced.

A selection mimicking the preselection used in the main analysis is applied to the samples: The SS leptons are required to have $p_T > 20$ GeV, and > 10 GeV is required for the OS lepton. The associated b-jet is required to have $p_T > 25$ GeV, and all physics objects are required to fall in a range of $|\eta| < 2.5$.

The kinematics of these samples after the selection has been applied are shown below:

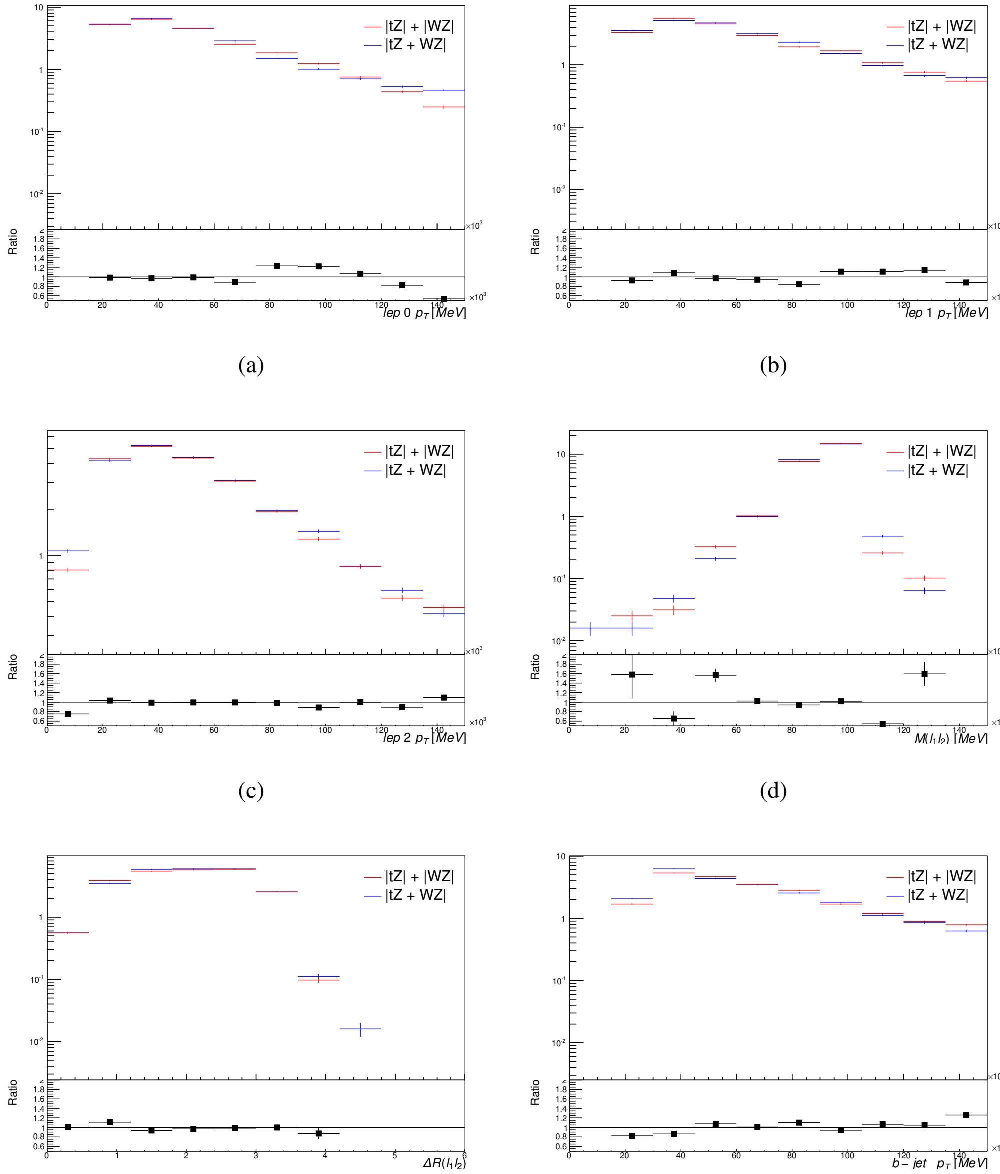

(a) (b) (c) (d) (e) (f)

Figure 8: Comparisons between (a) the p_T of the lepton from the W, (b) and (c) show the p_T of the lepton from the Z, (d) the invariant mass of the Z-candidate, (e) ΔR of the leptons from the Z, and (f) the p_T of the b-jet, for WZ and tZ events generated with interference effects (blue) and without interference effects (red).

388 The overall cross-section of the two methods agree within error, and no significant differences
389 in the kinematic distributions are seen. It is therefore concluded that interference effects do not

significantly impact the results.

6 Event Selection and Signal Region Definitions

Event are required to pass a preselection described in Section 6.1 and summarized in Table 6. Those that pass this preselection are divided into various fit regions described in Section 6.2, based on the number of jets in the event, and the b-tag score of those jets.

6.1 Event Preselection

Events are required to include exactly three reconstructed light leptons passing the requirement described in 4.2, which have a total charge of ±1.

The leptons are ordered in the analysis code as 0, 1, and 2. Lepton 0 is the lepton whose charge is opposite the other two. Lepton 1 is the lepton closest to the opposite charge lepton, i.e. the smallest ΔR, leaving lepton 2 as the lepton further from the opposite charge lepton. Lepton 0 is required to have $p_T > 10$ GeV, as it is found to be prompt the vast majority of the time, while the same sign leptons, 1 and 2, are required to have $p_T > 20$ GeV to reduce the contribution of non-prompt leptons, as non-prompt leptons tend to be soft.

The invariant mass of at least one pair of opposite sign, same flavor leptons is required to fall within 10 GeV of the mass of the Z boson, 91.2 GeV. Events where one of the opposite sign pairs has an invariant mass less than 12 GeV are rejected in order to suppress low mass resonances.

An additional requirement is placed on the missing transverse energy, E_T^{miss} > 20 GeV, and the transverse mass of the W candidate, $m(E_T^{miss} + l_{other}) > 30$ GeV, defined as $\sqrt{2p_T^{lep}E_T^{miss} * (1 - \cos(\phi_{lep} - \phi_{E_T^{miss}}))}$. Here E_T^{miss} is the missing transverse energy, and l_{other} is the lepton not included in the Z-candidate.

Events are required to have one or two reconstructed jets passing the selection described in Section 4.3. Events with more than two jets are rejected in order to reduce the contribution of backgrounds such as $t\bar{t}Z$ and $t\bar{t}W$, which tend to have higher jet multiplicity.

Event Selection
Exactly three leptons with total charge ± 1
Two same-charge leptons with $p_T > 20$ GeV
One opposite charge lepton with $p_T > 10$ GeV
$m(l^+l^-)$ within 10 GeV of 91.2 GeV
Transverse mass of W-candidate, $\sqrt{2p_T^{lep}E_T^{miss} * (1 - \cos(\phi_{lep} - \phi_{E_T^{miss}}))} > 30$ GeV
Missing transverse energy, $E_T^{miss} > 20$ GeV
One or two jets with $p_T > 25$ GeV

Table 6: Summary of the selection applied to events for inclusion in the fit

The event yields in the preselection region for both data and Monte Carlo are summarized in Table 6.1, which shows good agreement between data and Monte Carlo, and demonstrates that this region consists primarily of WZ + jets events. The WZ events are split into WZ + b, WZ + c, and WZ + l based on the truth flavor of the associated jet in the event. Specifically, this determination is made based on the `HadronConeExclTruthLabelID` of the jet, as recommended by the b-tagging working group [24]. In this ordering b-jet supersede charm, which supersides light. That is, WZ + light events contain no charm and no b jets at truth level, WZ + c contain at least one truth charm and no b-jets, and WZ + b contains at least one truth b-jet.

Process	Events
$WZ + b$	143 ± 43
$WZ + c$	930 ± 280
$WZ + l$	6250 ± 1900
Other VV	16.6 ± 4.1
ZZ	460 ± 55
$t\bar{t}W$	14.8 ± 2.1
$t\bar{t}Z$	96 ± 14
Single top	0.1 ± 0.2
Three top	0.003 ± 0.002
Four top	0.01 ± 0.01
$t\bar{t}WW$	0.20 ± 0.04
$Z + \text{jets}$	320 ± 70
$V + \gamma$	75 ± 43
tZ	164 ± 37
tW	4.9 ± 1.2
WtZ	21 ± 11
VVV	23 ± 11
VH	67 ± 6
$t\bar{t}$	84 ± 9
$t\bar{t}H$	3.6 ± 0.4
Total	8700 ± 2300
Data	8696

Table 7: Event yields in the preselection region at 139.0 fb^{-1}

Here Other VV represents diboson processes other than WZ, and consists predominantly of $ZZ \rightarrow llll$ events where one of the leptons is not reconstructed.

Simulations are further validated by comparing the kinematic distributions of the Monte Carlo with data, which are shown in Figure 9. Here, bins with 5% or more WZ+b are blinded.

WZ Fit Region - Inclusive

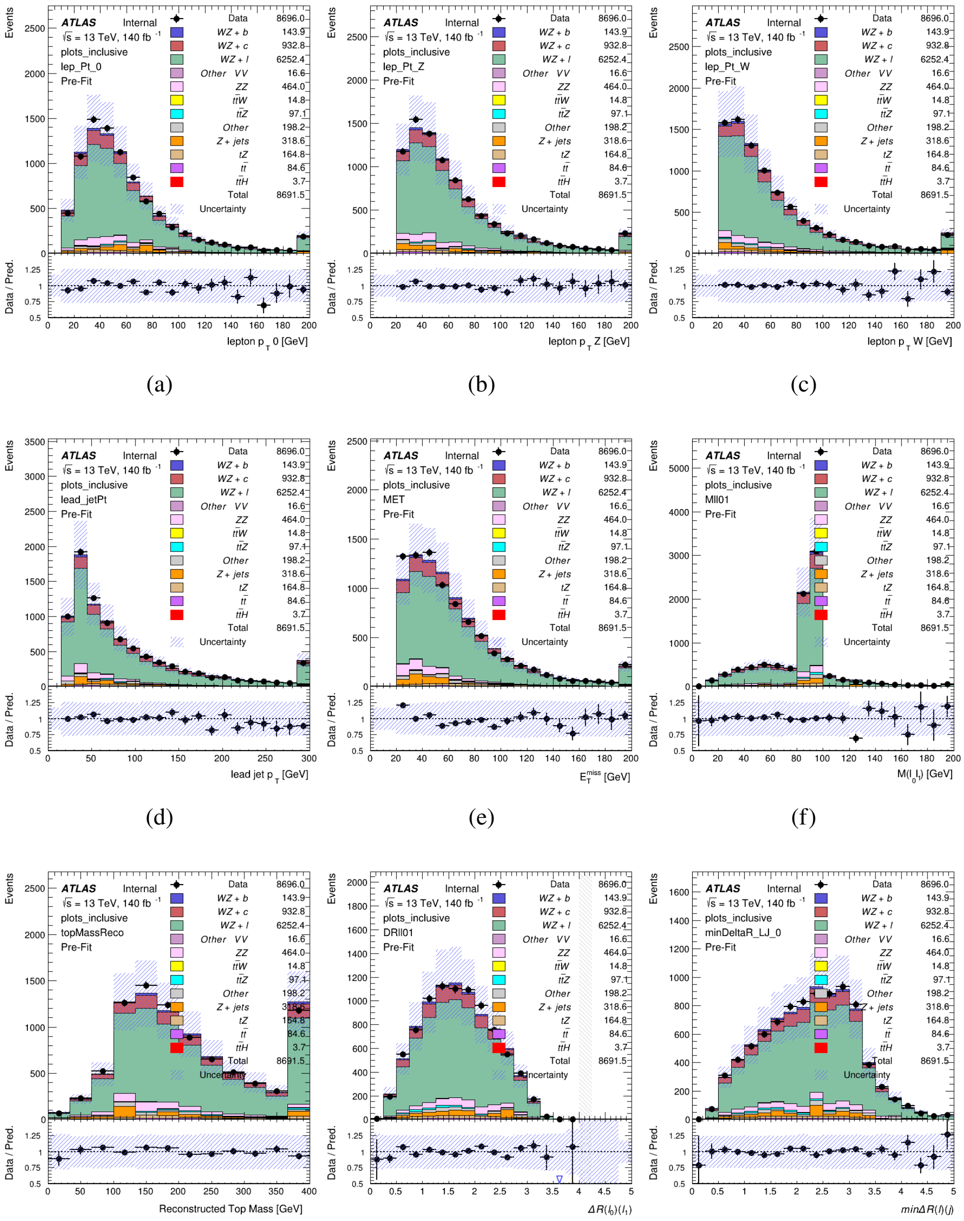

(a) (b) (c)

(d) (e) (f)

(g) (h) (i)

Figure 9: Comparisons between the data and MC distributions in the preselection region for (a) the p_T of the opposite sign lepton, (b) the p_T of the other lepton from the Z candidate, (c) the p_T of the lepton from the W candidate, (d) the leading jet p_T, (e) the E_T^{miss}, and (f) the invariant mass of leptons 0 and 1, (g) the reconstructed top mass, (h) $\Delta(R)$ between lepton 0 and 1, (i) the $\Delta(R)$ between the closest lepton and jet.

6.2 Fit Regions

Once preselection has been applied, the remaining events are categorized into one of twelve orthogonal regions. The regions used in the fit are summarized in Table 8.

Table 8: A list of the regions used in the fit and the selection used for each.

Region	Selection
1j, <85%	N_{jets} = 1, nJets_DL1r_85 = 0
1j, 85%-77%	N_{jets} = 1, nJets_DL1r_85 = 1, nJets_DL1r_77=0
1j, 77%-70%	N_{jets} = 1, nJets_DL1r_77 = 1, nJets_DL1r_70=0
1j, 70%-60%	N_{jets} = 1, nJets_DL1r_70 = 1, nJets_DL1r_60=0
1j, 60%	N_{jets} = 1, nJets_DL1r_60 = 1, tZ BDT > 0.12
1j tZ CR	N_{jets} = 1, nJets_DL1r_60 = 1, tZ BDT < 0.12
2j, <85%	N_{jets} = 2, nJets_DL1r_85 = 0
2j, 85%-77%	N_{jets} = 2, nJets_DL1r_85 >= 1, nJets_DL1r_77=0
2j, 77%-70%	N_{jets} = 2, nJets_DL1r_77 >= 1, nJets_DL1r_70=0
2j, 70%-60%	N_{jets} = 2, nJets_DL1r_70 >= 1, nJets_DL1r_60=0
2j, 60%	N_{jets} = 2, nJets_DL1r_60 >= 1, tZ BDT > 0.12
2j tZ CR	N_{jets} = 2, nJets_DL1r_60 >= 1, tZ BDT < 0.12

The working points discussed in Section 4.4 are used to separate events into fit regions based on the highest working point reached by a jet in each event. Because the background composition differs significantly based on the number of b-jets, events are further subdivided into 1-jet and 2-jet regions in order to minimize the impact of background uncertainties.

An unfolding procedure is performed to account for differences in the number of reconstructed jets compared to the number of truth jets in each event. The `AntiKt4TruthDressedWZJets` truth jet collection is used to make this determination. In order to account for migration of WZ+1-jet and WZ+2-jet events between the 1-jet and 2-jet bins at reco level, the signal samples are separated based on the number of truth jets. Events with 0 jets or more than 3 jets at truth level, yet fall within one of the categories listed in Table 8, are categorized as WZ + other, and treated as a background. The migration matrix in the number of jets at truth level versus reco level is shown in Figure 10. The composition of the number of truth jets in each reco jet bin is taken from MC, with uncertainties in these estimates described in detail in Section 7.

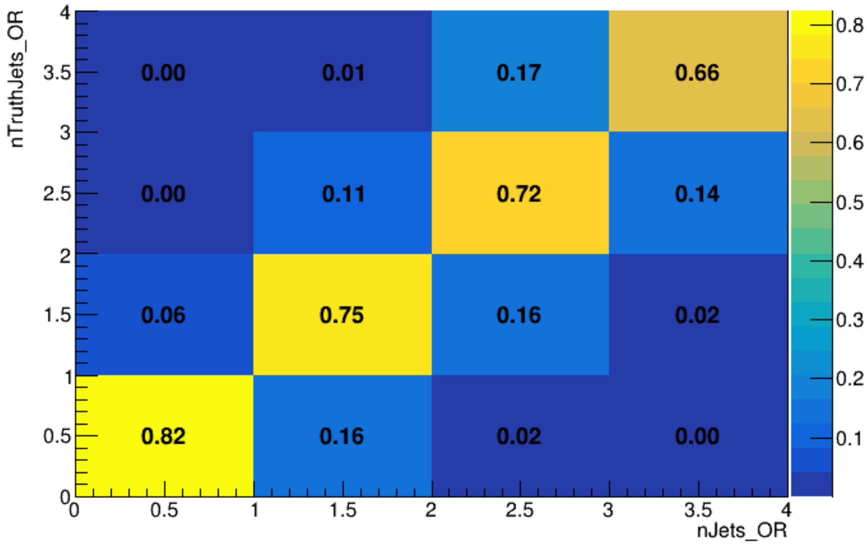

Figure 10: Number of truth jets compared to the number of reconstructed jets in each WZ event falling in the preselection region. Each row is normalized to unity, with overflow bins not shown included in the normalization. That is, each bin represents the absolute fraction of events with a particular truth jet multiplicity that include the corresponding number of reconstructed jets.

An additional tZ control region is created based on the BDT described in Section 5. The region with 1-jet passing the 60% working point is split in two - a signal enriched region of events with a BDT score greater than 0.12, and a tZ control region including events with a score less than 0.12. This cutoff is arrived at by performing a fit an Asimov dataset with a variety of cutoffs, and selecting the value that produces the highest significance for the measurement of WZ + b.

The modeling in each region is validated by comparing data and MC predictions for various kinematic distributions. Events containing 5% or more WZ + b are blinded. These plot are shown in Figures 11-24.

WZ Fit Region - 1j Inclusive

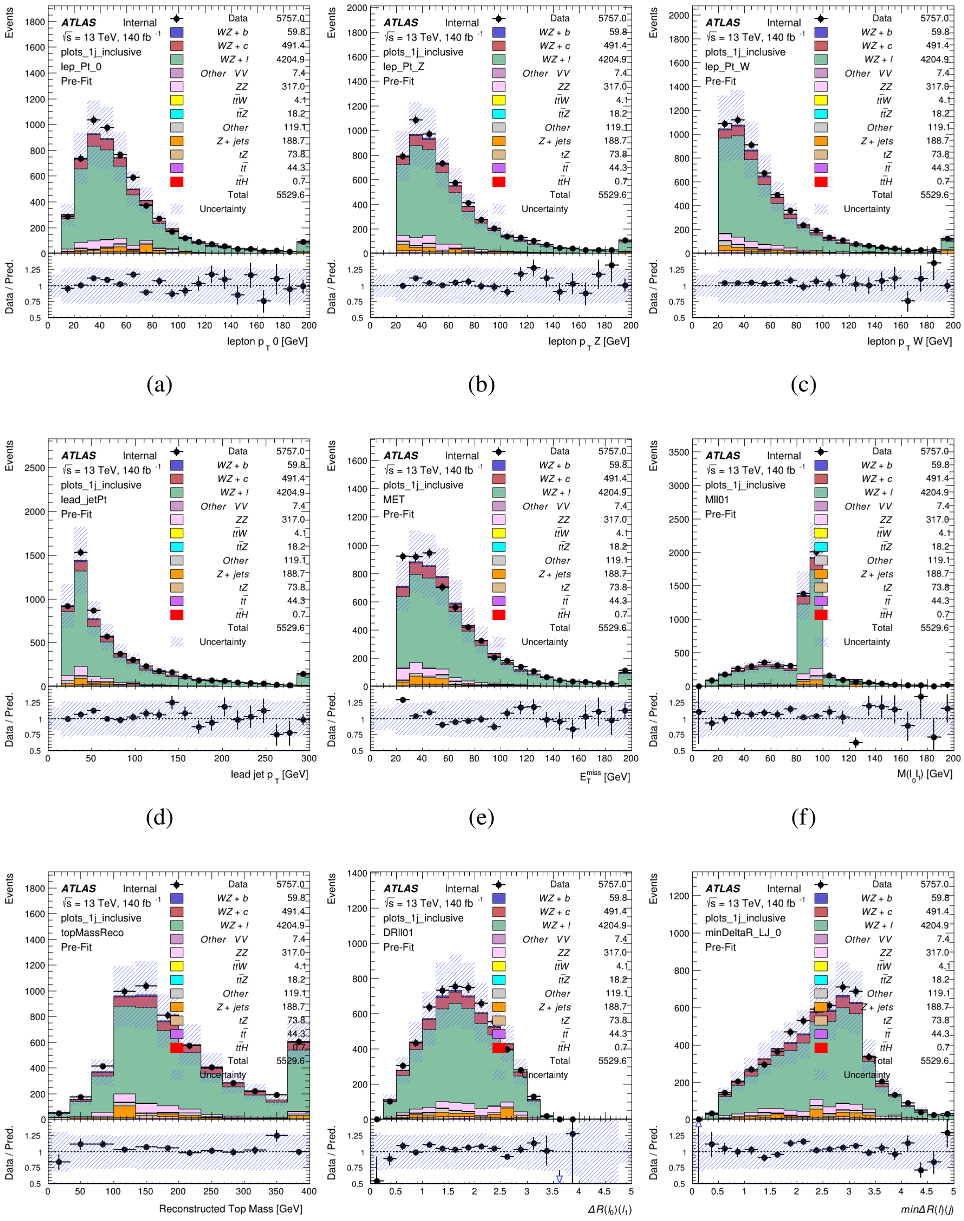

(a) (b) (c)

(d) (e) (f)

(g) (h) (i)

Figure 11: Comparisons between the data and MC distributions in the preselection region for (a) the p_T of the opposite sign lepton, (b) the p_T of the other lepton from the Z candidate, (c) the p_T of the lepton from the W candidate, (d) the leading jet p_T, (e) the E_T^{miss}, and (f) the invariant mass of leptons 0 and 1, (g) the reconstructed top mass, (h) $\Delta(R)$ between lepton 0 and 1, (i) the $\Delta(R)$ between the closest lepton and jet.

WZ Fit Region - 1j < 85% WP

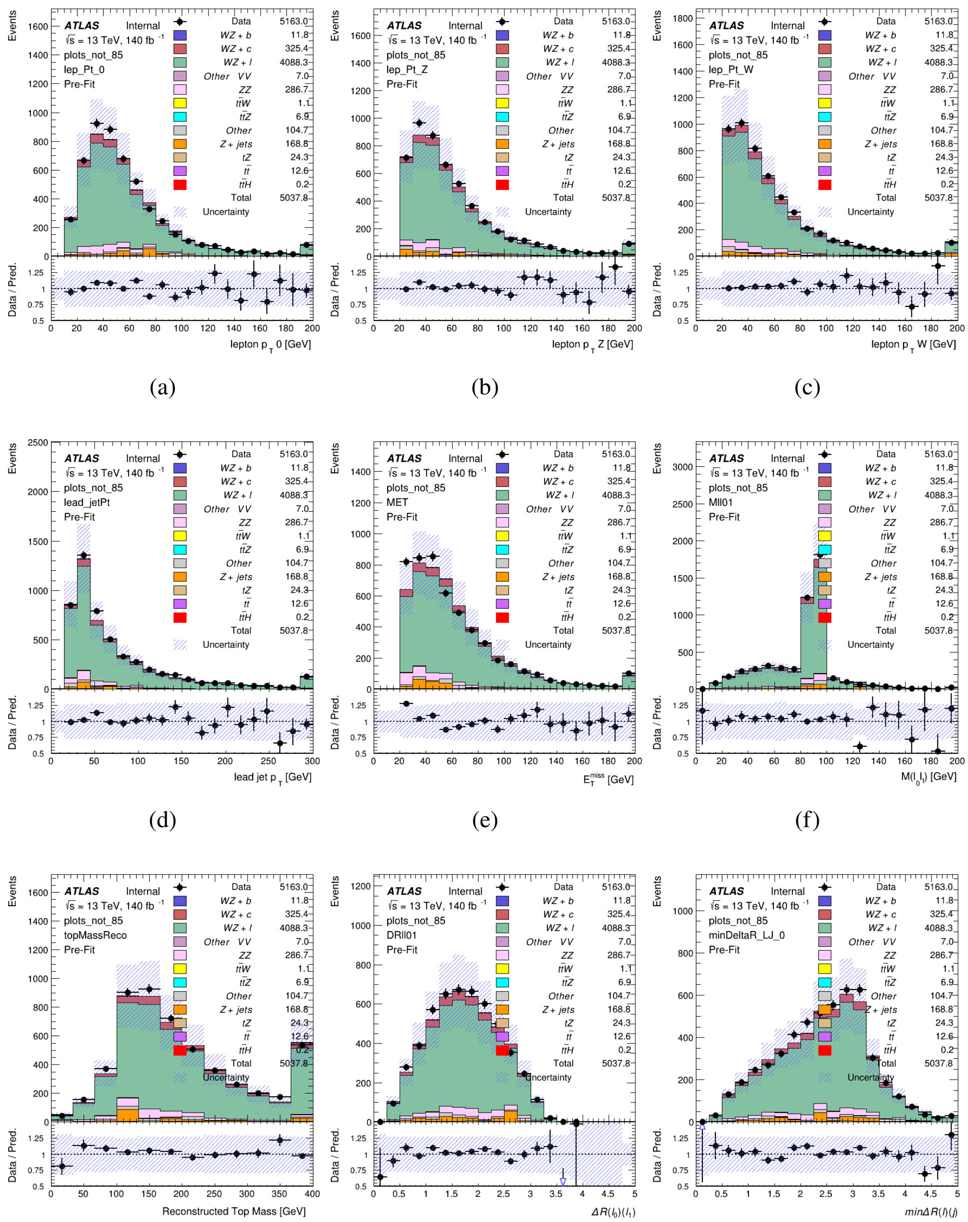

(a) (b) (c)

(d) (e) (f)

(g) (h) (i)

Figure 12: Comparisons between the data and MC distributions in the preselection region for (a) the p_T of the opposite sign lepton, (b) the p_T of the other lepton from the Z candidate, (c) the p_T of the lepton from the W candidate, (d) the leading jet p_T, (e) the E_T^{miss}, and (f) the invariant mass of leptons 0 and 1, (g) the reconstructed top mass, (h) $\Delta(R)$ between lepton 0 and 1, (i) the $\Delta(R)$ between the closest lepton and jet.

WZ Fit Region - 1j 77-85% WP

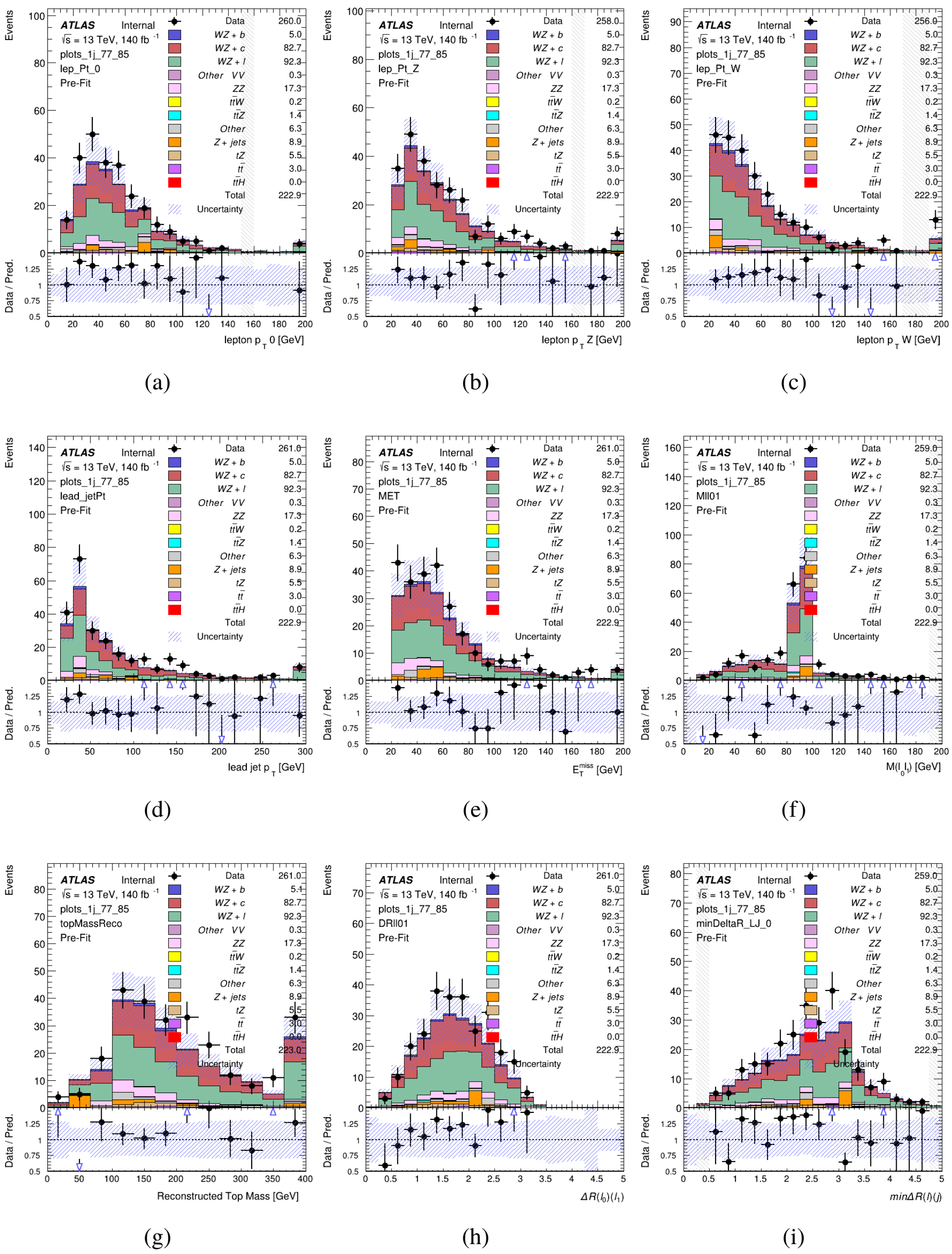

Figure 13: Comparisons between the data and MC distributions in the preselection region for (a) the p_T of the opposite sign lepton, (b) the p_T of the other lepton from the Z candidate, (c) the p_T of the lepton from the W candidate, (d) the leading jet p_T, (e) the E_T^{miss}, and (f) the invariant mass of leptons 0 and 1, (g) the reconstructed top mass, (h) $\Delta(R)$ between lepton 0 and 1, (i) the $\Delta(R)$ between the closest lepton and jet.

WZ Fit Region - 1j 70-77% WP

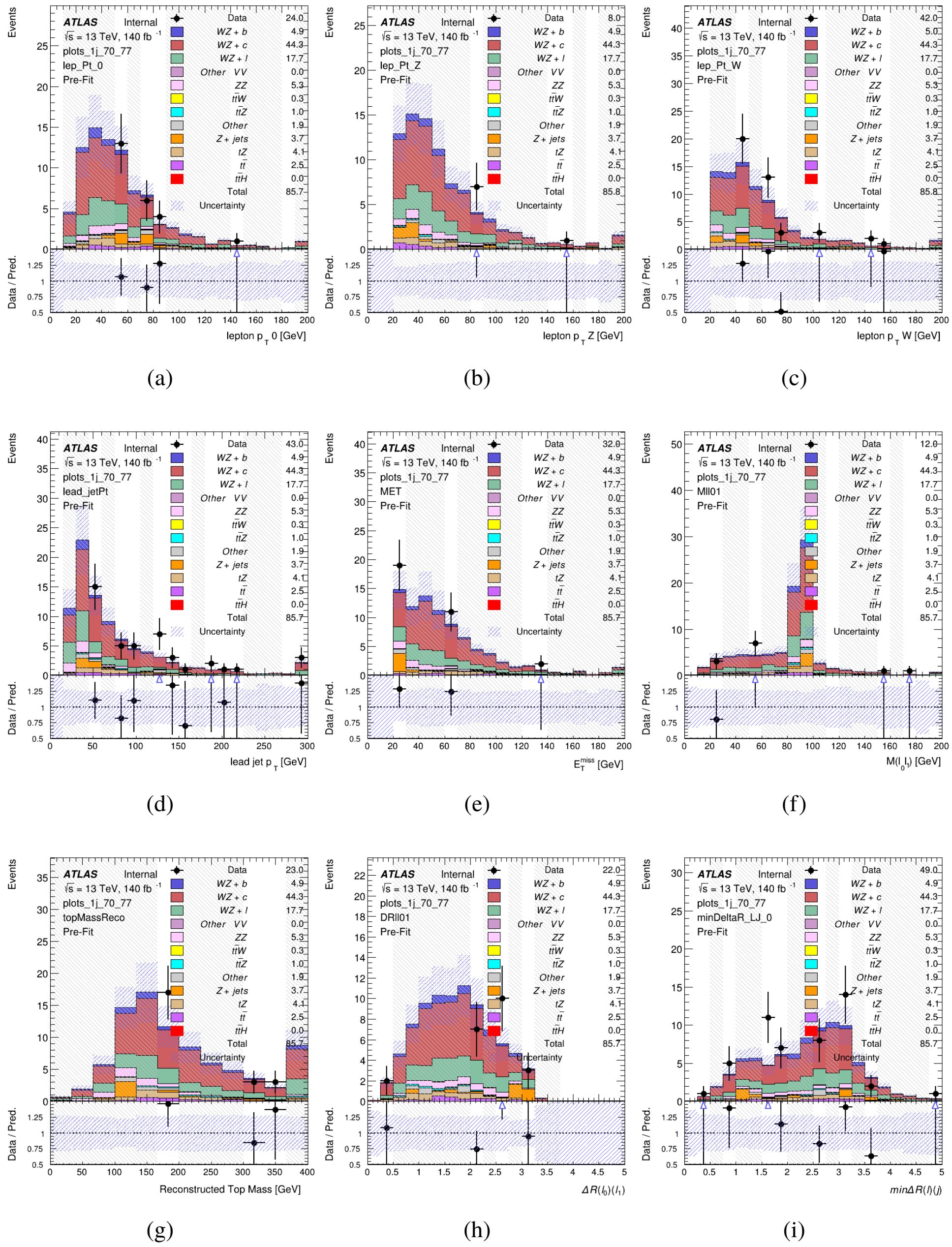

Figure 14: Comparisons between the data and MC distributions in the preselection region for (a) the p_T of the opposite sign lepton, (b) the p_T of the other lepton from the Z candidate, (c) the p_T of the lepton from the W candidate, (d) the leading jet p_T, (e) the E_T^{miss}, and (f) the invariant mass of leptons 0 and 1, (g) the reconstructed top mass, (h) $\Delta(R)$ between lepton 0 and 1, (i) the $\Delta(R)$ between the closest lepton and jet.

WZ Fit Region - 1j 60-70% WP

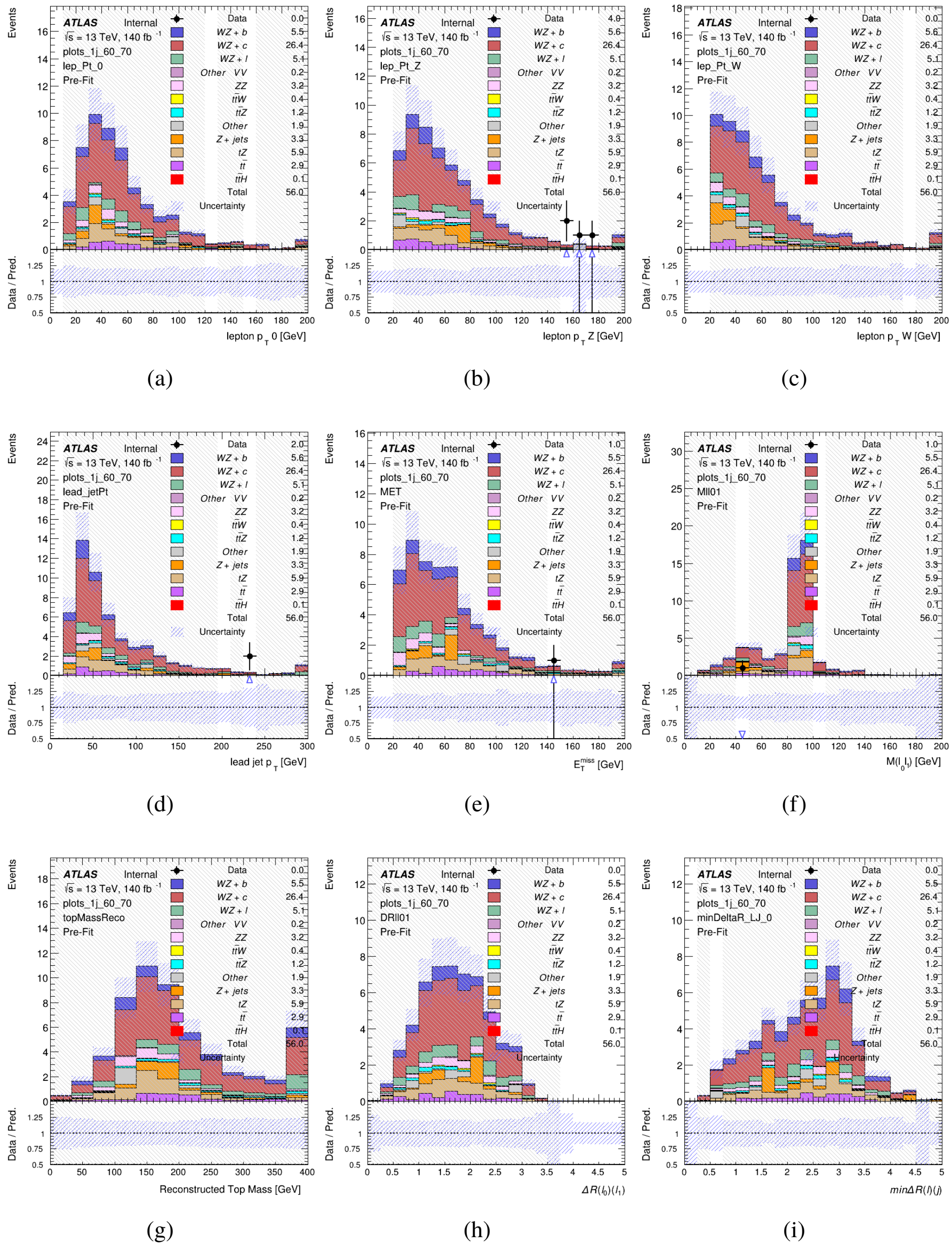

Figure 15: Comparisons between the data and MC distributions in the preselection region for (a) the p_T of the opposite sign lepton, (b) the p_T of the other lepton from the Z candidate, (c) the p_T of the lepton from the W candidate, (d) the leading jet p_T, (e) the E_T^{miss}, and (f) the invariant mass of leptons 0 and 1, (g) the reconstructed top mass, (h) $\Delta(R)$ between lepton 0 and 1, (i) the $\Delta(R)$ between the closest lepton and jet.

WZ Fit Region - 1j 60% WP

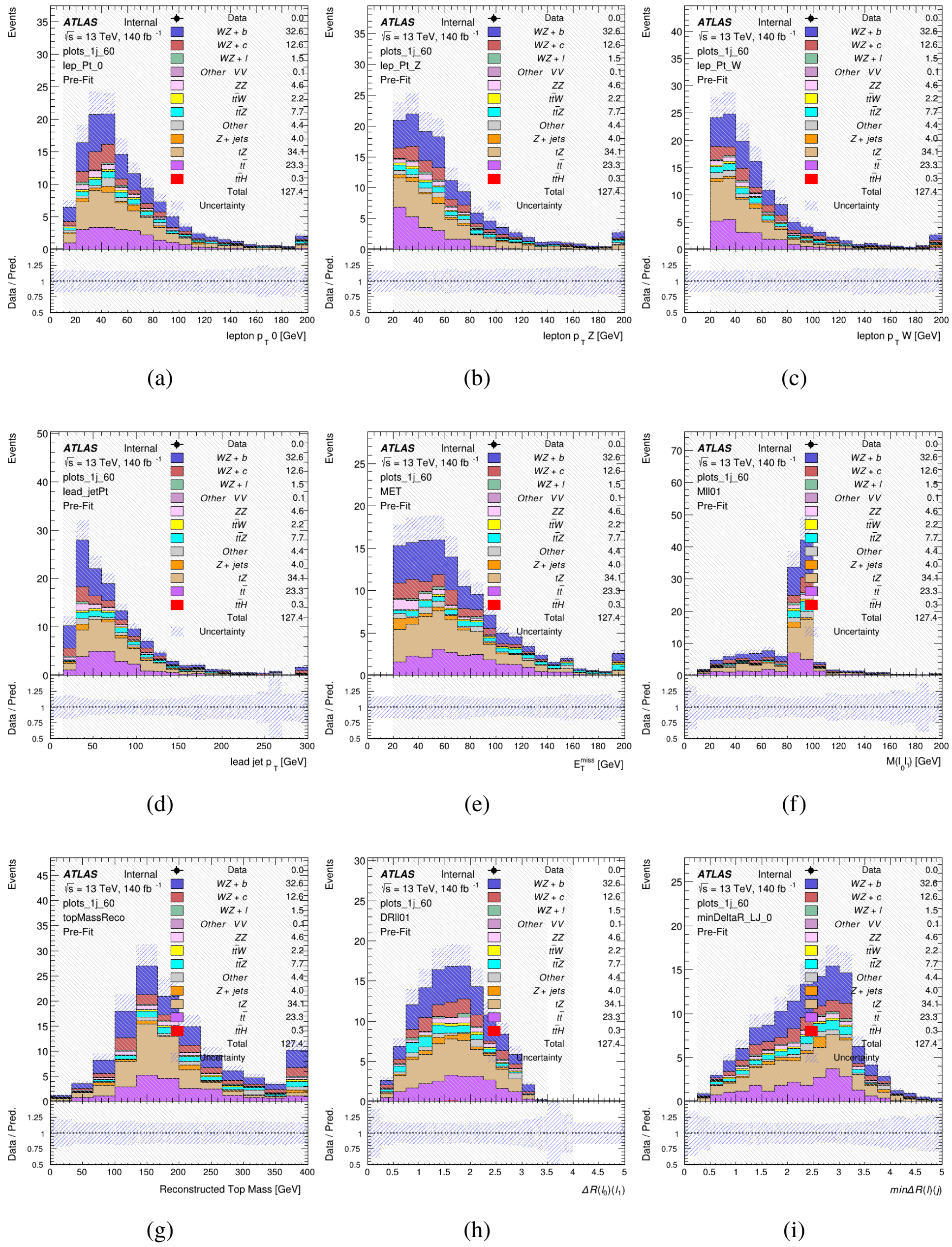

Figure 16: Comparisons between the data and MC distributions in the preselection region for (a) the p_T of the opposite sign lepton, (b) the p_T of the other lepton from the Z candidate, (c) the p_T of the lepton from the W candidate, (d) the leading jet p_T, (e) the E_T^{miss}, and (f) the invariant mass of leptons 0 and 1, (g) the reconstructed top mass, (h) $\Delta(R)$ between lepton 0 and 1, (i) the $\Delta(R)$ between the closest lepton and jet.

WZ Fit Region - tZ-CR

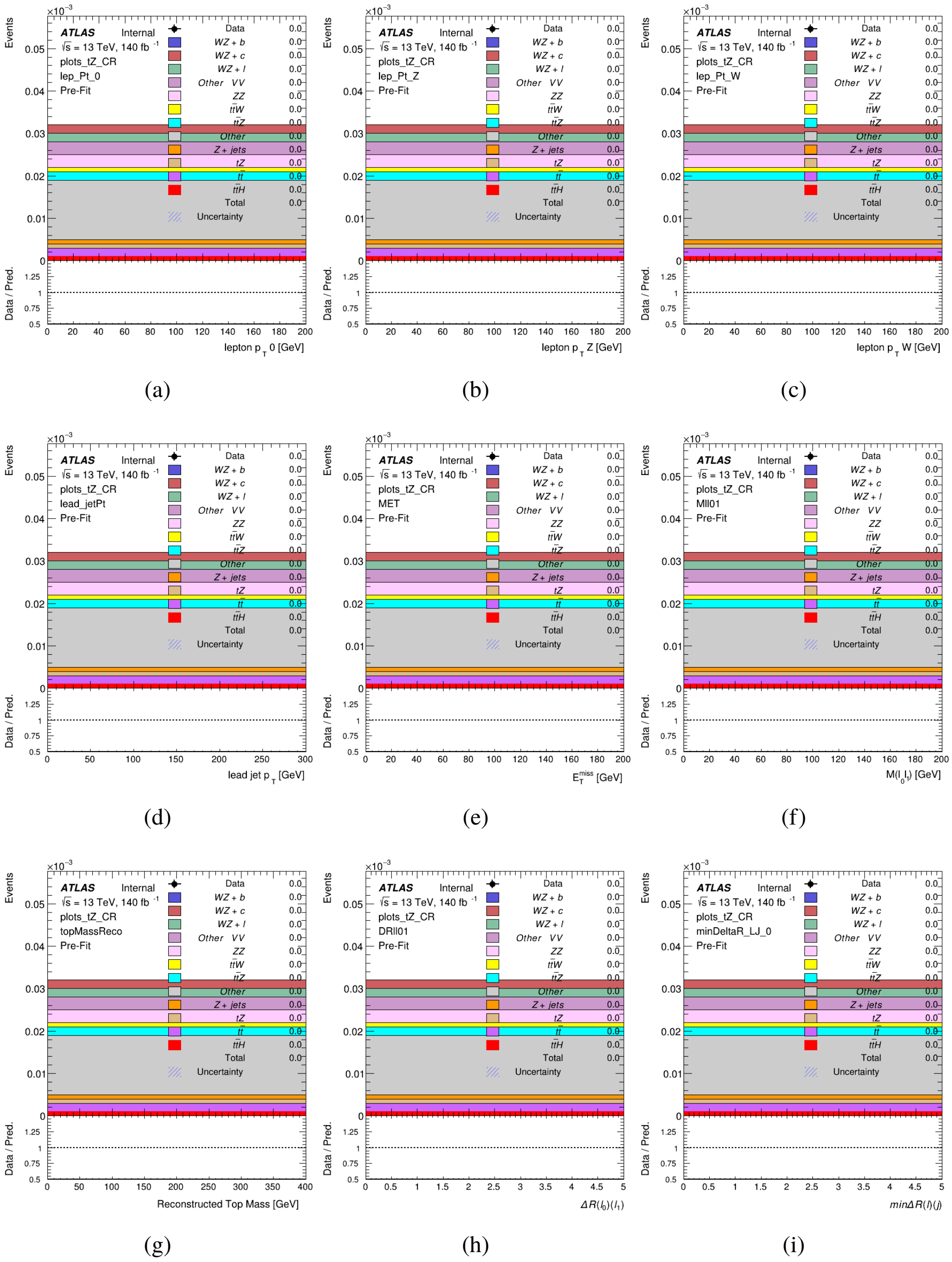

Figure 17: Comparisons between the data and MC distributions in the preselection region for (a) the p_T of the opposite sign lepton, (b) the p_T of the other lepton from the Z candidate, (c) the p_T of the lepton from the W candidate, (d) the leading jet p_T, (e) the E_T^{miss}, and (f) the invariant mass of leptons 0 and 1, (g) the reconstructed top mass, (h) $\Delta(R)$ between lepton 0 and 1, (i) the $\Delta(R)$ between the closest lepton and jet.

WZ Fit Region - 2j Inclusive

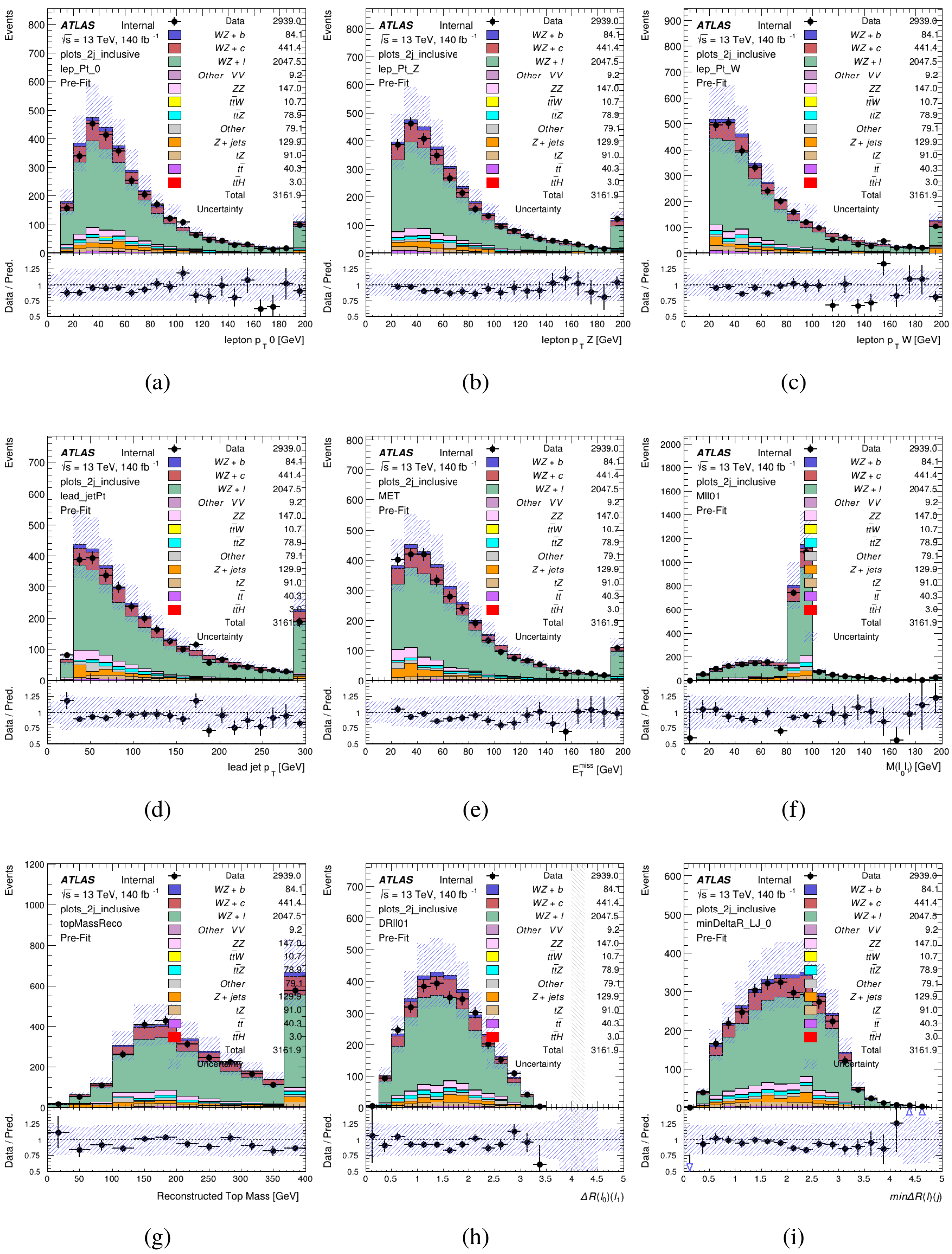

Figure 18: Comparisons between the data and MC distributions in the preselection region for (a) the p_T of the opposite sign lepton, (b) the p_T of the other lepton from the Z candidate, (c) the p_T of the lepton from the W candidate, (d) the leading jet p_T, (e) the E_T^{miss}, and (f) the invariant mass of leptons 0 and 1, (g) the reconstructed top mass, (h) $\Delta(R)$ between lepton 0 and 1, (i) the $\Delta(R)$ between the closest lepton and jet.

WZ Fit Region - 2j < 85% WP

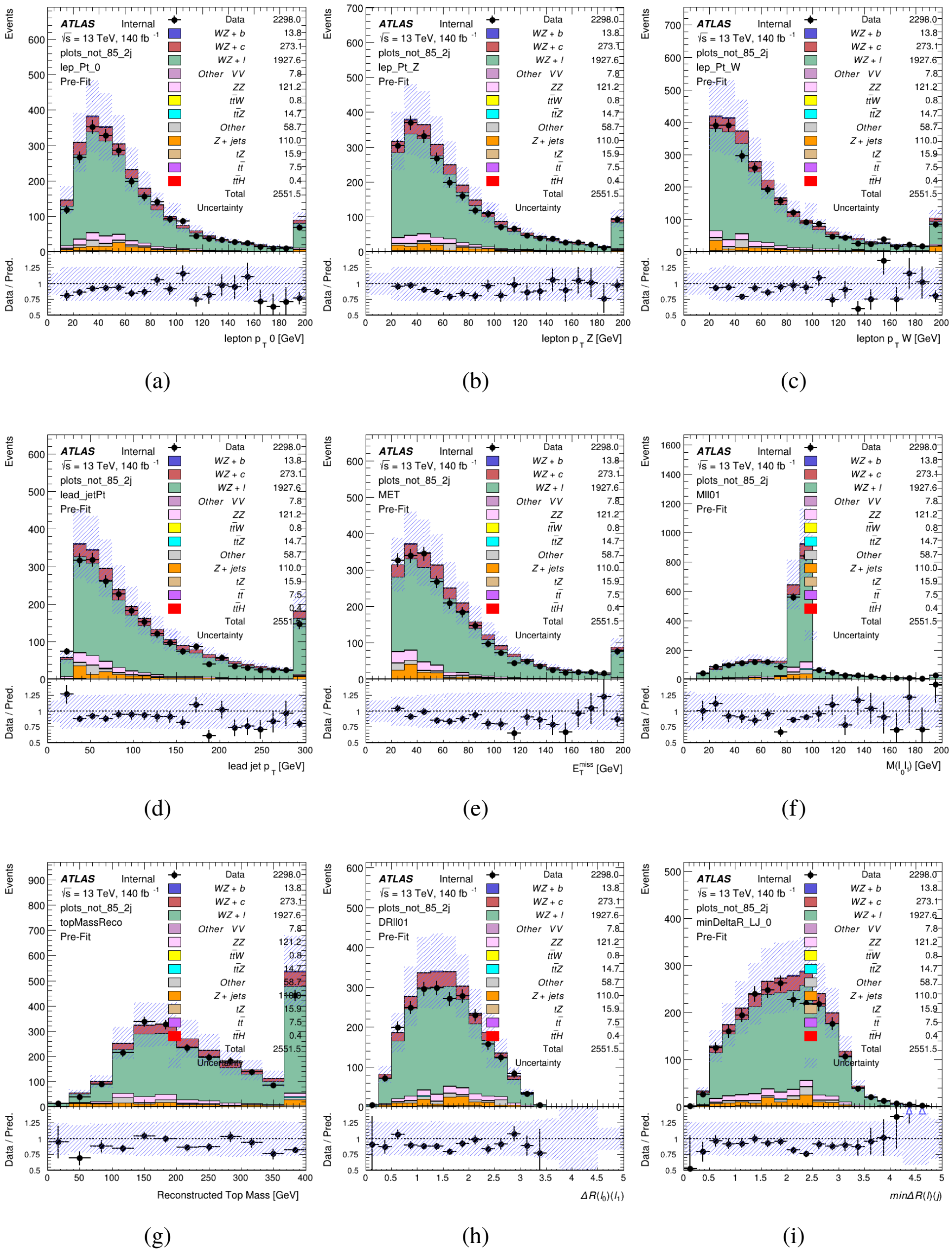

Figure 19: Comparisons between the data and MC distributions in the preselection region for (a) the p_T of the opposite sign lepton, (b) the p_T of the other lepton from the Z candidate, (c) the p_T of the lepton from the W candidate, (d) the leading jet p_T, (e) the E_T^{miss}, and (f) the invariant mass of leptons 0 and 1, (g) the reconstructed top mass, (h) $\Delta(R)$ between lepton 0 and 1, (i) the $\Delta(R)$ between the closest lepton and jet.

WZ Fit Region - 2j 77-85% WP

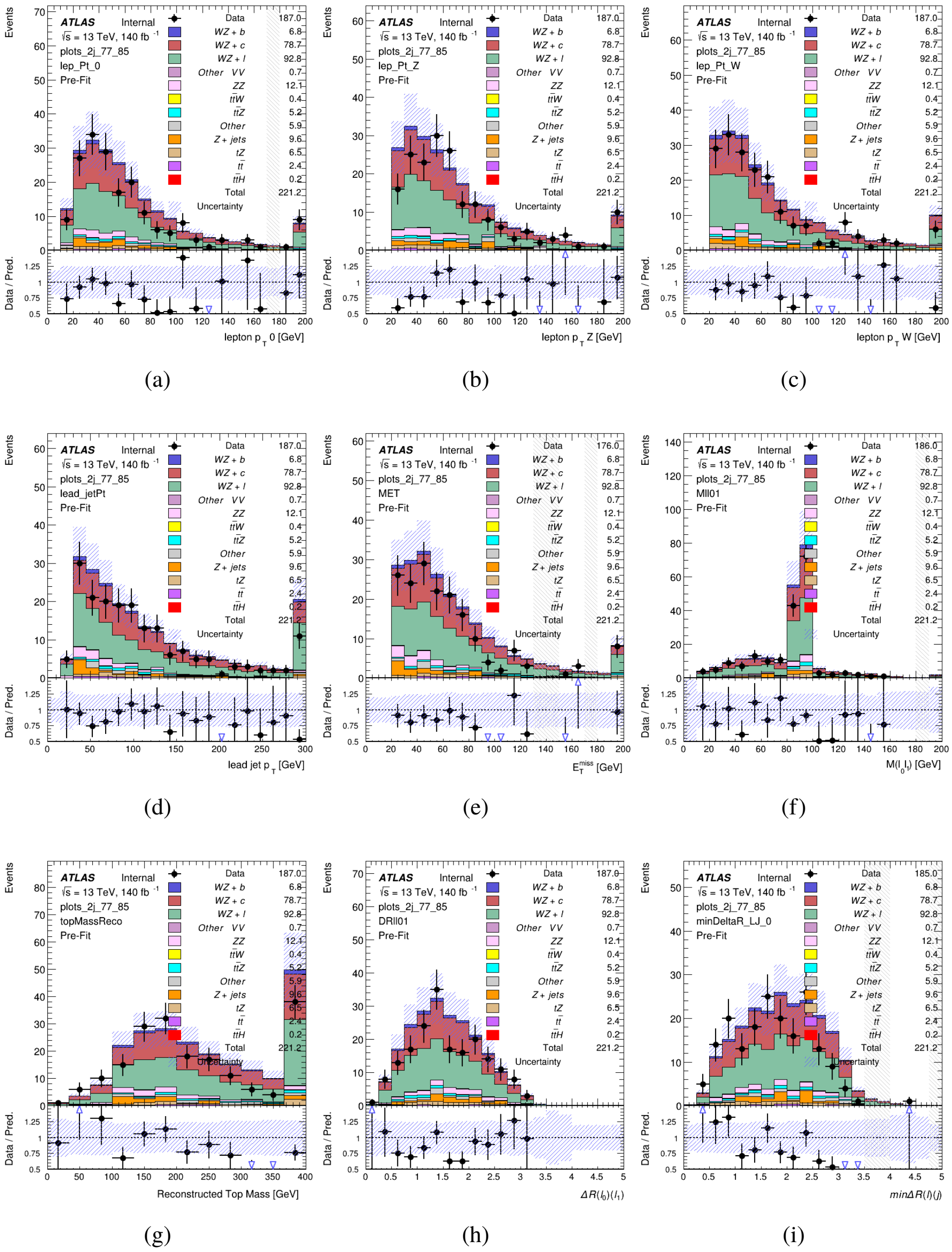

Figure 20: Comparisons between the data and MC distributions in the preselection region for (a) the p_T of the opposite sign lepton, (b) the p_T of the other lepton from the Z candidate, (c) the p_T of the lepton from the W candidate, (d) the leading jet p_T, (e) the E_T^{miss}, and (f) the invariant mass of leptons 0 and 1, (g) the reconstructed top mass, (h) $\Delta(R)$ between lepton 0 and 1, (i) the $\Delta(R)$ between the closest lepton and jet.

WZ Fit Region - 2j 70-77% WP

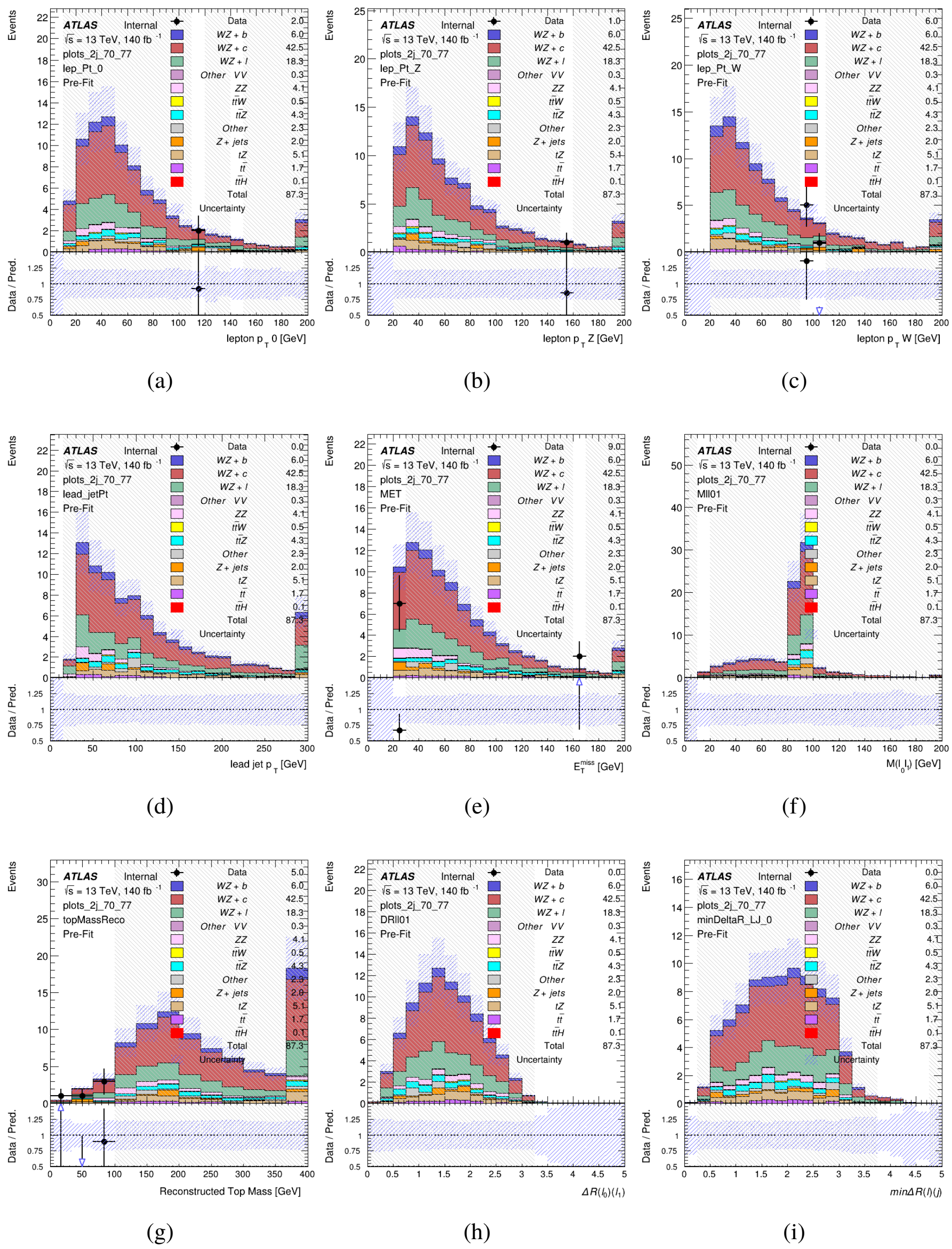

Figure 21: Comparisons between the data and MC distributions in the preselection region for (a) the p_T of the opposite sign lepton, (b) the p_T of the other lepton from the Z candidate, (c) the p_T of the lepton from the W candidate, (d) the leading jet p_T, (e) the E_T^{miss}, and (f) the invariant mass of leptons 0 and 1, (g) the reconstructed top mass, (h) $\Delta(R)$ between lepton 0 and 1, (i) the $\Delta(R)$ between the closest lepton and jet.

WZ Fit Region - 2j 60-70% WP

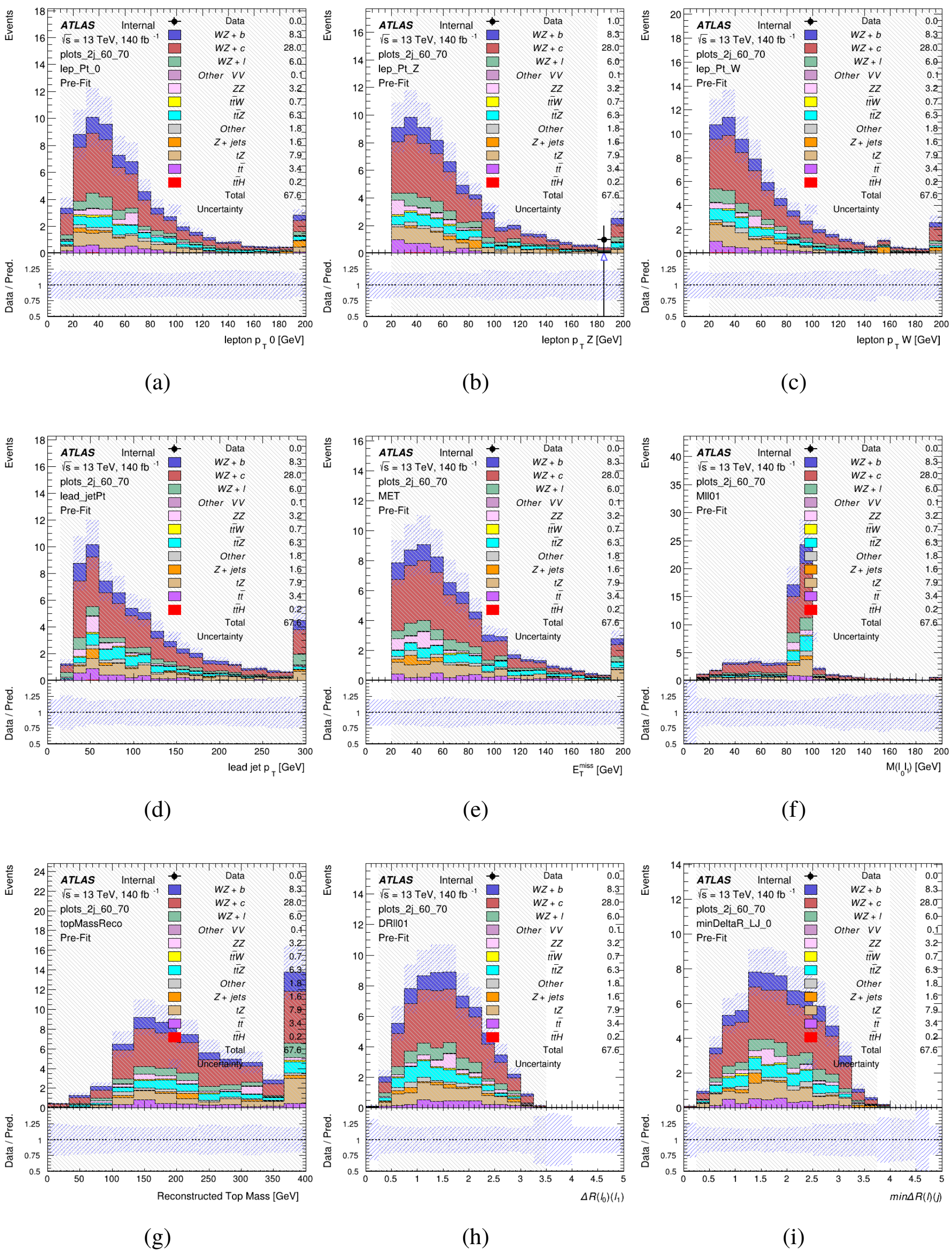

(a) (b) (c)

(d) (e) (f)

(g) (h) (i)

Figure 22: Comparisons between the data and MC distributions in the preselection region for (a) the p_T of the opposite sign lepton, (b) the p_T of the other lepton from the Z candidate, (c) the p_T of the lepton from the W candidate, (d) the leading jet p_T, (e) the E_T^{miss}, and (f) the invariant mass of leptons 0 and 1, (g) the reconstructed top mass, (h) $\Delta(R)$ between lepton 0 and 1, (i) the $\Delta(R)$ between the closest lepton and jet.

WZ Fit Region - 2j 60% WP

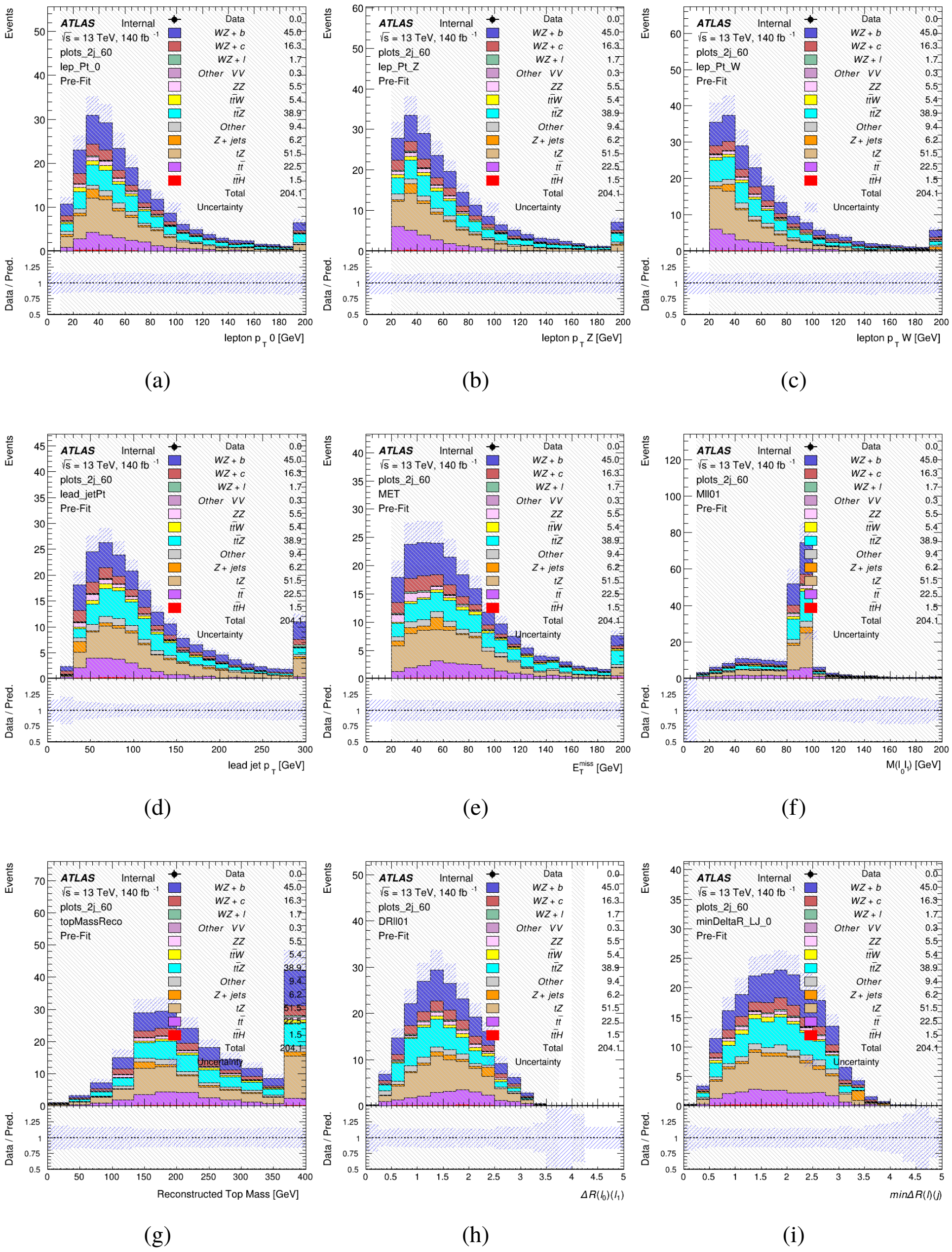

Figure 23: Comparisons between the data and MC distributions in the preselection region for (a) the p_T of the opposite sign lepton, (b) the p_T of the other lepton from the Z candidate, (c) the p_T of the lepton from the W candidate, (d) the leading jet p_T, (e) the E_T^{miss}, and (f) the invariant mass of leptons 0 and 1, (g) the reconstructed top mass, (h) $\Delta(R)$ between lepton 0 and 1, (i) the $\Delta(R)$ between the closest lepton and jet.

WZ Fit Region - tZ-CR-2j

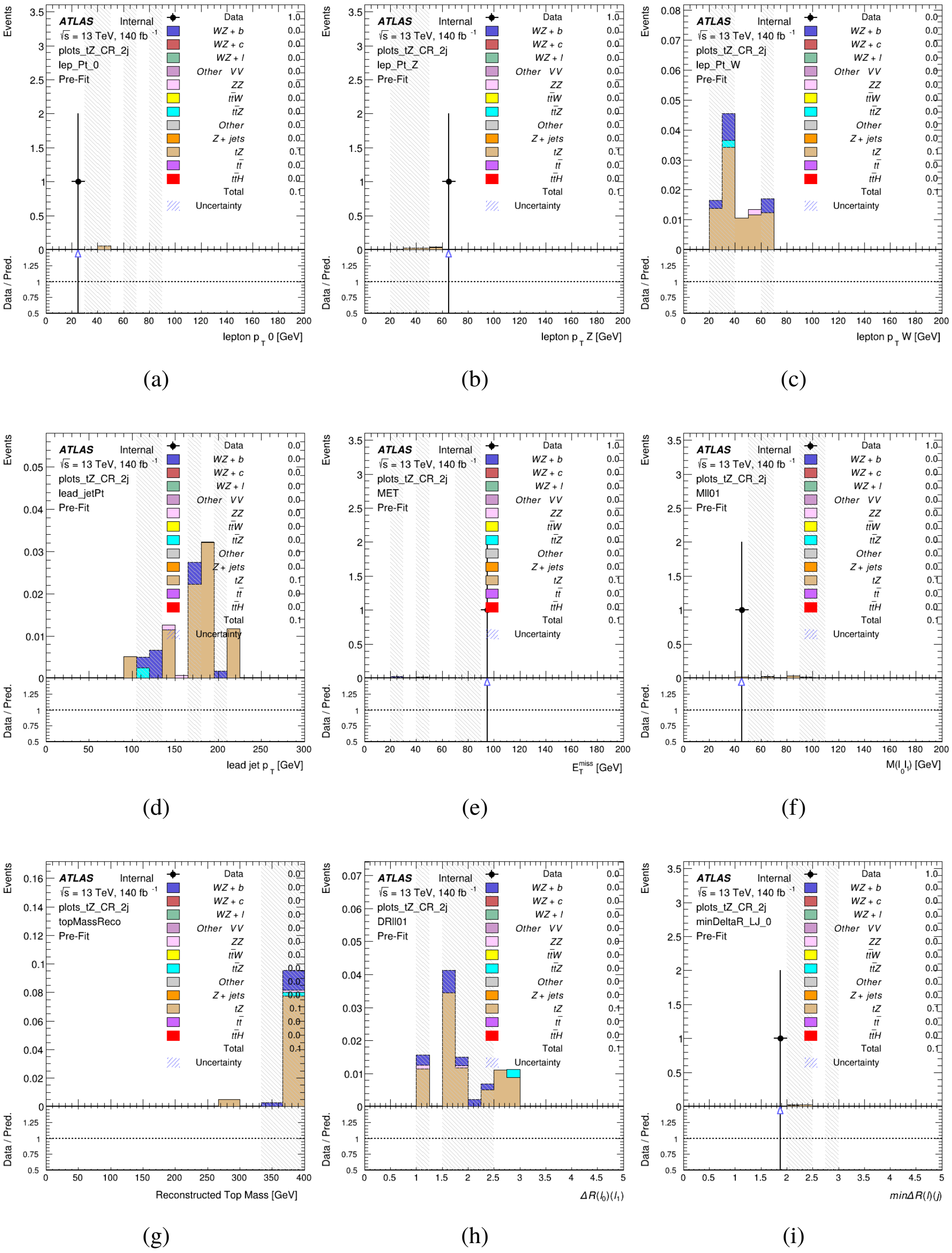

Figure 24: Comparisons between the data and MC distributions in the preselection region for (a) the p_T of the opposite sign lepton, (b) the p_T of the other lepton from the Z candidate, (c) the p_T of the lepton from the W candidate, (d) the leading jet p_T, (e) the E_T^{miss}, and (f) the invariant mass of leptons 0 and 1, (g) the reconstructed top mass, (h) $\Delta(R)$ between lepton 0 and 1, (i) the $\Delta(R)$ between the closest lepton and jet.

6.3 Non-Prompt Lepton Estimation

Two processes act as sources of non-prompt leptons appear in the analysis: $t\bar{t}$ and Z+jet production both produce two prompt leptons, and each contribute to the 3l region when an additional non-prompt lepton appears in the event. The contribution of these processes is estimated with Monte Carlo simulations, which are validated using enriched validation regions.

The modelling in the Z+jets and $t\bar{t}$ CRs is further validated for each of the pseudo-continuous b-tag regions used in the analysis. The relevant lepton p_T spectrum in each b-tag region is shown in Appendix A.2 for these CRs after the correction factors derived below have been applied.

6.3.1 $t\bar{t}$ Validation

$t\bar{t}$ events can produce two prompt leptons from the decay of each of the tops. These top decays produce two b-quarks, the decay of which can produce additional non-prompt leptons, which occasionally pass the event preselection. In order to validate that the Monte Carlo accurately simulates this process accurately, the MC prediction in a non-prompt $t\bar{t}$ enriched validation region is compared to data.

The $t\bar{t}$ validation region is similar to the preselection region - three leptons meeting the criteria described in Section 6 are required, and the requirements on E_T^{miss} remain the same. However, the selection requiring that a lepton pair form a Z-candidate are reversed. Events where the invariant mass of any two opposite sign, same flavor leptons falls within 10 GeV of 91.2 GeV are rejected. This ensures the $t\bar{t}$ validation region is orthogonal to the preselection region.

Further, because the jet multiplicity of $t\bar{t}$ events tends to be higher than WZ + jets, the number of jets in each event is required to be greater than 1. As b-jets are almost invariably produced from top decays, at least one b-tagged jet passing the 70% DL1r WP in each event is required. Various kinematic plots of this region are shown in Figure 25.

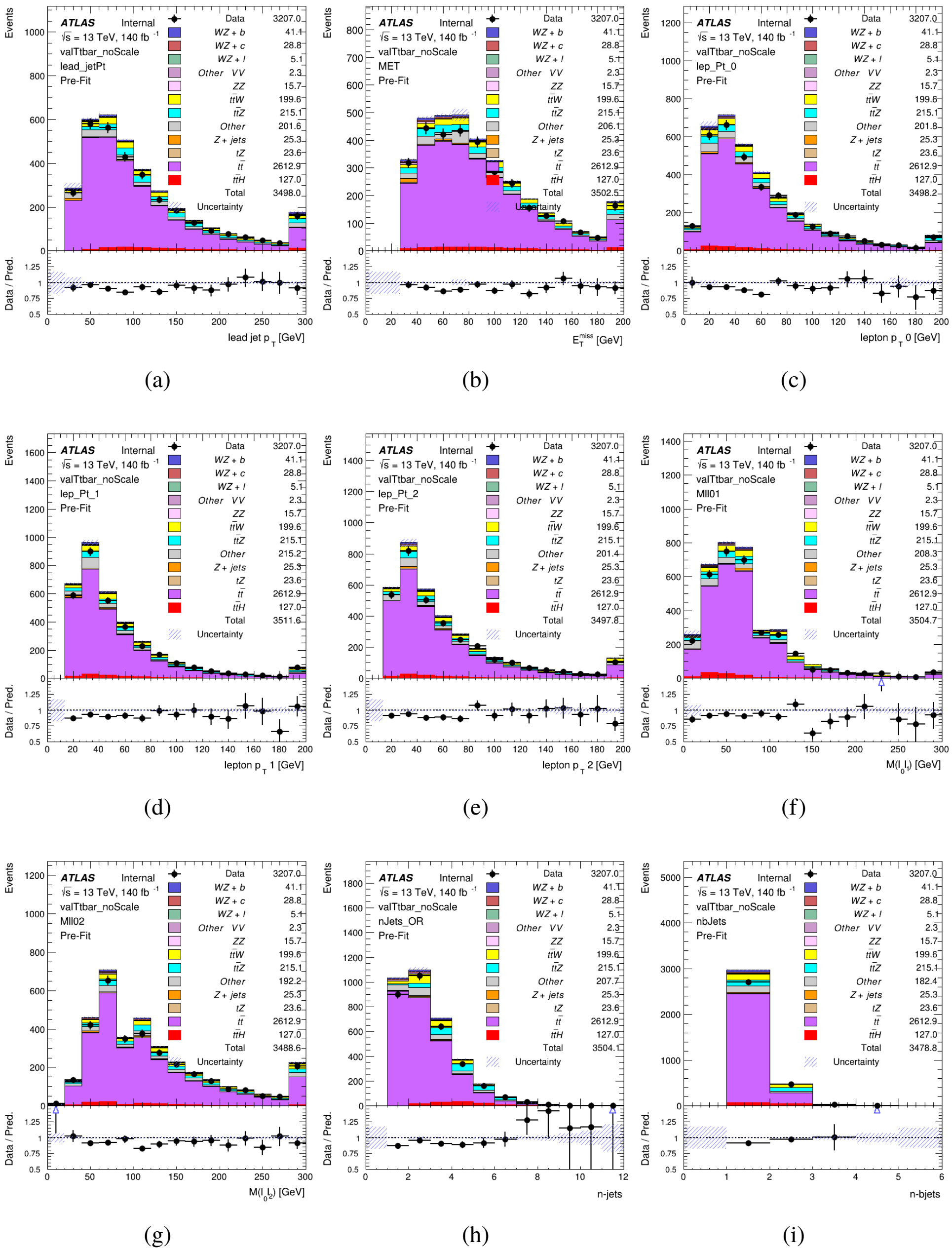

Figure 25: Comparisons between the data and MC distributions in the $t\bar{t}$ validation region for (a) the p_T of the leading jet, (b) the missing transverse energy, (c) the p_T of lepton 0, (d) p_T of lepton 1, (e) p_T of lepton 2, (f) the invariant mass of leptons 0 and 1, (g) the invariant mass of leptons 0 and 2, (h) the number of jets, (i) the number of b-tagged jets.

The shape of each distribution agrees quite well between data and MC, with a constant offset between the two. This is accounted for by applying a constant correction factor of 0.9 to the $t\bar{t}$

MC prediction. Plots showing the kinematics of the $t\bar{t}$ VR after this correction factor has been applied are shown in Figure 26.

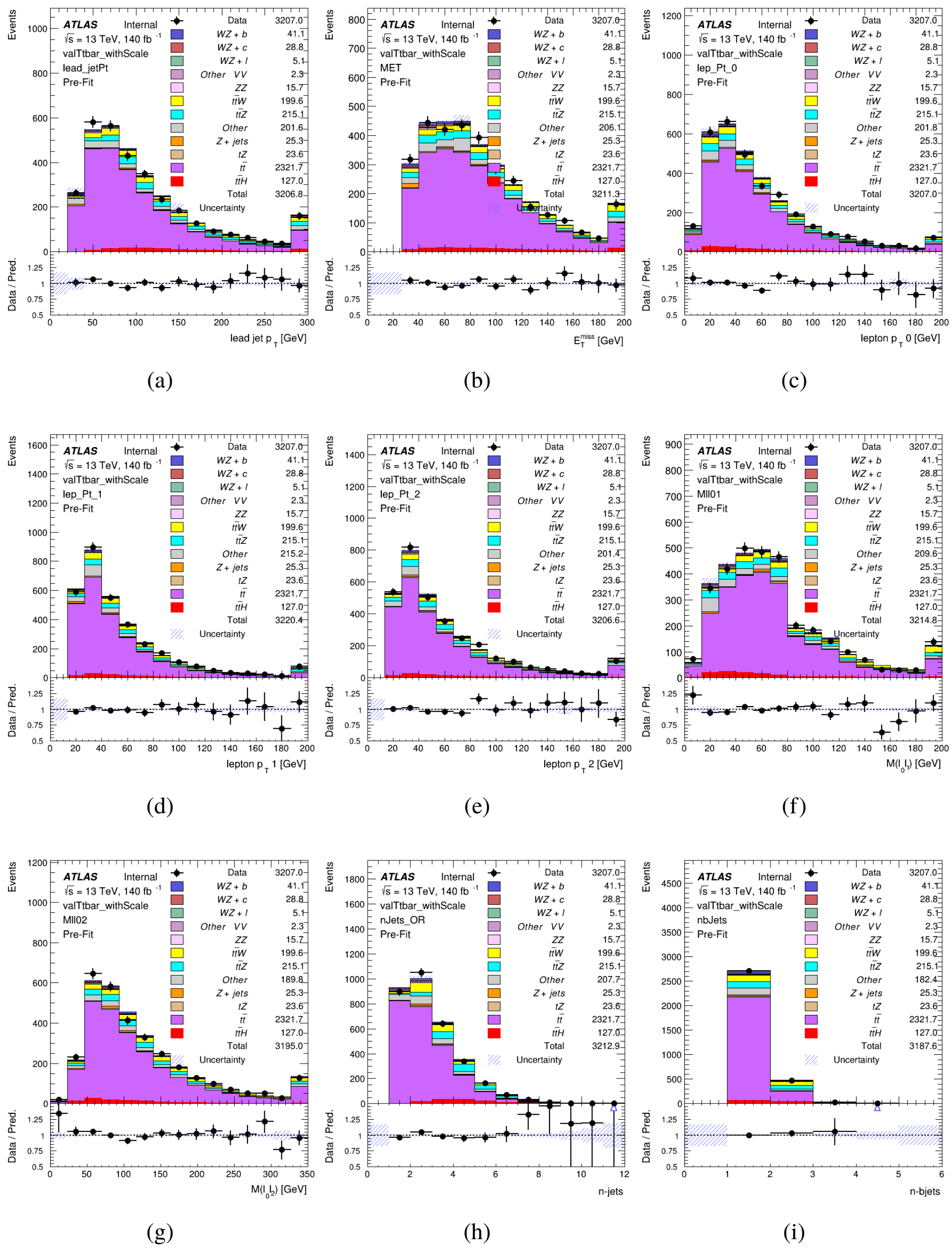

Figure 26: Comparisons between the data and MC distributions in the $t\bar{t}$ validation region after the correction factor has been applied for (a) the p_T of the leading jet, (b) the missing transverse energy, (c) the p_T of lepton 0, (d) p_T of lepton 1, (e) p_T of lepton 2, (f) the invariant mass of leptons 0 and 1, (g) the invariant mass of leptons 0 and 2, (h) the number of jets, (i) the number of b-tagged jets.

The modeling is further validated by looking at the yield in the $t\bar{t}$ VR for each DL1r WP, giving a clearer correspondence to the signal regions used in the fit. For these plots, the requirement that each event contain at least one b-tagged jet is removed. Each region shown in Figure 27 requires one or more jets pass the listed WP, with no jets passing the next highest WP.

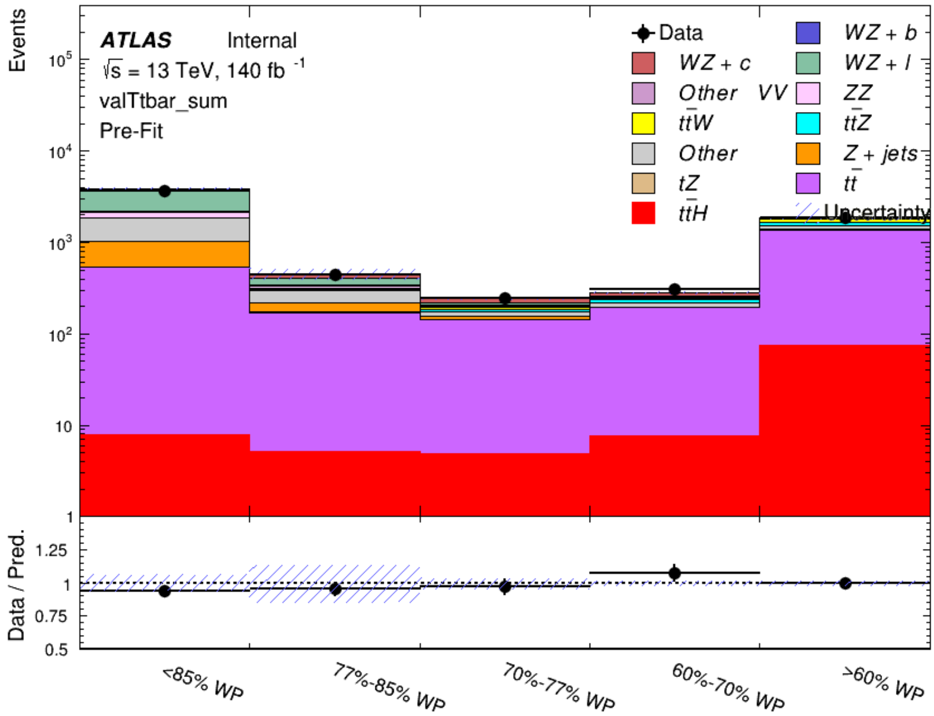

Figure 27: Data and MC comparisons for each DL1r WP for both 1-jet and 2-jet regions, after the $t\bar{t}$ VR selection and correction factor have been applied

As data and MC are found to agree within 20% for each of these working points, a 20% systematic uncertainty on the $t\bar{t}$ prediction is included for the analysis.

6.3.2 Z+jets Validation

Similar to $t\bar{t}$, a non-prompt Z+jets validation region is produced in order to validate the MC predictions. The lepton requirements remain the same as the preselection region. Because no neutrinos are present for this process, the E_T^{miss} cut is reversed, requiring $E_T^{miss} < 30$ GeV. This also ensures this validation region is orthogonal to the preselection region. Further, the number of jets in each event is required to be greater than or equal to one. Various kinematic plots of this region are shown below. The general agreement between data and MC in each of these suggests that the non-prompt contribution of Z+jets is well modeled by Monte Carlo.

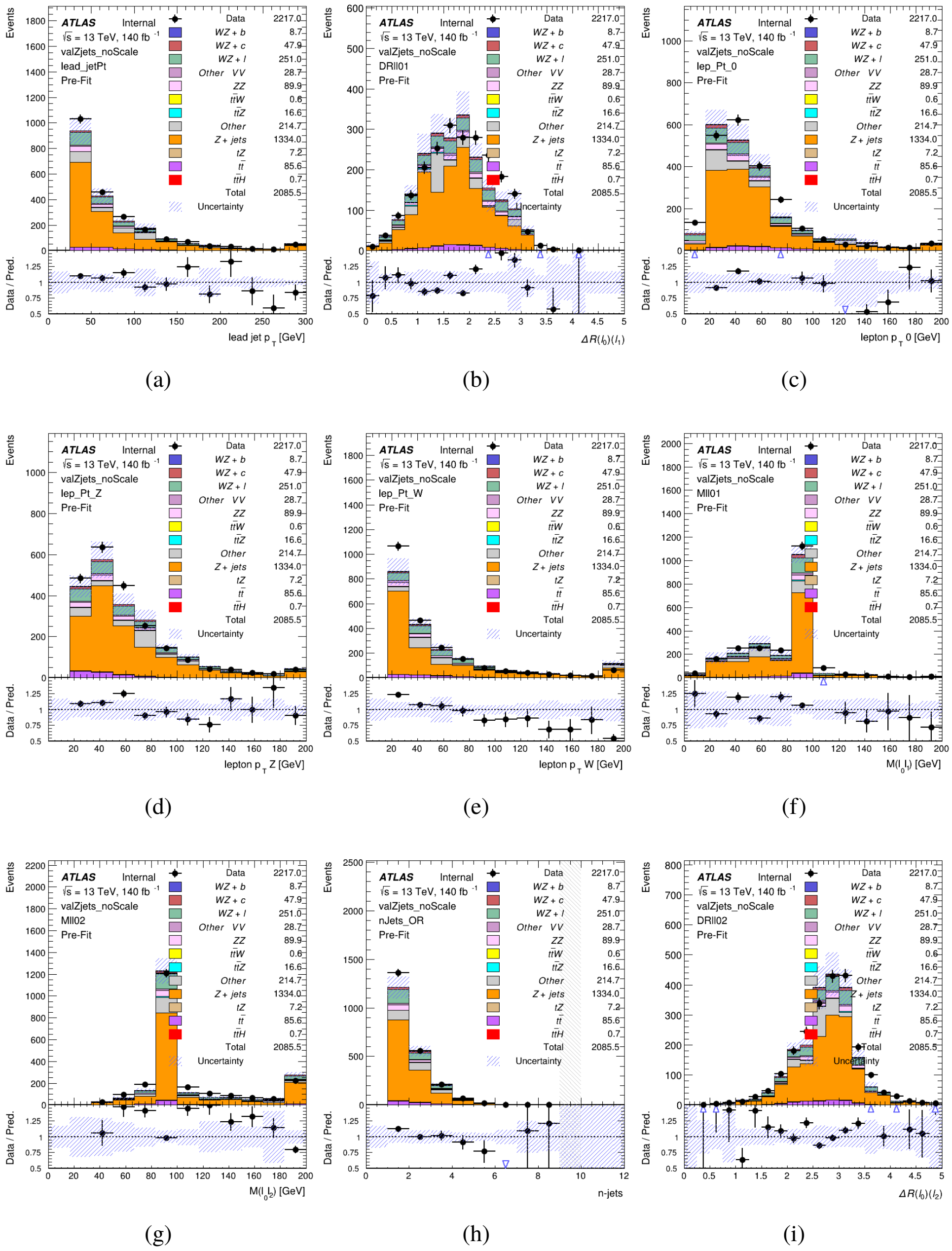

Figure 28: Comparisons between the data and MC distributions in the Z+jets validation region for (a) the p_T of the leading jet, (b) ΔR between leptons 0 and 1, (c) the p_T of lepton 0, (d) p_T of SS lepton from the Z candidate, (e) p_T of the SS lepton from the W candidate, (f) the invariant mass of leptons 0 and 1, (g) the invariant mass of leptons 0 and 2, (h) the number of jets, (i) ΔR between leptons 0 and 2. Includes only statistical uncertainties

491 While there is general agreement between data and MC within statistical uncertainty, the shape

of the p_T spectrum of the lepton from the W candidate is found to differ. As this is the lepton not included in the Z-candidate, in the case of Z+jets, this lepton is most often the non-prompt lepton. A similar effect is seen for both non-prompt muons and electrons in the Z+jets validation region, as shown in Figure 29.

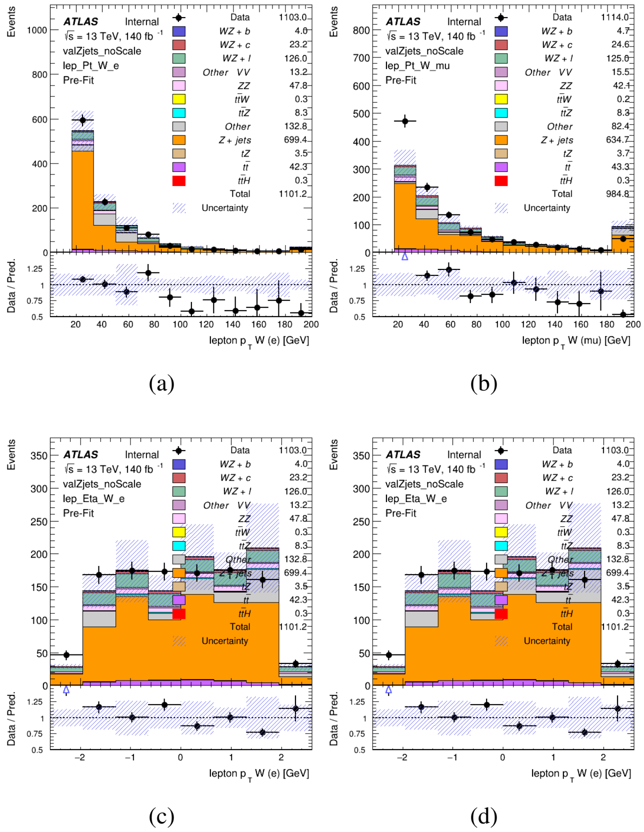

Figure 29: p_T spectrum of the lepton from the W candidate for (a) electrons and (b) muons, as well as η spetrum for (c) electrons and (d) muons, before the correction has been applied

To account for this discrepency, a variable correction factor is applied to Z+jets. χ^2 minimization of the W lepton p_T spectrum is performed to derive a correction factor as a function of this p_T. Kinematic plots of the Z + jets validation region after this correction factor has been aplied are shown in Figure 30.

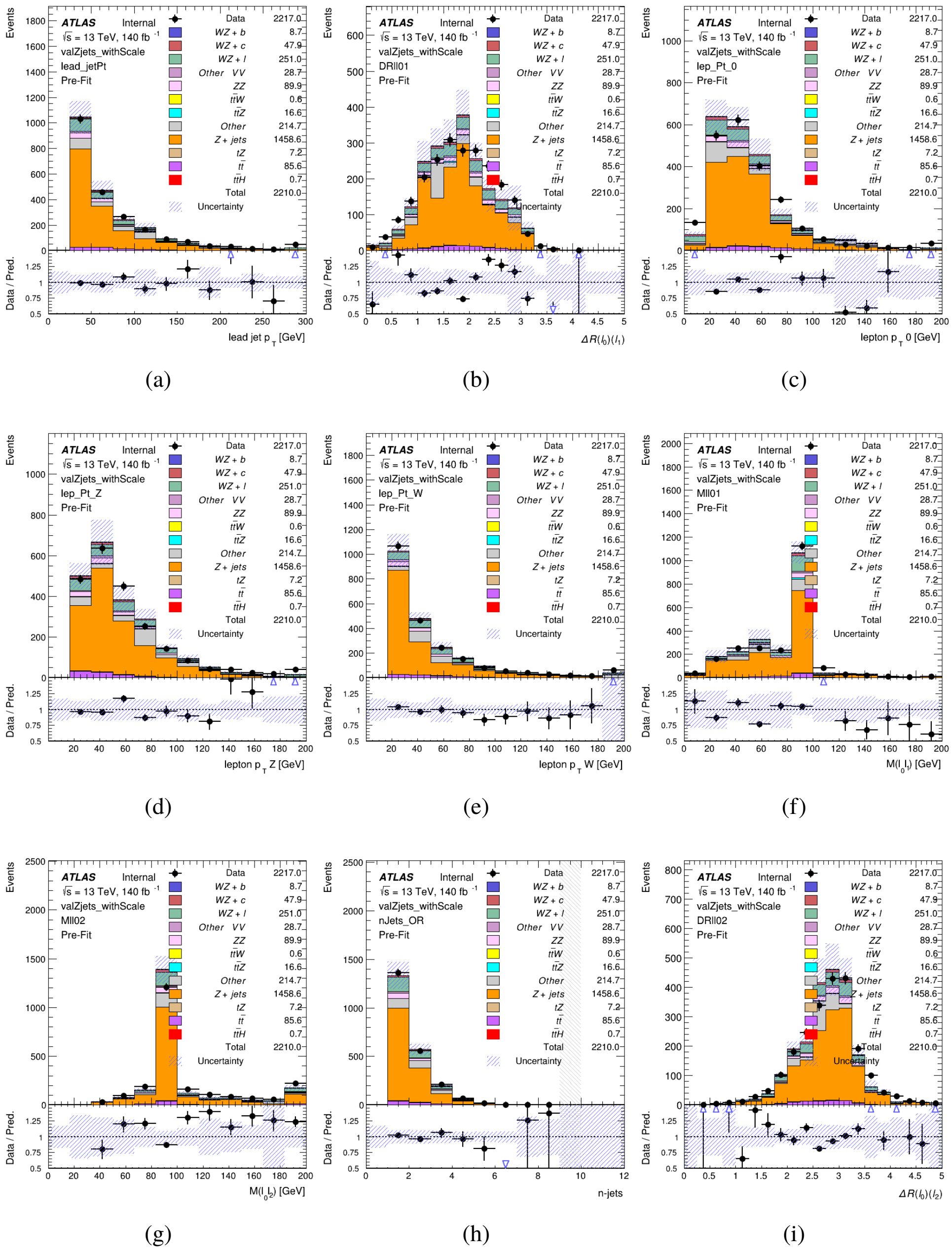

Figure 30: Comparisons between the data and MC distributions in the Z+jets validation region after the correction factor has been applied for (a) the p_T of the leading jet, (b) ΔR between leptons 0 and 1, (c) the p_T of lepton 0, (d) p_T of SS lepton from the Z candidate, (e) p_T of the SS lepton from the W candidate, (f) the invariant mass of leptons 0 and 1, (g) the invariant mass of leptons 0 and 2, (h) the number of jets, (i) ΔR between leptons 0 and 2

The p_T and η of the lepton from the W candidate split by lepton flavor after this correction has

501 been applied is shown in figure 31.

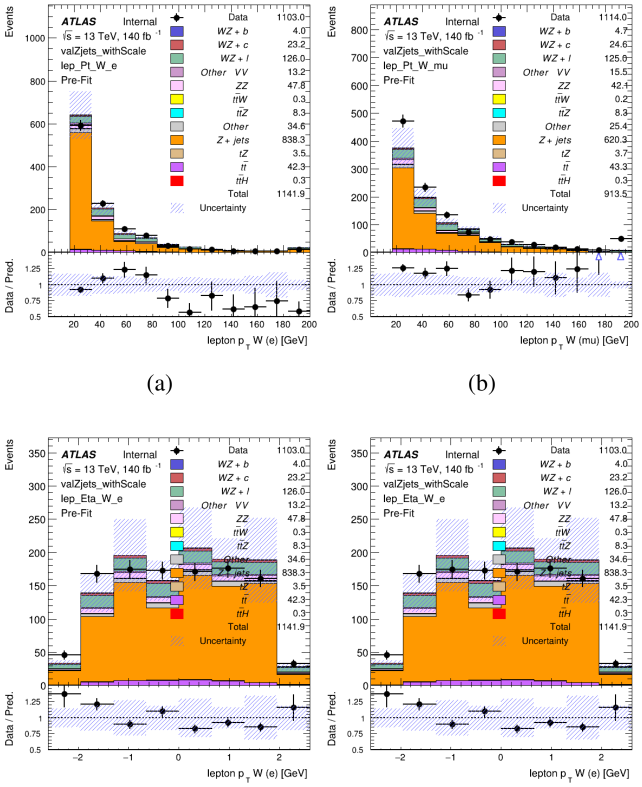

(a) (b)

(c) (d)

Figure 31: p_T spectrum of the lepton from the W candidate for (a) electrons and (b) muons, as well as η spetrum for (c) electrons and (d) muons, after the correction has been applied

502 The modeling is further validated by looking at the yield in the Z+jets VR for each DL1r WP,
503 giving a clearer correspondence to the signal regions used in the fit. Each region shown in Figure
504 32 requires one or more jets pass the listed WP, with no jets passing the next highest WP.

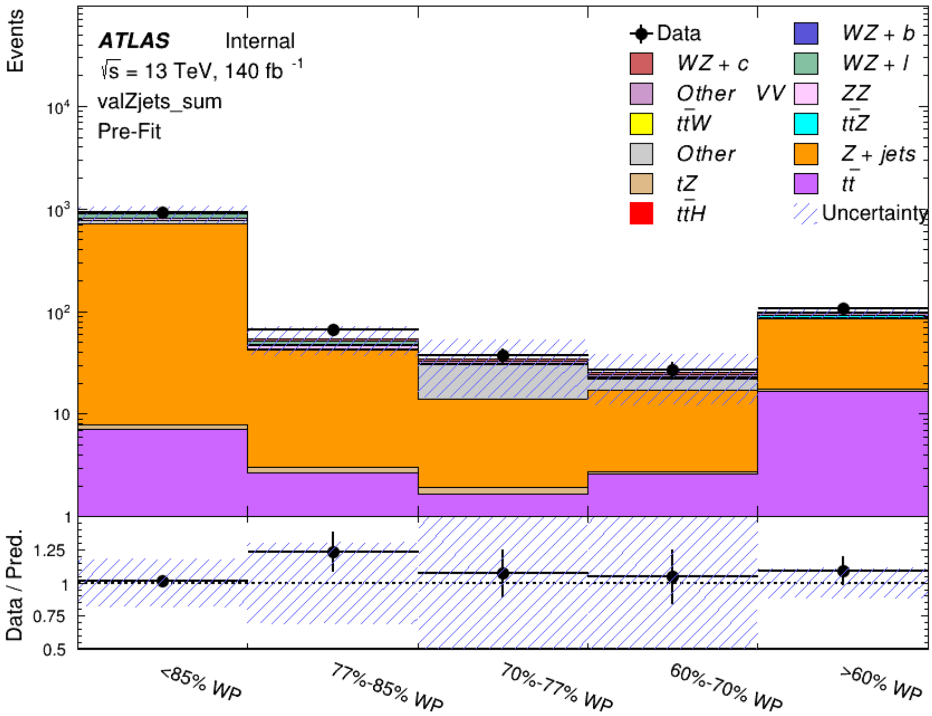

Figure 32: Data and MC comparisons for each DL1r WP for both 1-jet and 2-jet regions, after the Z+jets VR selection and correction factor have been applied

For each of the b-tagging working points considered, the data falls within 25% of the MC prediction once this correction factor has been applied. Therefore, a 25% systematic uncertainty is applied to Z + jets in the analysis.

7 Systematic Uncertainties

The systematic uncertainties that are considered are summarized in Table 9. These are implemented in the fit either as a normalization factors or as a shape variation or both in the signal and background estimations. These systematic uncertainties are treated as independent nuiscance parameters (NPs) in the fit, and are assumed to be gaussian. Each NP is varied up and down by its uncertainty, and the difference in the result of the fit is taken to be the systematic uncertainty of that NP. The numerical impact of each of these uncertainties is outlined in Section 8.

Table 9: Sources of systematic uncertainty considered in the analysis.

Systematic uncertainty	Components
Luminosity	1
Pileup reweighting	1
Physics Objects	
Electron	5
Muon	14
Prompt Lepton Veto	1
Jet energy scale	28
Jet energy resolution	8
Jet vertex fraction	1
Jet flavor tagging	131
E_T^{miss}	3
Total (Experimental)	194
Signal Modeling	
Shape modelling	3
Renormalization and factorization scales	5
nJet Migration	5
Background Modeling	
Cross section	15
Renormalization and factorization scales	12
Parton shower and hadronization model	2
Shower tune	4
Total (Signal and background modeling)	41
Total (Overall)	235

The uncertainty in the combined 2015–2018 integrated luminosity is 1.7% [25], obtained using the LUCID-2 detector [26] for the primary luminosity measurements.

The experimental uncertainties are related to the reconstruction and identification of light leptons and b-tagging of jets, and to the reconstruction of E_T^{miss}. The `TOTAL` electron ID correlation model is used, corresponding to 1 electron ID systematic [27]. Electron ID is found to be a subleading systematic that is unconstrained by the fit, making it an appropriate choice for this analysis.

The sources which contribute to the uncertainty in the jet energy scale (JES) [28] are decomposed into uncorrelated components and treated as independent sources in the analysis. The CategoryReduction model is used to account for JES uncertainties, which decomposes the uncertainties into 30 nuiscance parameters included in the fit. The SimpleJER model is used to account for jet energy resolution (JER) uncertainties, and 8 JER uncertainty components included as NPs in the fit.

The uncertainties in the b-tagging efficiencies measured in dedicated calibration analyses [19] are also decomposed into uncorrelated components. The large number of components for b-tagging is due to the use of the full continuous b-tagging spectrum: The calibration of the distribution of the MVA discriminant for each of the individual working points considered for $b-$ $c-$ and light jets, and the correlations between them, produces a large number of systematic uncertainties.

The full list of systematic uncertainties considered in the analysis is summarized in Tables 10, 11 and 12.

Experimental Systematics on Leptons and E_T^{miss}			
Type	Description	Systematics Name	Application
Trigger			
Scale Factors	Trigger Efficiency	lepSFTrigTight_MU(EL)_SF_Trigger_STAT(SYST)	Event Weight
Muons			
Efficiencies	Reconstruction and Identification	lepSFObjTight_MU_SF_ID_STAT(SYST)	Event Weight
	Isolation	lepSFObjTight_MU_SF_Isol_STAT(SYST)	Event Weight
	Track To Vertex Association	lepSFObjTight_MU_SF_TTVA_STAT(SYST)	Event Weight
p_T Scale	p_T Scale	MUONS_SCALE	p_T Correction
Resolution	Inner Detector Energy Resolution	MUONS_ID	p_T Correction
	Muon Spectrometer Energy Resolution	MUONS_MS	p_T Correction
Electrons			
Efficiencies	Reconstruction	lepSFObjTight_EL_SF_ID	Event Weight
	Identification	lepSFObjTight_EL_SF_Reco	Event Weight
	Isolation	lepSFObjTight_EL_SF_Isol	Event Weight
Scale Factor	Energy Scale	EG_SCALE_ALL	Energy Correction
Resolution	Energy Resolution	EG_RESOLUTION_ALL	Energy Correction
E_T^{miss}			
Soft Tracks Terms	Resolution	MET_SoftTrk_ResoPerp	p_T Correction
	Resolution	MET_SoftTrk_ResoPara	p_T Correction
	Scale	MET_SoftTrk_ScaleUp	p_T Correction
	Scale	MET_SoftTrk_ScaleDown	p_T Correction

Table 10: Summary of experimental systematics considered for leptons and E_T^{miss}. Includes type, description, name of systematic as used in the fit, and mode of application. The mode of application indicates the systematic evaluation, e.g. as an overall event re-weighting (Event Weight) or rescaling (p_T Correction).

Experimental Systematics on Jets			
Type	Origin	Systematics Name	Application
Jet Vertex Tagger		JVT	Event Weight
Energy Scale	Calibration Method	JET_21NP_	p_T Correction
		JET_EffectiveNP_1-19	p_T Correction
	η inter-calibration	JET_EtaIntercalibration_Modelling	p_T Correction
		JET_EtaIntercalibration_NonClosure	p_T Correction
		JET_EtaIntercalibration_TotalStat	p_T Correction
	High p_T jets	JET_SingleParticle_HighPt	p_T Correction
	Pile-Up	JET_Pileup_OffsetNPV	p_T Correction
		JET_Pileup_OffsetMu	p_T Correction
		JET_Pileup_PtTerm	p_T Correction
		JET_Pileup_RhoTopology	p_T Correction
	Non Closure	JET_PunchThrough_MC15	p_T Correction
	Flavour	JET_Flavor_Response	p_T Correction
		JET_BJES_Response	p_T Correction
		JET_Flavor_Composition	p_T Correction
Resolution		JET_JER_EffectiveNP_NP_1-8	Event Weight

Table 11: Jet systematics take into account effects of jets calibration method, η inter-calibration, high p_T jets, pile-up, and flavor response. They are all diagonalised into effective parameters.

Experimental Systematics on b-tagging		
Type	Origin	Systematic Name
Scale Factors	DL1r b-tagger efficiency on b originated jets in bins of η	DL1r_Continuous_EventWeight_B0-29
	DL1r b-tagger efficiency on c originated jets in bins of η	DL1r_Continuous_EventWeight_C0-19
	DL1r b-tagger efficiency on light flavoured originated jets in bins of η and p_T	DL1r_Continuous_EventWeight_Light0-79
	DL1r b-tagger extrapolation efficiency	DL1r_Continuous_EventWeight_extrapolation DL1r_Continuous_EventWeight_extrapolation_from_charm

Table 12: Summary of experimental systematics to be included for b-tagging of jets in the analysis, using the continuous DL1r tagging algorithm. All of the b-tagging related systematics are applied as event weights. From left: type, description, and the name of systematic used in the fit.

Theoretical uncertainties applied to MC predictions, including cross section, PDF, and scale uncertainties are taken from theory calculations, with the exception of non-prompt and diboson backgrounds. The cross-section uncertainty on tZ is taken from [29]. Derivation of the non-prompt background uncertainties, Z+jets and $t\bar{t}$, are explained in detail in Section 6.3. These normalization uncertainties are chosen so as to account for the complete uncertainty in the non-prompt contribution, and therefore no additional modelling uncertainties are considered for Z+jets and $t\bar{t}$.

The other VV + heavy flavor processes (namely VV+b and VV+charm, which primarily consist of ZZ events) are also poorly understood, because these processes involve the same physics as WZ + heavy flavor, and have also not been measured. Therefore, an arbitrary 50% uncertainty is applied to those samples, as it is found to have little impact on the significance of the final result: Fits are performed with this uncertainty decreased to 25% and increased to 75% and no change in the final result was observed.

The theory uncertainties applied to the predominate background estimates are summarized in Table 13.

Process	X-section [%]
WZ	QCD Scale: $^{+3.7}_{-3.4}$ PDF($+\alpha_S$): ± 3.1
tZ	X-sec: ± 15.2
$t\bar{t}$ H (aMC@NLO+Pythia8)	QCD Scale: $^{+5.8}_{-9.2}$ PDF($+\alpha_S$): $\pm$ 3.6
$t\bar{t}$ Z (aMC@NLO+Pythia8)	QCD Scale: $^{+9.6}_{-11.3}$ PDF($+\alpha_S$): $\pm$ 4
$t\bar{t}$ W (aMC@NLO+Pythia8)	QCD Scale: $^{+12.9}_{-11.5}$ PDF($+\alpha_S$): $\pm$ 3.4
VV + b/charm (Sherpa 2.2.1)	± 50
VV + light (Sherpa 2.2.1)	± 6
$t\bar{t}$	± 20
Z + jets	± 25
Others	± 50

Table 13: Summary of theoretical uncertainties for MC predictions in the analysis.

Due to its importance as a background, additional modelling uncertainties are considered for tZ. Alternative tZ samples with variations in scale (DSID 412064-5) and shower modelling (DSID 501046) are included as systematics..

The fit involves varying the overall normalization of signal templates over the regions described in Section 6.2, which are defined by the flavor and number of associated jets at truth-level. The modelling of these template shapes therefore significantly impacts the final result. Additional signal uncertainties, probing the shape of the signal templates as well as the rate of migrations between the number of truth-jets and reconstructed jets, are estimated by comparing estimates from the nominal Sherpa WZ samples with alternative WZ samples generated with Powheg+Pythia8 (DSID 361601). Separate systematics are included in the fit for WZ + b, WZ + c and WZ + light, where the distribution among each of the fit regions is varied based on the prediction of the Powheg sample.

The variations in the signal templates are shown in Figures 33 and 34. Each of these plots are normalized to unity in order to capture the relevant differences in shape.

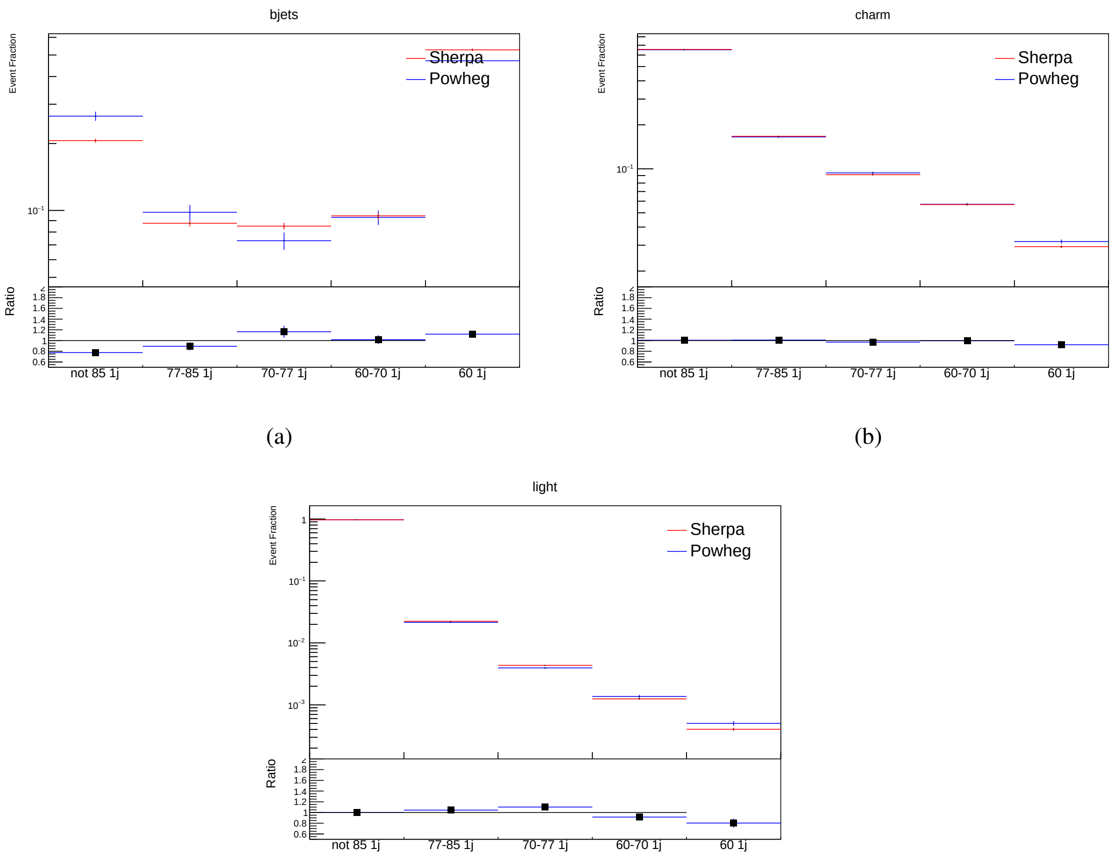

(a) (b) (c)

Figure 33: Comparison between Sherpa and Powheg predictions of the distribution of (a) WZ + b, (b) WZ + charm, and (c) WZ + light among the various b-tag WPs used in the 1-jet fit.

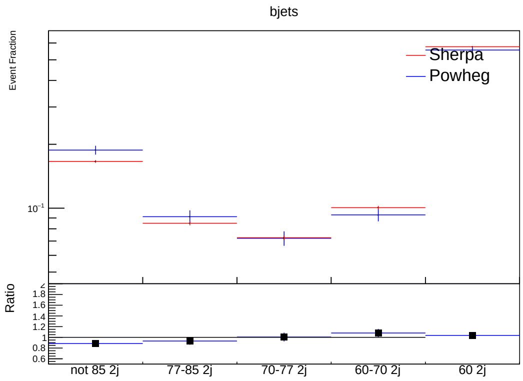

(a)

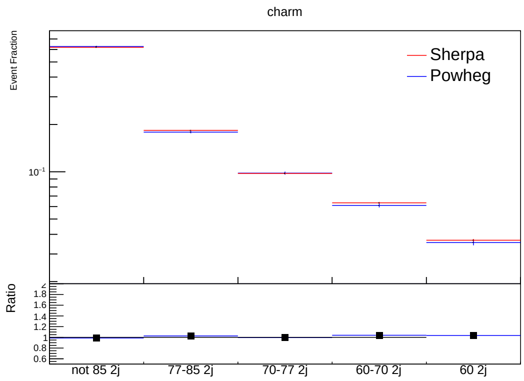

(b)

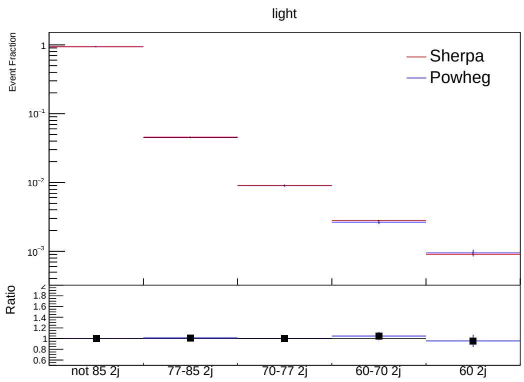

(c)

Figure 34: Comparison between Sherpa and Powheg predictions of the distribution of (a) WZ + b, (b) WZ + charm, and (c) WZ + light among the various b-tag WPs used in the 2-jet fit.

Separate systematics are included in the fit for WZ + b, WZ + charm and WZ + light, where the distribution among each of the fit regions is varied based on the prediction of the Powheg sample.

A similar approach is taken to account for uncertainties in migrations between the number of reco and truth jets. The fraction of events with 1 truth jet which fall into the 1 jet bin versus the 2 jet bin at reco level is compared for Sherpa and Powheg. The same is done for events with 2 truth jets. This comparison is shown is figure 35.

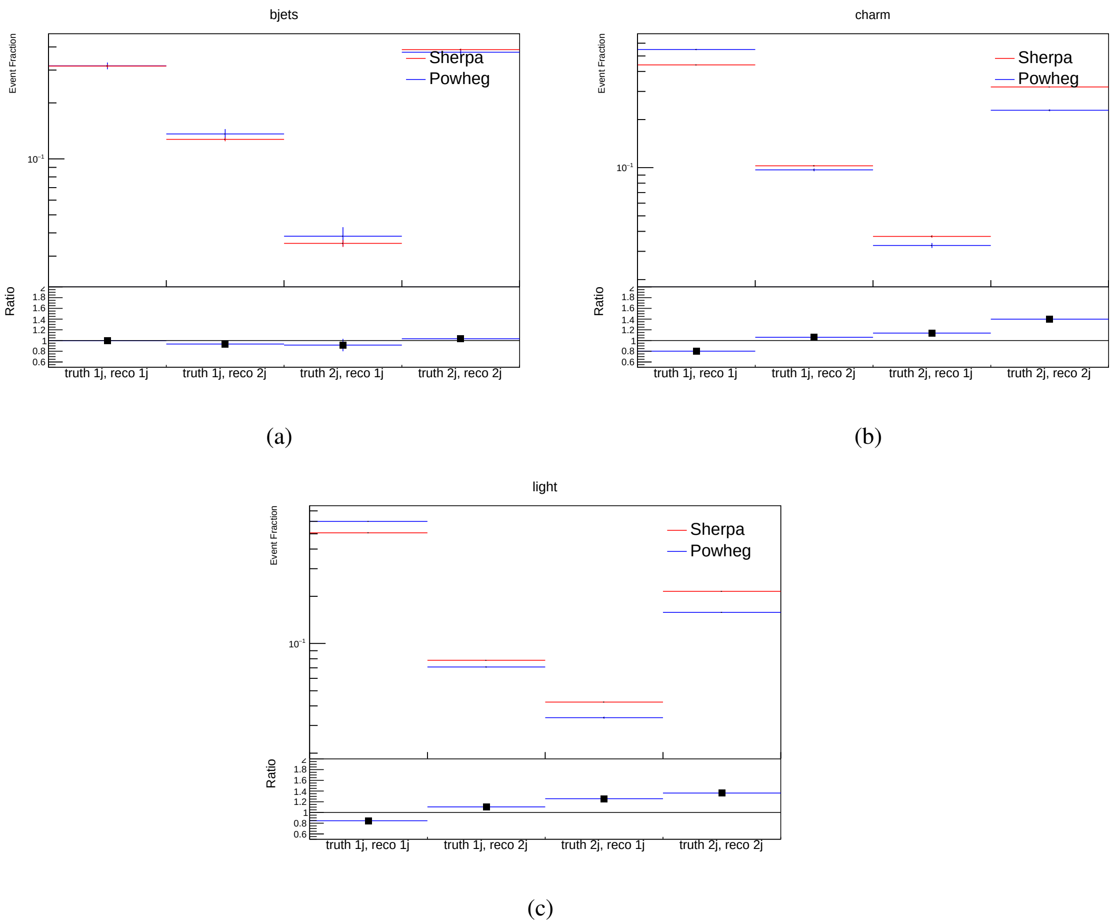

Figure 35: Comparison between Sherpa and Powheg predictions for truth jet migrations between the 1 and 2 jet reco bins for (a) WZ + b, (b) WZ + charm, and (c) WZ + light

A systematic is included where events are shifted between the 1-jet and 2-jet regions based on the differences between these two shapes. This is done independently for each of the WZ + b, WZ + charm, and WZ + light templates.

Additional systematics are included to account for the uncertainty in the contamination of 0 jet and 3 or more jet events (at truth level) in the 1 and 2 reco jet bins. Because these events fall outside the scope of this measurement, these events are included as a background. As such, a normalization, rather than a shape, uncertainty is applied for this background.

The number of WZ events with 0-jets and >=3-jets in the reconstructed 1-jet and 2-jet regions are compared for Sherpa and Powheg, as seen in figure 36. These differences are taken as separate normalization systematics on the yield of WZ+0-jet and WZ+>=3-jet events.

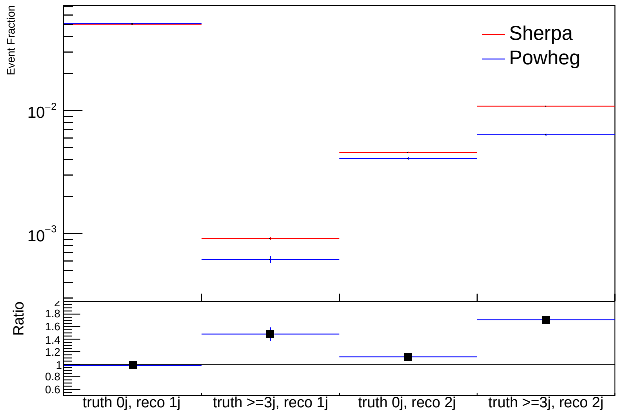

Figure 36: Comparison between Sherpa and Powheg predictions for 0 and >=3 truth jet contributions in the 1 and 2 jet reco bins

8 Results

8.1 Fit Procedure

A maximum-likelihood fit is performed over the unfolded signal templates in the various fit regions described in Section 6 in order to extract the best-fit value of the WZ + b-jet and WZ + charm jet contributions for events with both 1 and 2 associated jets.

Because the fit regions are defined by the number of associated jets at reco-level, an unfolding procedure is applied to the signal in order to account for differences in the number of truth jets compared to the number of reco-jets. The WZ + b, WZ + charm and WZ + light contributions are separated into independent samples based on the number of truth jets in each event. WZ + 1 truth-jet and WZ + 2 truth-jets are treated as signal samples, while WZ + 0 truth-jets and WZ + >=3 truth-jets are treated as an additional background.

A maximum likelihood fit to data is performed simultaneously in the regions described in Section 6, summarized in figure 37. The six signal templates, which include WZ+b 1-jet, WZ+c 1-jet, WZ+l 1-jet, WZ+b 2-jets, WZ+c 2-jets, WZ+l 2-jets, are allowed to float, while the remaining background contributions are held fixed. The parameters $\mu_{WZ+b-1-jet}$, $\mu_{WZ+charm1-jet}$, $\mu_{WZ+light-1-jet}$, $\mu_{WZ+b-2-jet}$, $\mu_{WZ+charm2-jet}$, $\mu_{WZ+light-2-jet}$, where $\mu = \sigma_{observed}/\sigma_{SM}$, are extracted from the fit. A simultaneous fit is performed over all 1-jet and 2-jet regions.

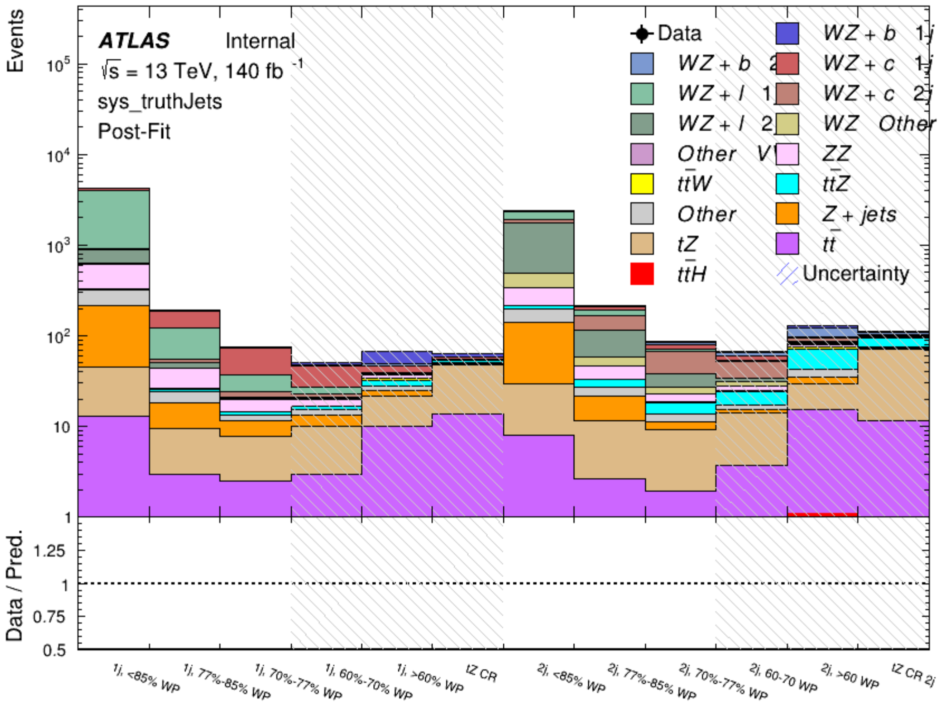

Figure 37: Post-fit summary of the fit regions.

As described in Section 7, there are 235 systematic uncertainties that are considered as NPs in the fit. These NPs are constrained by Gaussian or log-normal probability density functions. The latter are used for normalisation factors to ensure that they are always positive. The expected number of signal and background events are functions of the likelihood. The prior for each NP is added as a penalty term, decreasing the likelihood as it is shifted away from its nominal value.

Several alternative fit strategies are documented in Sections 8.3-8.4.1. These include a measurement of WZ + 1 or 2 jets inclusively, a fit where tZ is allowed to float, and a case where tZ is included as part of the signal.

8.2 Results of the Simultaneous Fit

The Asimov fit for 1-jet events gives an expected μ value of $1.00^{+0.47}_{-0.43}(\mathrm{stat})^{+0.30}_{-0.27}(\mathrm{sys})$ for WZ + b. The normalization factors extracted from the fit for WZ + charm and WZ + light are $1.00 \pm 0.17 \pm 0.17$ and $1.00 \pm 0.06 \pm 0.14$, respectively.

The expected cross-section of WZ+b with 1-jet in the fiducial region outlined in Section 2 is $1.74^{+0.82}_{-0.75}(\mathrm{stat})^{+0.53}_{-0.48}(\mathrm{sys})$ fb, and $14.6 \pm 2.5(\mathrm{stat}) \pm 2.3(\mathrm{sys})$ fb for WZ + charm, with a correlation of -0.15 between them. An expected significance of 2.0 is observed for WZ + b in this region.

For 2-jet events, the fit gives an expected μ value of $1.00^{+0.53}_{-0.51}(\mathrm{stat})^{+0.39}_{-0.34}(\mathrm{sys})$ for WZ + b. The fitted cross-section modifiers for WZ + charm and WZ + light are $1.00 \pm 0.25 \pm 0.21$ and $1.00 \pm 0.06 \pm 0.16$, respectively.

The expected WZ + b cross-section in the fiducial region with 2 associated jets is $2.5^{+1.3}_{-1.3}(\mathrm{stat})^{+0.95}_{-0.83}(\mathrm{sys})$ fb with an expected significance of 1.7σ. The 2-jet expected cross-section of WZ + charm is $12.7 \pm 3.2(\mathrm{stat}) \pm 2.7(\mathrm{sys})$ fb, and the correlation between WZ + charm and WZ + b is -0.22.

The results of the fit to an Asimov dataset for the fiducial regions considered, including both the normalization factors as well as the expected cross-sections, along with their uncertainties, are summarized in Table 14.

Process	μ	σ
WZ + b - 1-jet	$1.00^{+0.47}_{-0.43}(\mathrm{stat})^{+0.30}_{-0.27}(\mathrm{sys})$	$1.74^{+0.82}_{-0.75}(\mathrm{stat})^{+0.53}_{-0.48}(\mathrm{sys})$ fb
WZ + c - 1-jet	$1.00 \pm 0.17(\mathrm{stat}) \pm 0.17(\mathrm{sys})$	$14.6 \pm 2.5(\mathrm{stat}) \pm 2.3(\mathrm{sys})$ fb
WZ + b - 2-jet	$1.00^{+0.53}_{-0.51}(\mathrm{stat})^{+0.39}_{-0.34}(\mathrm{sys})$	$2.5^{+1.3}_{-1.3}(\mathrm{stat})^{+0.95}_{-0.83}(\mathrm{sys})$ fb
WZ + c - 2-jet	$1.00^{+0.25}_{-0.24}(\mathrm{stat})^{+0.32}_{-0.27}(\mathrm{sys})$	$12.7^{+3.3}_{-3.2}(\mathrm{stat})^{+3.9}_{-3.4}(\mathrm{sys})$ fb

Table 14: Normalization factors and cross-sections extracted from the fit for each of the fiducial regions considered

An expected significance of 2.0σ is observed for WZ + b with 1-jet, and 1.7σ for WZ + b with two jets. A summary of the correlations between these various measurements is shown in Figure 38.

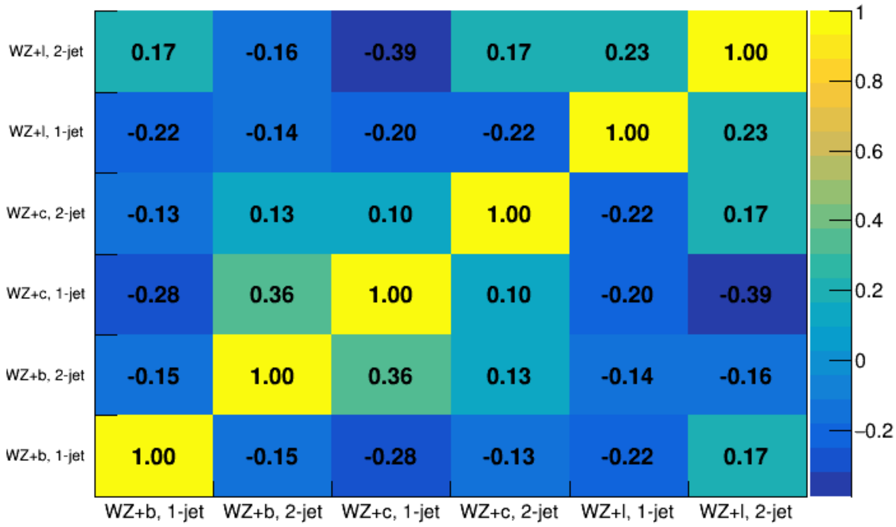

Figure 38: Correlations between the various measured components of WZ.

The pre-fit yields in each of the 1-jet regions used in the fit are shown in Table 15.

Sample	1j, <85% WP	1j, 77%-85% WP	1j, 70%-77% WP	1j, 60%-70% WP	1j, 60% WP	tZ CR
$WZ + b - 1j$	8.1 ± 1.6	4.7 ± 0.5	4.6 ± 0.4	5.1 ± 0.4	18.1 ± 2.4	5.0 ± 0.6
$WZ + c - 1j$	260 ± 22	81 ± 6	43.1 ± 3.6	25.8 ± 2.6	9.4 ± 1.8	2.9 ± 0.6
$WZ + l - 1j$	3090 ± 250	91 ± 13	17 ± 3	4.9 ± 1.6	1.3 ± 0.4	0.2 ± 0.1
$WZ + b - 2j$	1.10 ± 0.37	0.44 ± 0.11	0.39 ± 0.06	0.62 ± 0.14	2.1 ± 0.5	0.59 ± 0.14
$WZ + c - 2j$	21 ± 5	5.6 ± 1.2	3.0 ± 0.7	2.0 ± 0.5	0.70 ± 0.20	0.30 ± 0.08
$WZ + l - 2j$	250 ± 60	5.7 ± 1.6	0.73 ± 0.53	0.31 ± 0.15	0.07 ± 0.06	0.01 ± 0.01
$WZ - \mathrm{Other}$	13 ± 5	1.4 ± 0.4	0.42 ± 0.08	0.2 ± 0.01	0.30 ± 0.05	0.67 ± 0.15
Other VV	6.2 ± 0.6	0.2 ± 0.4	0.2 ± 0.04	0.07 ± 0.1	0.1 ± 0.1	0.1 ± 0.2
ZZ	336 ± 26	17.8 ± 2.1	4.3 ± 0.6	1.7 ± 0.5	0.36 ± 0.08	0.10 ± 0.03
$t\bar{t}W$	1.1 ± 0.2	0.2 ± 0.1	0.3 ± 0.1	0.4 ± 0.1	1.5 ± 0.3	0.7 ± 0.2
$t\bar{t}Z$	6.8 ± 1.2	1.4 ± 0.3	1.0 ± 0.2	1.2 ± 0.2	4.4 ± 0.8	3.2 ± 0.6
$Z +$ jets	169 ± 38	8.9 ± 1.9	3.7 ± 0.8	3.3 ± 0.7	3.2 ± 0.7	0.8 ± 0.17
$V + \gamma$	45 ± 28	1.9 ± 2.4	0.1 ± 0.1	0.02 ± 0.01	1.0 ± 0.9	0.02 ± 0.03
tZ	31.8 ± 4.3	6.4 ± 1.1	5.3 ± 0.8	7.2 ± 1.1	11.8 ± 2.0	33.9 ± 4.5
tW	1.4 ± 0.8	0.2 ± 0.5	0.0 ± 0.2	0.7 ± 0.6	0.26 ± 0.42	0.39 ± 0.41
WtZ	2.3 ± 1.2	0.6 ± 0.3	0.3 ± 0.21	0.27 ± 0.2	1.1 ± 0.7	0.6 ± 0.5
VVV	12.4 ± 0.5	0.93 ± 0.06	0.35 ± 0.03	0.13 ± 0.02	0.14 ± 0.03	0.02 ± 0.01
VH	40 ± 6	2.6 ± 1.4	0.9 ± 0.8	0.7 ± 0.8	0.5 ± 0.6	0.0 ± 0.0
$t\bar{t}$	12.1 ± 1.6	2.9 ± 0.6	2.5 ± 0.5	2.8 ± 0.5	11.2 ± 1.4	10.9 ± 1.5
$t\bar{t}H$	0.24 ± 0.03	0.05 ± 0.01	0.04 ± 0.01	0.06 ± 0.01	0.20 ± 0.03	0.13 ± 0.02
Total	5010 ± 260	227 ± 24	88 ± 12	57 ± 8	76 ± 16	53 ± 8

Table 15: Pre-fit yields in each of the 1-jet regions.

Here <85% includes jets that fail to pass the 85% WP, and 60% includes jets that pass the highest WP. The post-fit yields in each region are summarized in Table 16.

	1j, <85% WP	1j, 77%-85% WP	1j, 70%-77% WP	1j, 60%-70% WP	1j, 60% WP	tZ CR
$WZ+b-1j$	8.1 ± 4.9	4.7 ± 2.0	4.6 ± 2.0	5.1 ± 2.1	18 ± 10	5.0 ± 2.5
$WZ+c-1j$	260 ± 60	80 ± 14	43 ± 7	26 ± 5	7.4 ± 2.3	2.1 ± 0.7
$WZ+l-1j$	3090 ± 130	90 ± 11	17.3 ± 2.8	4.9 ± 1.6	1.3 ± 0.4	0.23 ± 0.13
$WZ+b-2j$	1.10 ± 0.37	0.44 ± 0.11	0.39 ± 0.06	0.62 ± 0.14	2.1 ± 0.5	0.59 ± 0.14
$WZ+c-2j$	21 ± 5	5.6 ± 1.2	3.0 ± 0.7	2.0 ± 0.5	0.70 ± 0.20	0.30 ± 0.08
$WZ+l-2j$	250 ± 60	5.7 ± 1.6	0.73 ± 0.53	0.31 ± 0.15	0.07 ± 0.06	0.01 ± 0.01
$WZ-\mathrm{Other}$	13 ± 5	1.4 ± 0.4	0.42 ± 0.08	0.2 ± 0.01	0.30 ± 0.05	0.67 ± 0.15
Other VV	6.2 ± 0.6	0.92 ± 0.07	0.02 ± 0.01	0.01 ± 0.01	0.01 ± 0.01	0.01 ± 0.01
ZZ	346 ± 57	19 ± 5	4.3 ± 0.8	2.7 ± 0.5	2.4 ± 0.1	2.1 ± 0.6
$t\bar{t}W$	1.09 ± 0.21	0.2 ± 0.1	0.1 ± 0.1	0.4 ± 0.1	1.5 ± 0.3	0.1 ± 0.2
$t\bar{t}Z$	6.8 ± 1.2	1.4 ± 0.3	1.0 ± 0.2	1.2 ± 0.2	4.4 ± 0.7	3.2 ± 0.5
rare Top	0.14 ± 0.04	0.04 ± 0.02	0.04 ± 0.0	0.1 ± 0.03	0.14 ± 0.04	0.15 ± 0.05
$t\bar{t}WW$	0.04 ± 0.03	0.01 ± 0.02	0.01 ± 0.01	0.01 ± 0.01	0.01 ± 0.02	0.01 ± 0.01
$Z+\mathrm{jets}$	169 ± 37	8.9 ± 1.9	3.7 ± 0.8	3.3 ± 0.7	3.2 ± 0.7	0.8 ± 0.2
$W+\mathrm{jets}$	0.01 ± 0.01	0.01 ± 0.01	0.01 ± 0.01	0.01 ± 0.01	0.01 ± 0.01	0.01 ± 0.01
$V+\gamma$	46 ± 28	1.9 ± 2.4	0.1 ± 0.1	0.0 ± 0.2	1.0 ± 0.9	0.0 ± 0.0
tZ	31 ± 4	6.0 ± 1.0	5.3 ± 0.8	7.2 ± 1.0	11.8 ± 1.8	33.9 ± 4.5
tW	1.37 ± 0.82	0.18 ± 0.26	0.01 ± 0.12	0.67 ± 0.64	0.26 ± 0.42	0.39 ± 0.41
WtZ	2.3 ± 1.2	0.6 ± 0.3	0.3 ± 0.2	0.3 ± 0.2	1.1 ± 0.6	0.6 ± 0.3
VVV	12.4 ± 0.4	0.9 ± 0.1	0.4 ± 0.1	0.13 ± 0.02	0.14 ± 0.03	0.02 ± 0.01
VH	40 ± 6	2.6 ± 1.4	0.9 ± 0.8	0.7 ± 0.8	0.4 ± 0.6	0.01 ± 0.01
$t\bar{t}$	12.1 ± 1.6	2.9 ± 0.6	2.5 ± 0.5	2.8 ± 0.5	11.2 ± 1.5	10.9 ± 1.4
$t\bar{t}H$	0.24 ± 0.03	0.05 ± 0.01	0.04 ± 0.01	0.06 ± 0.01	0.20 ± 0.03	0.13 ± 0.02
Total	5100 ± 110	227 ± 12	87 ± 6	56.7 ± 4.4	76 ± 9	52.5 ± 4.2

Table 16: Post-fit yields in each of the 1-jet regions.

The impact of each NP is calculated by performing the fit with the parameter of interest held fixed, varied from its fitted value by its uncertainty, and calculating $\Delta\mu$ relative to the baseline fit. The impact of the most significant sources of systematic uncertainties on WZ + b with one associated jet is summarized in Table 17.

Uncertainty Source	$\Delta\mu$	
WZ + 1-jet light cross-section	0.13	-0.15
WZ + 1-jet charm cross-section	-0.10	0.12
Jet Energy Scale	0.1	-0.13
Other Diboson + b cross-section	-0.09	0.09
tZ cross-section	-0.08	0.08
WZ 1-jet/2-jet Migration	0.08	-0.07
Jet Energy Resolution	-0.07	0.08
Luminosity	-0.06	0.07
Flavor tagging	0.05	0.05
$t\bar{t}$ cross-section	-0.05	0.05
Total Systematic Uncertainty	0.28	0.33

Table 17: Summary of the most significant sources of systematic uncertainty on the measurement of $WZ + b$ with exactly one associated jet.

Uncertainty Source	$\Delta\sigma/\sigma_{nominal}$	
WZ + c 1j/2j migration	0.12	-0.09
Flavor Tagging	0.09	0.08
WZ + b, 1-jet cross-section	-0.04	0.05
Luminosity	-0.04	0.04
Jet Energy Resolution	0.04	0.04
WZ + b, 2-jet cross-section	0.04	-0.03
WZ cross-section - QCD scale	-0.04	0.04
Jet Energy Scaling	0.04	0.02
WZ cross-section - PDF	-0.03	0.03
WZ + light, 1-jet cross-section	0.03	-0.03
total	0.1879	0.1753

Table 18: Summary of the most significant sources of systematic uncertainty on the measurement of WZ + c with exactly one associated jet.

The ranking and impact of those nuisance parameters with the largest contribution to the overall uncertainty is shown in Figure 39.

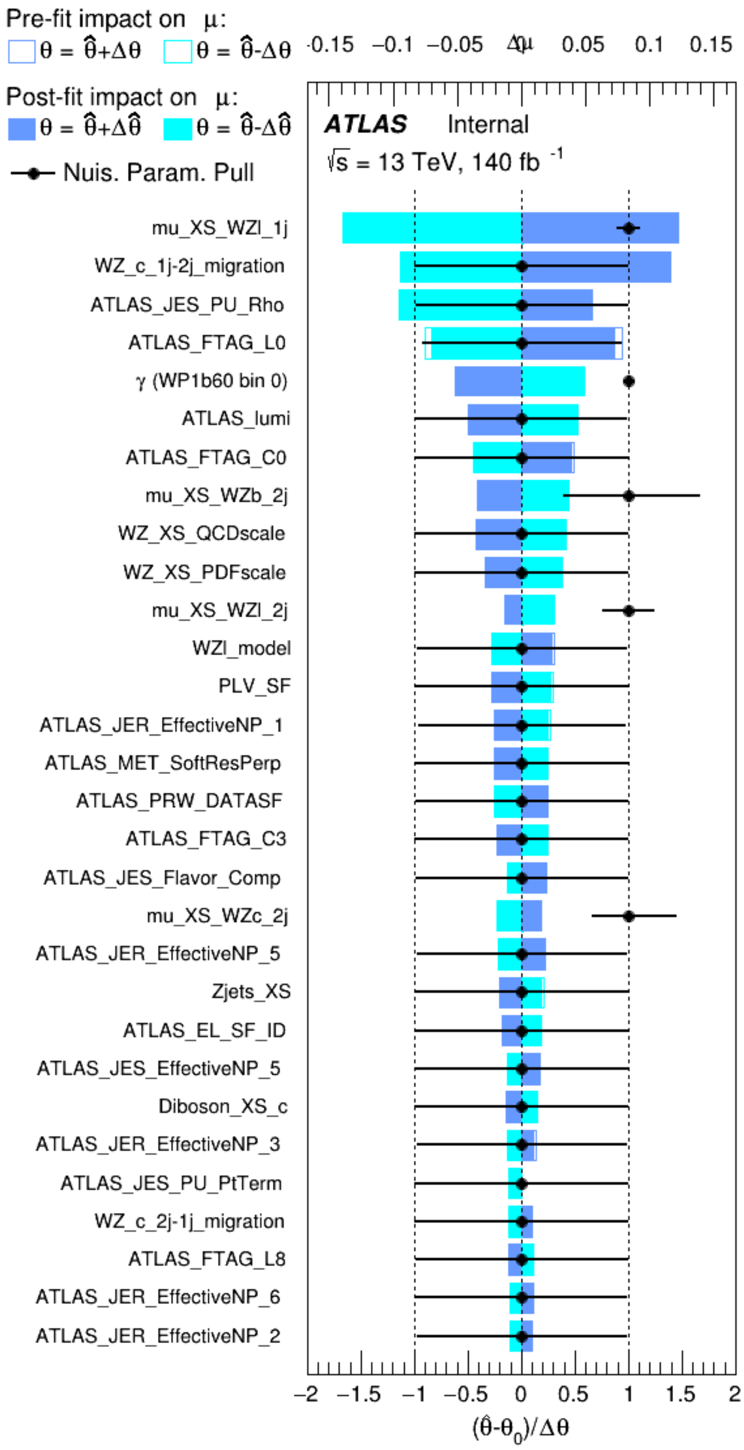

Figure 39: Impact of systematic uncertainties on the signal-strength of WZ + b for events with exactly one jet

Here γ represents the impact of the statistical uncertainty of the MC prediction in that particular bin. The large impact of the Jet Energy Scale and Jet Flavor Tagging is unsurprising, as the definition of the fit regions depends heavily on the modeling of the jets. The other major sources of uncertainty come from background modelling and cross-section uncertainty.

Pre-fit yields in each of the 2-jet fit are shown in Table 19.

	2j, <85% WP	2j, 77%-85% WP	2j, 70%-77% WP	2j, 60%-70% WP	2j, 60% WP	tZ CR 2j
$WZ + b - 2j$	3.1 ± 1.6	6.7 ± 0.5	5.6 ± 0.4	8.0 ± 0.6	24 ± 2	5 ± 1
$WZ + c - 2j$	180 ± 20	54 ± 6	41 ± 3	24 ± 3	17 ± 2	7.0 ± 0.6
$WZ + l - 2j$	1250 ± 150	90 ± 14	18 ± 3	5.8 ± 1.4	1.4 ± 0.4	0.25 ± 0.15
$WZ + b - 1j$	3.4 ± 0.6	1.52 ± 0.35	1.58 ± 0.23	1.95 ± 0.39	7.8 ± 1.1	0.8 ± 0.6
$WZ + c - 1j$	56 ± 14	17.6 ± 4.0	8.6 ± 2.2	6.3 ± 1.8	3.0 ± 0.9	0.7 ± 0.2
$WZ + l - 1j$	427 ± 120	24 ± 7	4.7 ± 2.3	1.6 ± 0.7	0.3 ± 0.2	0.01 ± 0.01
$WZ - \mathrm{Other}$	129 ± 29	6.1 ± 4.6	1.2 ± 0.3	0.3 ± 0.2	2.9 ± 0.5	3.6 ± 0.6
Other VV	7.63 ± 0.63	0.6 ± 0.5	0.16 ± 0.03	0.01 ± 0.01	0.1 ± 0.1	0.1 ± 0.1
ZZ	135 ± 20	14.1 ± 3.2	4.7 ± 0.8	4.0 ± 0.6	4.1 ± 0.7	3.1 ± 0.5
$t\bar{t}W$	0.8 ± 0.2	0.4 ± 0.1	0.5 ± 0.1	0.7 ± 0.2	4.3 ± 0.6	3.9 ± 0.6
$t\bar{t}Z$	14.7 ± 2.2	5.6 ± 0.8	4.5 ± 0.7	6.5 ± 1.1	25.4 ± 4.0	21.9 ± 3.4
rare Top	0.14 ± 0.04	0.07 ± 0.03	0.03 ± 0.02	0.09 ± 0.03	0.37 ± 0.07	0.6 ± 0.1
$t\bar{t}WW$	0.04 ± 0.03	0.02 ± 0.02	0.01 ± 0.01	0.01 ± 0.00	0.03 ± 0.03	0.01 ± 0.01
$Z +$ jets	110.0 ± 22.9	9.6 ± 2.0	2.1 ± 0.50	1.6 ± 0.4	5.1 ± 1.1	1.5 ± 0.3
$W +$ jets	0.0 ± 0.0	0.0 ± 0.0	0.0 ± 0.0	0.0 ± 0.0	0.0 ± 0.0	0.0 ± 0.0
$V + \gamma$	25 ± 18	0.5 ± 0.2	0.1 ± 0.1	0.1 ± 0.1	0.0 ± 0.02	0.05 ± 0.07
tZ	21.9 ± 2.9	9.6 ± 1.3	9.1 ± 1.0	10.0 ± 1.5	14.7 ± 3.2	60 ± 6
tW	0.9 ± 0.7	0.2 ± 0.3	0.0 ± 0.1	0.0 ± 0.0	0.8 ± 0.6	0.2 ± 0.2
WtZ	4.9 ± 2.5	1.5 ± 0.8	1.1 ± 0.6	1.3 ± 0.7	4.6 ± 2.4	3.3 ± 1.7
VVV	7.4 ± 0.3	1.0 ± 0.1	0.4 ± 0.1	0.2 ± 0.1	0.13 ± 0.03	0.04 ± 0.01
VH	19.5 ± 4.2	2.8 ± 1.6	0.7 ± 0.7	0.1 ± 0.2	0.0 ± 0.0	0.0 ± 0.0
$t\bar{t}$	0.7 ± 0.4	0.1 ± 0.1	0.05 ± 0.06	0.15 ± 0.13	0.8 ± 0.5	2.3 ± 1.2
$t\bar{t}$	6.8 ± 1.0	2.4 ± 0.5	1.8 ± 0.4	3.3 ± 0.6	8.4 ± 1.2	13.6 ± 1.7
$t\bar{t}H$	0.4 ± 0.1	0.2 ± 0.1	0.16 ± 0.02	0.23 ± 0.03	0.94 ± 0.11	1.03 ± 0.12
Total	2580 ± 160	229 ± 24	89 ± 13	69 ± 11	120 ± 15	108 ± 11

Table 19: Pre-fit yields in each of the 2-jet regions.

The post-fit yields in each region are summarized in Table 20.

	2j, <85% WP	2j, 77%-85% WP	2j, 70%-77% WP	2j, 60%-70% WP	2j, 60% WP	tZ CR 2j
$WZ + b$	13 ± 6	6.7 ± 2.9	5.8 ± 2.5	8.0 ± 3.5	31 ± 13	14 ± 5
$WZ + c$	260 ± 60	77 ± 15	41 ± 8	26 ± 5	10.9 ± 2.4	4.8 ± 1.1
$WZ + l$	1860 ± 90	90 ± 12	17.6 ± 2.8	5.8 ± 1.3	1.4 ± 0.4	0.3 ± 0.2
$WZ + b - 1j$	3.4 ± 0.6	1.52 ± 0.35	1.58 ± 0.23	1.95 ± 0.39	6.7 ± 1.1	1.9 ± 0.6
$WZ + c - 1j$	56 ± 14	17.6 ± 4.0	8.6 ± 2.2	6.3 ± 1.8	3.0 ± 0.9	0.7 ± 0.2
$WZ + l - 1j$	427 ± 120	24 ± 7	4.7 ± 2.3	1.6 ± 0.7	0.3 ± 0.2	0.01 ± 0.01
$WZ - \mathrm{Other}$	129 ± 29	6.1 ± 4.6	1.2 ± 0.3	0.3 ± 0.2	2.9 ± 0.5	3.6 ± 0.6
Other VV	7.6 ± 0.6	0.3 ± 0.3	0.3 ± 0.1	0.1 ± 0.06	0.03 ± 0.02	0.1 ± 0.1
ZZ	145 ± 30	11.3 ± 4.4	2.7 ± 1.6	1.0 ± 0.3	4.0 ± 0.1	2.4 ± 0.1
$t\bar{t}W$	0.8 ± 0.2	0.4 ± 0.1	0.54 ± 0.12	0.74 ± 0.15	4.3 ± 0.6	3.9 ± 0.6
$t\bar{t}Z$	14.7 ± 2.2	5.6 ± 0.8	4.5 ± 0.7	6.5 ± 1.0	25.4 ± 3.9	21.9 ± 3.3
rare Top	0.14 ± 0.04	0.07 ± 0.03	0.03 ± 0.02	0.09 ± 0.03	0.4 ± 0.1	0.6 ± 0.1
$t\bar{t}WW$	0.04 ± 0.03	0.02 ± 0.02	0.01 ± 0.01	0.01 ± 0.01	0.03 ± 0.03	0.01 ± 0.01
$Z + \mathrm{jets}$	110 ± 23	9.6 ± 2.0	2.1 ± 0.5	1.6 ± 0.4	5.1 ± 1.1	1.5 ± 0.3
$W + \mathrm{jets}$	0.0 ± 0.0	0.0 ± 0.0	0.0 ± 0.0	0.0 ± 0.0	0.0 ± 0.0	0.0 ± 0.0
$V + \gamma$	25 ± 19	0.5 ± 0.2	0.1 ± 0.1	0.13 ± 0.14	0.0 ± 0.02	0.05 ± 0.07
tZ	21.9 ± 2.7	9.6 ± 1.2	7.1 ± 0.9	10.0 ± 1.4	14.7 ± 3.0	60 ± 6
tW	0.1 ± 0.7	0.2 ± 0.3	0.0 ± 0.1	0.0 ± 0.0	0.8 ± 0.6	0.2 ± 0.2
WtZ	4.9 ± 2.5	1.5 ± 0.8	1.1 ± 0.6	1.3 ± 0.7	4.6 ± 2.3	3.3 ± 1.7
VVV	7.4 ± 0.3	1.0 ± 0.1	0.36 ± 0.03	0.19 ± 0.03	0.13 ± 0.03	0.04 ± 0.01
VH	19 ± 4	2.8 ± 1.6	0.7 ± 0.7	0.1 ± 0.2	0.0 ± 0.0	0.0 ± 0.0
$t\bar{t}$	6.8 ± 1.0	2.4 ± 0.5	1.8 ± 0.4	3.3 ± 0.6	8.4 ± 1.2	13.6 ± 1.7
$t\bar{t}H$	0.40 ± 0.05	0.19 ± 0.03	0.16 ± 0.02	0.23 ± 0.03	0.94 ± 0.11	1.03 ± 0.11
Total	2580 ± 60	229 ± 11	89 ± 6	69.1 ± 4.1	120 ± 10	108 ± 6

Table 20: Post-fit yields in each of the 2-jet regions.

The same set of systematic uncertainties consider for the 1-jet fit are included in the 2-jet fit as well. The impact of the most significant systematic uncertainties is summarized in Table 21.

Uncertainty Source	$\Delta\mu$	
WZ + c 2-jet cross-section	-0.13	0.16
WZ + l 2-jet cross-section	0.12	-0.09
ttZ cross-section - QCD scale	-0.10	0.13
WZ + b 1-jet cross-section	-0.11	0.10
Jet Energy Scale	-0.11	0.11
Luminosity	-0.11	0.12
tZ cross-section	-0.11	0.11
WtZ cross-section	-0.07	0.07
Flavor tagging	0.05	0.05
Other VV + b cross-section	-0.05	0.05
Total	0.35	0.37

Table 21: Summary of the most significant sources of systematic uncertainty on the measurement of $WZ + b$ 2-jet events.

Uncertainty Source	$\Delta\sigma/\sigma_{nominal}$	
WZ + c 1j/2j migration	-0.17	0.25
Flavor Tagging	0.14	0.13
WZ + b, 1-jet cross-section	-0.09	0.09
Jet Energy Scale	0.06	0.08
Jet Energy Resolution	0.05	0.05
WZ >=3j/2j migration	-0.04	0.04
WZ + c 2j/1j migration	-0.04	0.04
WZ cross-section - QCD scale	-0.04	0.04
WZ + light modelling	0.04	-0.03
Luminosity	-0.03	0.03
total	0.2694	0.3274

Table 22: Summary of the most significant sources of systematic uncertainty on the measurement of WZ + c with 2 associated jets.

The ranking and impact of those nuisance parameters with the largest contribution to the overall uncertainty is shown in Figure 40.

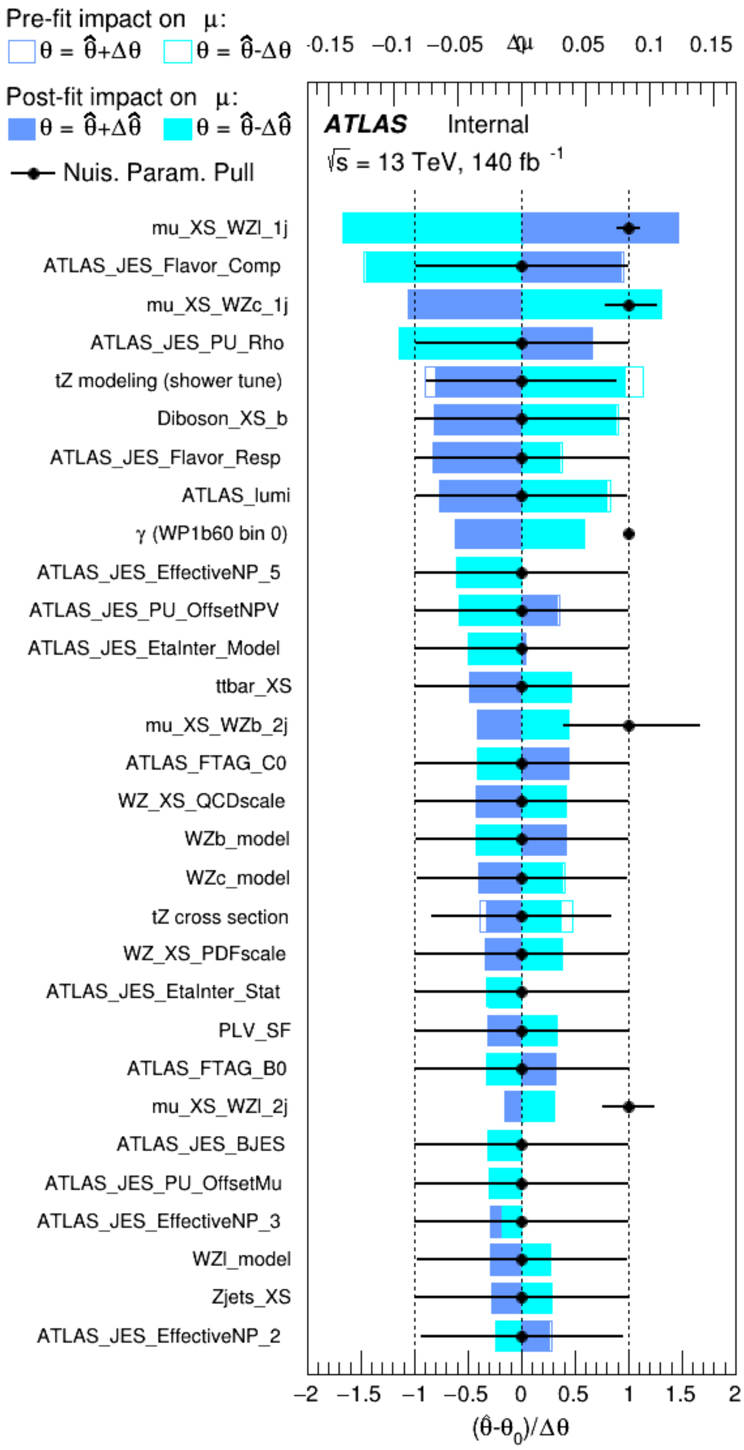

Figure 40: Impact of systematic uncertainties on the signal-strength of WZ + b in 2-jet events.

The large impact of the Jet Energy Scale and Jet Flavor Tagging is unsurprising, as the shape of the fit regions depends heavily on the modeling of the jets. The other major sources of uncertainty come from background modelling and cross-section uncertainty.

8.3 Inclusive 1+2 Jet Fit

An alternative fit is performed which combines the WZ + 1-jet and WZ + 2-jet samples rather than fitting them independently. This is done primarily as a cross-check of the nominal analysis, to see if measuring 1-jet and 2-jet events separately and combining them gives drastically different results than measuring them together.

For this study, three signal templates, WZ + b, WZ + charm and WZ + light, are fit to data, and the systematics accounting for migrations between 1-jet and 2-jet bins are removed. All other background and nuiscance parameters remain the same as the nominal fit.

The measured μ value for WZ + b is $\mu = 1.00^{+0.30}_{-0.29}(stat)^{+0.25}_{-23}(sys)$, with a significance of 2.8σ, and the uncertainty on WZ + charm is $\mu = 1.00 \pm 0.12(stat) \pm 0.13(sys)$. This is compared to combined uncertainty of $\mu = 1.00^{+0.32}_{-0.30}(stat)^{+0.24}_{-23}(sys)$ for WZ + b when 1-jet and 2-jet events are measured separately and then combined.

A post-fit summary plot of the fit regions is shown in Figure 41:

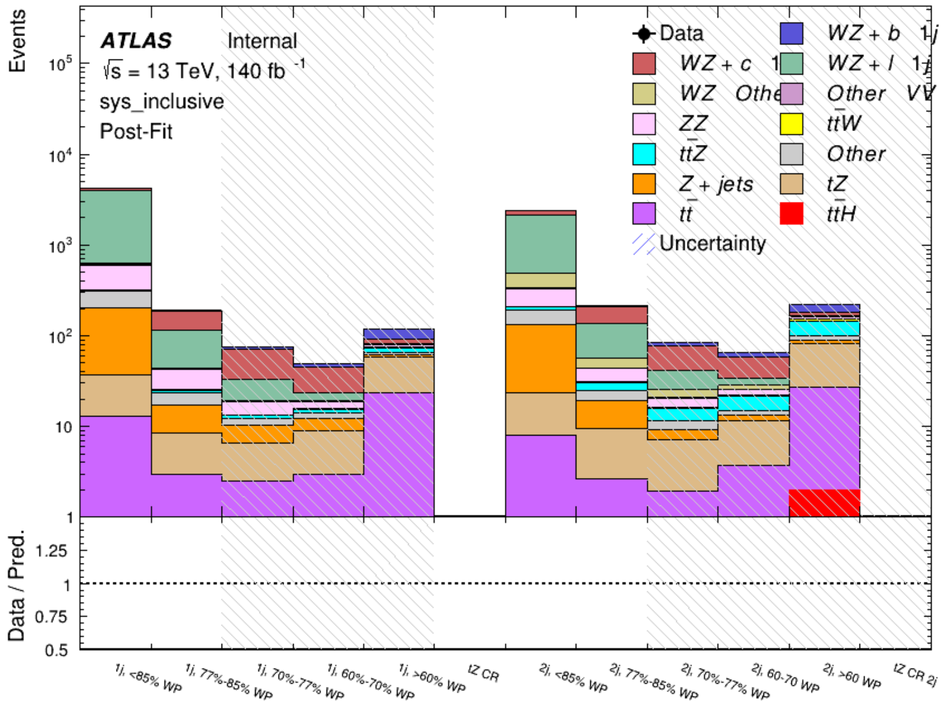

Figure 41: Post-fit summary of the 1-jet fit regions.

666 The impact of the most significant sources of systematic uncertainties on the measurement of
667 WZ+b is summarized in Table 23.

Uncertainty Source	$\Delta\mu$	
WZ + light cross-section	0.13	-0.12
WZ + charm cross-section	-0.10	0.12
Jet Energy Scale	0.08	0.13
tZ cross-section	-0.10	0.10
Jet Energy Resolution	-0.10	0.10
Luminosity	-0.08	0.09
Other Diboson + b cross-section	-0.07	0.07
Flavor tagging	0.05	0.05
$t\bar{t}$ cross-section	-0.05	0.05
WZ cross-section - QCD scale	-0.04	0.03
Total Systematic Uncertainty	0.28	0.32

Table 23: Summary of the most significant sources of systematic uncertainty on the measurement of $WZ + b$ with one or two associated jets.

The ranking and impact of those nuisance parameters with the largest contribution to the overall uncertainty is shown in Figure 42.

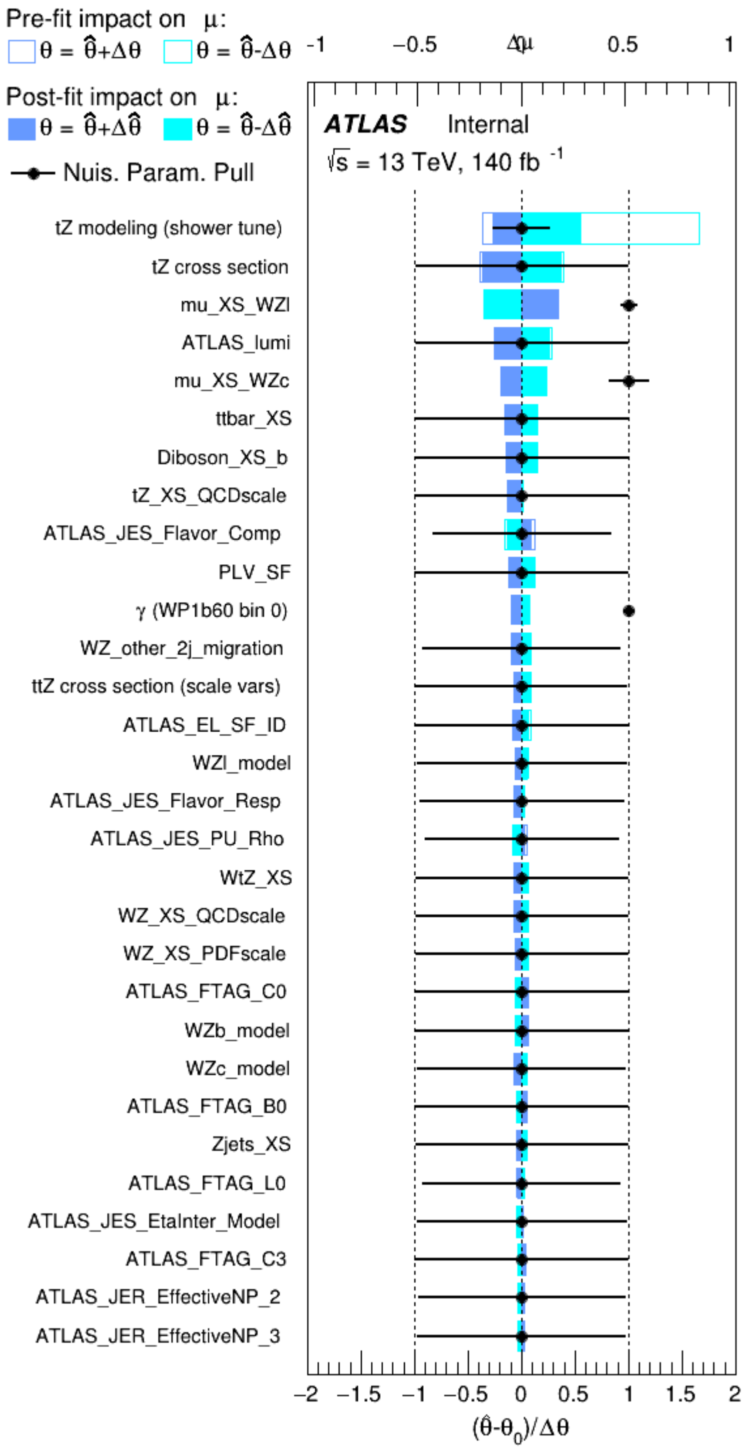

Figure 42: Impact of systematic uncertainties on the signal-strength of $WZ + \mathrm{b}$ for events with one or two jets

8.4 Alternate tZ Inclusive Fit

8.4.1 tZ Inclusive Fit

While tZ is often considered as a distinct process form WZ + b, this could also be considered part of the signal. Alternate studies are performed where, using the same framework as the nominal analysis, a measurement of WZ + b is performed that includes tZ as part of WZ+b.

Because of this change, the tZ CR is no longer necessary, and only the five pseudo-continuous b-tag regions are used in the fit. Further, systematics related to the tZ cross-section are removed from the fit, as they are now encompassed by the normalization measurement of WZ + b. All other systematic uncertainties are carried over from the nominal analysis.

An expected WZ + b cross-section of $4.1^{+0.78}_{-0.74}(stat)^{+0.53}_{-0.52}(sys)$ fb is extracted from the fit, with an expected significance of 4.0σ.

The impact of the predominate systematics are summarized in Table 24.

Uncertainty Source	$\Delta\mu$	
WZ + light cross-section	0.08	-0.08
Jet Energy Scale	-0.06	0.08
Luminosity	-0.05	0.06
WZ + charm cross-section	-0.04	0.05
Other Diboson + b cross-section	-0.04	0.04
WZ cross-section - QCD scale	-0.04	0.03
$t\bar{t}$ cross-section	-0.03	0.03
Jet Energy Resolution	-0.03	0.03
Flavor tagging	-0.03	0.03
Z+jets cross section	-0.02	0.02
Total Systematic Uncertainty	-0.15	0.16

Table 24: Summary of the most significant sources of systematic uncertainty on the measurement of $WZ + b$ with exactly one associated jet.

8.4.2 Floating tZ

In order to quantify the impact of the tZ uncertainty on the fit, an alternative fit strategy is used where the tZ normalization is allowed to float. This normalization factor replaces the cross-section uncertainty on tZ, and all other parameters of the fit remain the same.

An uncertainty of 17% on the normalization of tZ is extracted from the fit, compared to a theory uncertainty of 15% applied to the tZ cross-section. The measured uncertainties on WZ remain the same.

9 Conclusion

A measurement of WZ + heavy flavor is performed using 140 fb^{-1} of $\sqrt{s} = 13$ TeV proton-proton collision data collected by the ATLAS detector at the LHC. The expected cross-section of WZ+b with 1-jet is $1.74^{+0.82}_{-0.75}(\mathrm{stat})^{+0.53}_{-0.48}(\mathrm{sys})$ fb, and $14.6 \pm 2.5(\mathrm{stat}) \pm 2.3(\mathrm{sys})$ fb for WZ + charm, with a correlation of -0.22 between them. An expected significance of 2.0 is observed for WZ + b in this region.

For the 2-jet regions, an expected significance of 1.7 is observed for WZ + b, with an expected cross-section of $2.5^{+1.3}_{-1.3}(\mathrm{stat})^{+0.95}_{-0.83}(\mathrm{sys})$ fb. For WZ + charm, a cross-section of $12.7 \pm 3.2(\mathrm{stat}) \pm 2.7(\mathrm{sys})$ fb is expected for 2-jet events. A correlation of -0.26 is observed for WZ+b and WZ + charm.

This section will be include final results once unblinded.

References

[1] ATLAS Collaboration. 'Observation of electroweak $W^{\pm}Z$ boson pair production in association with two jets in pp collisions at $\sqrt{s} = 13$ TeV with the ATLAS detector'. In: *Phys. Lett.* B793 (2019), pp. 469–492. DOI: 10.1016/j.physletb.2019.05.012. arXiv: 1812.09740 [hep-ex].

[2] ATLAS Collaboration. 'Luminosity determination in pp collisions at $\sqrt{s} = 7$ TeV using the ATLAS detector at the LHC'. In: *Eur. Phys. J. C* 71 (2011), p. 1630. DOI: 10.1140/epjc/s10052-011-1630-5. arXiv: 1101.2185 [hep-ex].

[3] ATLAS Collaboration. 'Performance of the ATLAS detector using first collision data'. In: *JHEP* 09 (2010), p. 056. DOI: 10.1007/JHEP09(2010)056. arXiv: 1005.5254 [hep-ex].

[4] S. Agostinelli et al. 'GEANT4: A Simulation toolkit'. In: *Nucl. Instrum. Meth.* A506 (2003), pp. 250–303. DOI: 10.1016/S0168-9002(03)01368-8.

[5] T. Gleisberg et al. 'Event generation with SHERPA 1.1'. In: *JHEP* 02 (2009), p. 007. DOI: 10.1088/1126-6708/2009/02/007. arXiv: 0811.4622 [hep-ph].

[6] R. D. Ball et al. 'Parton distributions for the LHC Run II'. In: *JHEP* 04 (2015), p. 040. DOI: 10.1007/JHEP04(2015)040. arXiv: 1410.8849 [hep-ph].

[7] H.-L. Lai et al. 'New parton distributions for collider physics'. In: *Phys. Rev. D* 82 (2010), p. 074024. DOI: 10.1103/PhysRevD.82.074024. arXiv: 1007.2241 [hep-ph].

[8] J. Alwall et al. 'The automated computation of tree-level and next-to-leading order differential cross sections, and their matching to parton shower simulations'. In: *JHEP* 07 (2014), p. 079. DOI: 10.1007/JHEP07(2014)079. arXiv: 1405.0301 [hep-ph].

[9] M. Bahr et al. 'Herwig++ Physics and Manual'. In: *Eur. Phys. J. C* 58 (2008), p. 639. DOI: 10.1140/epjc/s10052-008-0798-9. arXiv: 0803.0883 [hep-ph].

[10] R. D. Ball et al. 'Parton distributions with LHC data'. In: *Nucl. Phys. B* 867 (2013), p. 244. DOI: 10.1016/j.nuclphysb.2012.10.003. arXiv: 1207.1303 [hep-ph].

[11] S. Frixione, G. Ridolfi and P. Nason. 'A positive-weight next-to-leading-order Monte Carlo for heavy flavour hadroproduction'. In: *JHEP* 09 (2007), p. 126. DOI: 10.1088/1126-6708/2007/09/126. arXiv: 0707.3088 [hep-ph].

[12] E. Re. 'Single-top Wt-channel production matched with parton showers using the POWHEG method'. In: *Eur. Phys. J. C* 71 (2011), p. 1547. DOI: 10.1140/epjc/s10052-011-1547-z. arXiv: 1009.2450 [hep-ph].

[13] ATLAS Collaboration. *Electron efficiency measurements with the ATLAS detector using the 2015 LHC proton–proton collision data*. ATLAS-CONF-2016-024. 2016. URL: https://cds.cern.ch/record/2157687.

[14] ATLAS Collaboration. 'Measurement of the muon reconstruction performance of the ATLAS detector using 2011 and 2012 LHC proton–proton collision data'. In: *Eur. Phys. J. C* 74 (2014), p. 3130. DOI: 10.1140/epjc/s10052-014-3130-x. arXiv: 1407.3935 [hep-ex].

[15] R. Narayan et al. *Measurement of the total and differential cross sections of a top-quark-antiquark pair in association with a W boson in proton-proton collisions at a centre-of-mass energy of 13 TeV with ATLAS detector at the Large Hadron Collider*. Tech. rep. ATL-COM-PHYS-2020-217. Geneva: CERN, Mar. 2020. URL: https://cds.cern.ch/record/2712986.

[16] ATLAS Collaboration. *Jet Calibration and Systematic Uncertainties for Jets Reconstructed in the ATLAS Detector at $\sqrt{s} = 13$ TeV*. ATL-PHYS-PUB-2015-015. 2015. URL: https://cds.cern.ch/record/2037613.

[17] ATLAS Collaboration. *Selection of jets produced in* 13 *TeV proton–proton collisions with the ATLAS detector*. ATLAS-CONF-2015-029. 2015. URL: https://cds.cern.ch/record/2037702.

[18] ATLAS Collaboration. 'Performance of pile-up mitigation techniques for jets in pp collisions at $\sqrt{s} = 8$ TeV using the ATLAS detector'. In: *Eur. Phys. J. C* 76 (2016), p. 581. DOI: 10.1140/epjc/s10052-016-4395-z. arXiv: 1510.03823 [hep-ex].

[19] ATLAS Collaboration. 'Performance of b -jet identification in the ATLAS experiment'. In: *Journal of Instrumentation* 11.04 (2016), P04008. URL: http://stacks.iop.org/1748-0221/11/i=04/a=P04008.

[20] ATLAS Collaboration. 'Performance of missing transverse momentum reconstruction with the ATLAS detector using proton–proton collisions at $\sqrt{s} = 13$ TeV'. In: *The European Physical Journal C* 78.11 (Nov. 2018). ISSN: 1434-6052. DOI: 10.1140/epjc/s10052-018-6288-9. URL: http://dx.doi.org/10.1140/epjc/s10052-018-6288-9.

[21] ATLAS Collaboration. 'Measurement of the fiducial and differential cross-section of a top quark pair in association with a Z boson at 13 TeV with the ATLAS detector'. In: ATL-COM-PHYS-2019-334 (Apr. 2019). URL: https://cds.cern.ch/record/2672207.

[22] T. Chen and C. Guestrin. 'XGBoost: A Scalable Tree Boosting System'. In: *Proceedings of the 22nd ACM SIGKDD International Conference on Knowledge Discovery and Data Mining*. KDD '16. San Francisco, California, USA: ACM, 2016, pp. 785–794. ISBN: 978-1-4503-4232-2. DOI: 10.1145/2939672.2939785. URL: http://doi.acm.org/10.1145/2939672.2939785.

[23] R. Frederix et al. 'The automation of next-to-leading order electroweak calculations'. In: *Journal of High Energy Physics* 2018.7 (July 2018). ISSN: 1029-8479. DOI: 10.1007/jhep07(2018)185. URL: http://dx.doi.org/10.1007/JHEP07(2018)185.

[24] 2021. URL: https://twiki.cern.ch/twiki/bin/view/AtlasProtected/BTagCalibrationRecommendationsRelease21#Tools_for_Flavor_Tagging_Calibra.

[25] 'Luminosity determination in pp collisions at $\sqrt{s} = 13$ TeV using the ATLAS detector at the LHC'. In: (June 2019).

[26] ATLAS Collaboration. 'The new LUCID-2 detector for luminosity measurement and monitoring in ATLAS'. In: *JINST* 13.07 (2018), P07017. DOI: 10.1088/1748-0221/13/07/P07017.

[27] A. Collaboration. 'Electron reconstruction and identification in the ATLAS experiment using the 2015 and 2016 LHC proton–proton collision data at $\sqrt{s} = 13$ TeV'. In: *The European Physical Journal C* 79.8 (Aug. 2019). ISSN: 1434-6052. DOI: 10.1140/epjc/s10052-019-7140-6. URL: http://dx.doi.org/10.1140/epjc/s10052-019-7140-6.

[28] ATLAS Collaboration. 'Jet energy scale measurements and their systematic uncertainties in proton–proton collisions at $\sqrt{s} = 13$ TeV with the ATLAS detector'. In: *Phys. Rev. D* 96 (2017), p. 072002. DOI: 10.1103/PhysRevD.96.072002. arXiv: 1703.09665 [hep-ex].

[29] ATLAS Collaboration. 'Observation of the associated production of a top quark and a Z boson in pp collisions at $\sqrt{s}$= 13 TeV with the ATLAS detector'. In: *Journal of High Energy Physics* 2020.7 (July 2020). ISSN: 1029-8479. DOI: 10.1007/jhep07(2020)124. URL: http://dx.doi.org/10.1007/JHEP07(2020)124.

A Appendices

A.1 Non-prompt lepton MVA

A lepton MVA has been developed to better reject non-prompt leptons than standard cut based selections based upon impact parameter, isolation and PID. The name of this MVA is `PromptLeptonVeto`. The full set of studies and detailed explanation can be found in [15].

The decays of W and Z bosons are commonly selected by the identification of one or two electrons or muons. The negligible lifetimes of these bosons mean that the leptons produced in the decay originate from the interaction vertex and are thus labelled “prompt”. Analyses using these light leptons impose strict reconstruction quality, isolation and impact parameter requirements to remove “fake” leptons. A significant source of the fake light leptons are non-prompt leptons produced in decays of hadrons that contain bottom (b) or charm (c) quarks. Such hadrons typically have microscopically significant lifetimes that can be detected experimentally.

These non-prompt leptons can also pass the tight selection criteria. In analyses that involve top (t) quarks, which decay almost exclusively into a W boson and a b quark, non-prompt leptons from the semileptonic decay of bottom and charm hadrons can be a significant source of background events. This is particularly the case in the selection of same-sign dilepton and multilepton final states.

The main idea is to identify non-prompt light leptons using lifetime information associated with a track jet that matches the selected light lepton. This lifetime information is computed using tracks contained within the jet. Typically, lepton lifetime is determined using the impact parameter of the track reconstructed by the inner tracking detector which is matched to the reconstructed lepton. Using additional reconstructed charged particle tracks increases the precision of identifying the displaced decay vertex of bottom or charm hadrons that produced a non-prompt light lepton. The MVA also includes information related to the isolation of the lepton to reject non-prompt leptons.

`PromptLeptonVeto` is a gradient boosted BDT. The training of the BDT is performed on leptons selected from the POWHEG+PYTHIA6 non-allhad $t\bar{t}$ MC sample. Eight variables are used to train the BDT in order to discriminate between prompt and non-prompt leptons. The track jets that are matched to the non-prompt leptons correspond to jets initiated by b or c quarks, and may contain a displaced vertex. Consequently, three of the selected variables are used to identify b-tag jets by standard ATLAS flavour tagging algorithms. Two variables use the relationship between the track jet and lepton: the ratio of the lepton p_T with respect to the track jet p_T and ΔR between the lepton and the track jet axis. Finally three additional variables test whether the reconstructed lepton is isolated: the number of tracks collected by the track jet and the lepton track and calorimeter isolation variables. Table 25 describes the variables used to train the BDT algorithm. The choice of input variables has been extensively discussed with Egamma, Muon, Tracking, and Flavour Tagging CP groups.

The output distribution of the BDT is shown in Figure A.1.

Variable	Description
N_{track} in track jet	Number of tracks collected by the track jet
IP2 $\log(P_b/P_{light})$	Log-likelihood ratio between the b and light jet hypotheses with the IP2D algorithm
IP3 $\log(P_b/P_{light})$	Log-likelihood ratio between the b and light jet hypotheses with the IP3D algorithm
$N_{TrkAtVtx}$ SV + JF	Number of tracks used in the secondary vertex found by the SV1 algorithm in addition to the number of tracks from secondary vertices found by the JetFitter algorithm with at least two tracks
$p_T^{lepton}/p_T^{track\ jet}$	The ratio of the lepton p_T and the track jet p_T
ΔR(lepton, track jet)	ΔR between the lepton and the track jet axis
p_TVarCone30$/p_T$	Lepton track isolation, with track collecting radius of $\Delta R < 0.3$
E_TTopoCone30$/p_T$	Lepton calorimeter isolation, with topological cluster collecting radius of $\Delta R < 0.3$

Table 25: A table of the variables used in the training of `PromptLeptonVeto`.

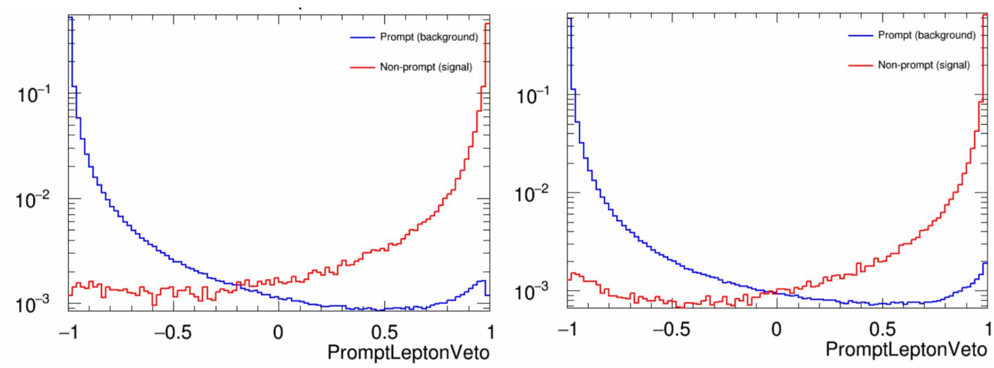

(a) (b)

Figure 43: Distribution of the PLV BDT discriminant for (a) electrons and (b) muons.

The ROC curve for the BDT response, compared to the standard `FixedCutTight` WP, is shown in figure A.1, which shows a clear improvement when using this alternative training.

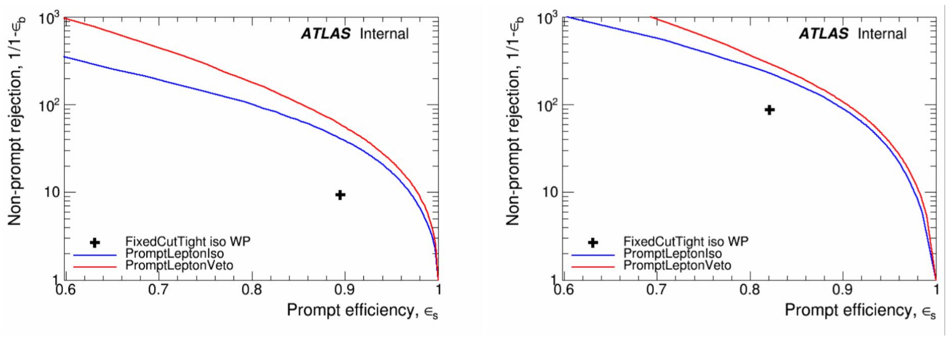

Figure 44: ROC curves for the PLV as well as the peformance of the standard FixedCutTight WP for (left) electrons and (right) muons. Plot also includes curves for PromptLeptonIso, which is not considered in this analysis.

A cutoff value of -0.7 for electrons and -0.5 for muons are chosen as the WPs for this MVA, based on an optimisation of $S/\sqrt{B}$ performed in the preselection regions of the $t\bar{t}H - ML$ analysis, which have a signiture similar to that of this analysis.

The efficiency of the tight `PromptLeptonVeto` working point is measured using the tag and probe method with $Z \rightarrow \ell^+\ell^-$ events. Such calibration are performed by analysers from this analysis in communication with the Egamma and Muon combined performance groups. The scale factor are approximately 0.92 for $10 < p_T < 15$ GeV, and averaging at 0.98 to 0.99 for higher p_T leptons. An extra systematic is applied to muons within $\Delta R < 0.6$ of a calorimeter jet, since there is a strong dependence on the scale factor due to the presence of these jets. For electrons, the dominant systematics is coming from pile-up dependence. Overall the systematics are a maximum of 3% at low p_T and decreasing at a function of p_T.

A.2 Non-prompt CR Modelling

In order to further validate the modeling in each of the non-prompt CRs, additional kinematic plots are made in the Z+jets CR and $t\bar{t}$ CR in each of the continuous b-tag regions, after the correction factors detailed in Section 6.3 have been applied.

In the case of the Z+jets CR, the p_T spectrum of the lepton originating from the W candidate is shown, as this is the distribution used to extract the scale factor applied to Z+jets. These plots are shown in Figures 45 and 46.

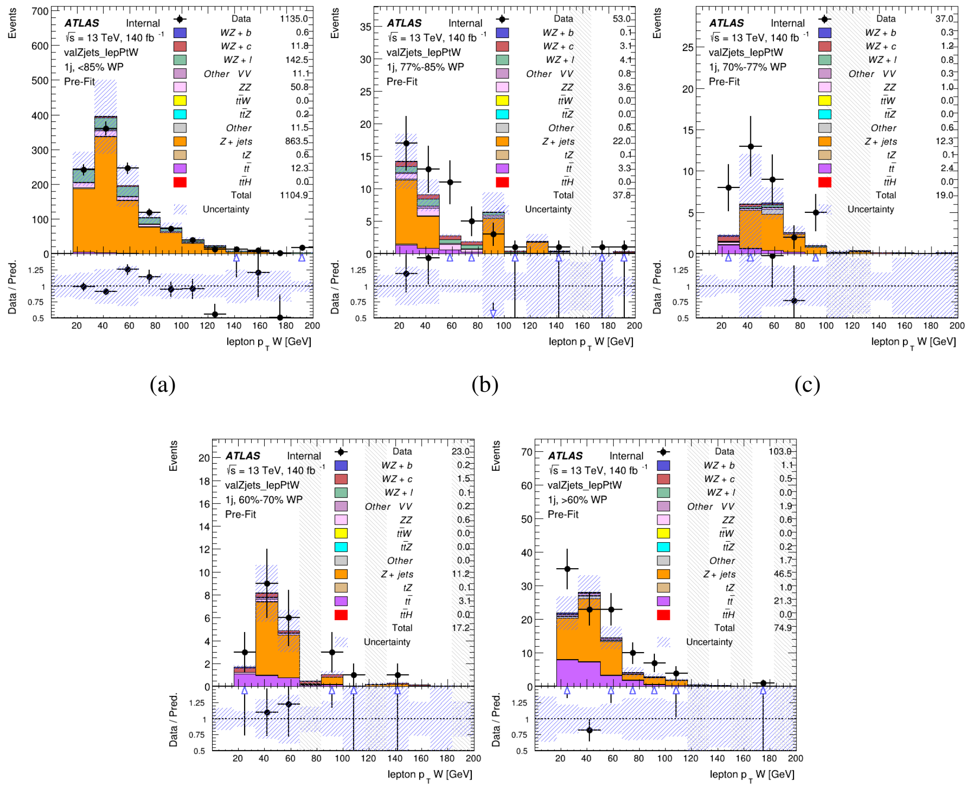

(a) (b) (c)

(d) (e)

Figure 45: Comparisons between the data and MC distributions of the p_T of the lepton originating from the W-candidate in the Z+jets CR for each of the 1-jet b-tag working point regions

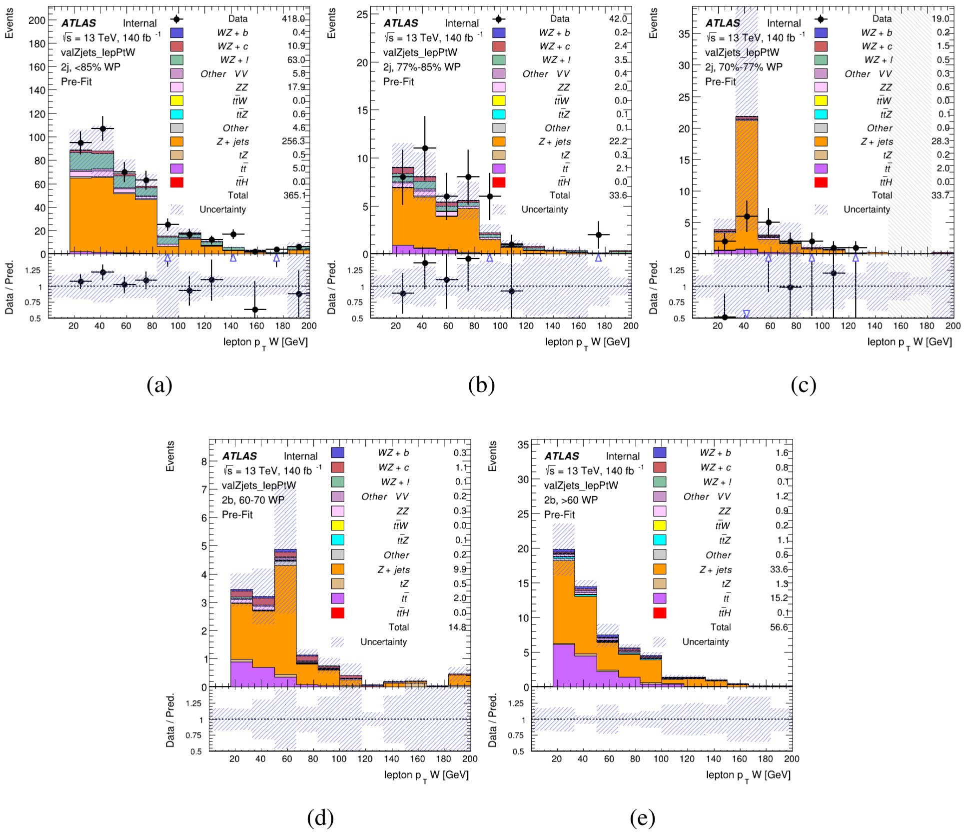

Figure 46: Comparisons between the data and MC distributions of the p_T of the lepton originating from the W-candidate in the Z+jets CR for each of the 2-jet b-tag working point regions

The same is shown for the $t\bar{t}$ CR, but the p_T of the OS lepton is used instead as a representation of the modeling, as the lepton from the W is not well defined for $t\bar{t}$ events. These plots are shown in Figures 47 and 48.

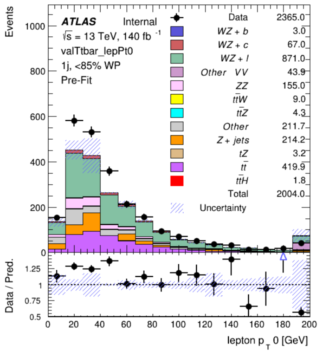

(a)

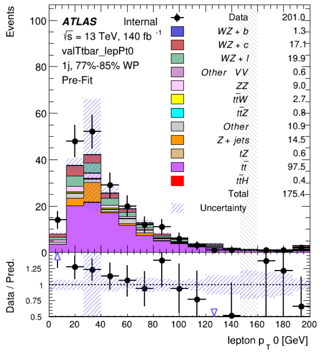

(b)

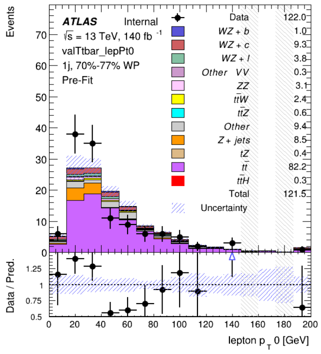

(c)

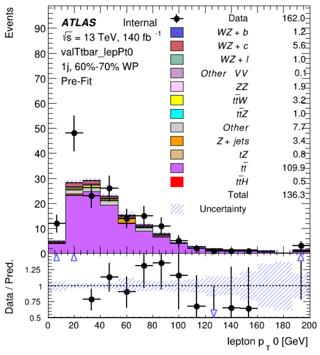

(d)

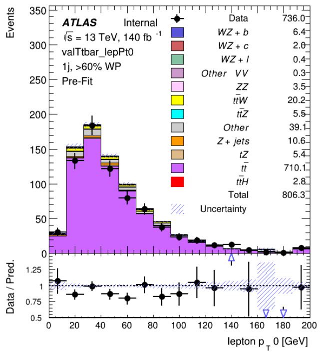

(e)

Figure 47: Comparisons between the data and MC distributions of the p_T of the OS lepton in the $t\bar{t}$ CR for each of the 1-jet b-tag working point regions

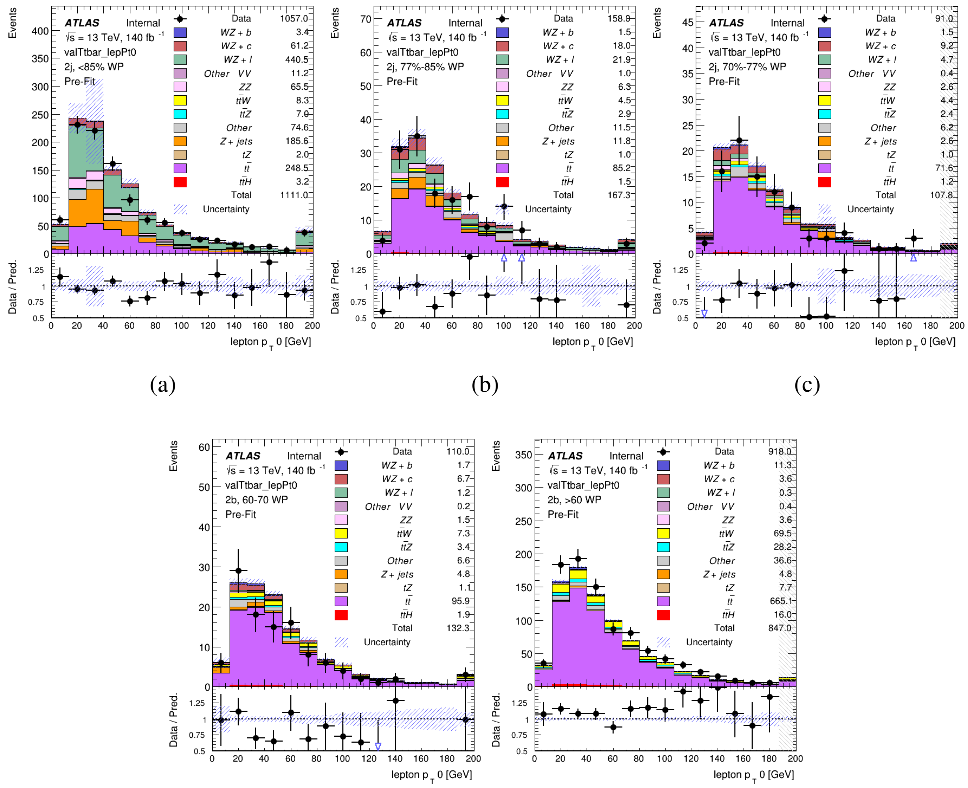

(a) (b) (c)

(d) (e)

Figure 48: Comparisons between the data and MC distributions of the p_T of the OS lepton in the $t\bar{t}$ CR for each of the 2-jet b-tag working point regions

854 A.3 DSID list

Data:
data15_13TeV.AllYear.physics_Main.PhysCont.DAOD_HIGG8D1.grp15_v01_p4134
data16_13TeV.AllYear.physics_Main.PhysCont.DAOD_HIGG8D1.grp16_v01_p4134
data17_13TeV.AllYear.physics_Main.PhysCont.DAOD_HIGG8D1.grp17_v01_p4134
data18_13TeV.AllYear.physics_Main.PhysCont.DAOD_HIGG8D1.grp18_v01_p4134

mc16a:
mc16_13TeV.361603.PowhegPy8EG_CT10nloME_AZNLOCTEQ6L1_ZZllll_mll4.deriv.DAOD_HIGG8D1.e4475_s3126_r9364_r9315_p4133
mc16_13TeV.361602.PowhegPy8EG_CT10nloME_AZNLOCTEQ6L1_WZlvvv_mll4.deriv.DAOD_HIGG8D1.e4054_s3126_r9364_r9315_p4133
mc16_13TeV.361604.PowhegPy8EG_CT10nloME_AZNLOCTEQ6L1_ZZvvll_mll4.deriv.DAOD_HIGG8D1.e4475_s3126_r9364_r9315_p4133
mc16_13TeV.361600.PowhegPy8EG_CT10nloME_AZNLOCTEQ6L1_WWlvlv.deriv.DAOD_HIGG8D1.e4616_s3126_r9364_r9315_p4133
mc16_13TeV.361605.PowhegPy8EG_CT10nloME_AZNLOCTEQ6L1_ZZvvvv_mll4.deriv.DAOD_HIGG8D1.e4054_s3126_s3136_r9364_r9315_p4133
mc16_13TeV.361601.PowhegPy8EG_CT10nloME_AZNLOCTEQ6L1_WZlvll_mll4.deriv.DAOD_HIGG8D1.e4475_s3126_r9364_r9315_p4133
mc16_13TeV.364286.Sherpa_222_NNPDF30NNLO_llvvjj_ss_EW4.deriv.DAOD_HIGG8D1.e6055_e5984_s3126_r9364_r9315_p3983 mc16_13TeV.364285.Sherpa_222_NNPD
mc16_13TeV.364740.MGPy8EG_NNPDF30NLO_A14NNPDF23LO_lvlljjEW6_OFPlus.deriv.DAOD_HIGG8D1.e7421_e5984_s3126_r9364_r9315_p4133
mc16_13TeV.364742.MGPy8EG_NNPDF30NLO_A14NNPDF23LO_lvlljjEW6_SFPlus.deriv.DAOD_HIGG8D1.e7421_e5984_s3126_r9364_r9315_p4133
mc16_13TeV.364253.Sherpa_222_NNPDF30NNLO_lllv.deriv.DAOD_HIGG8D1.e5916_s3126_r9364_r9315_p4133
mc16_13TeV.364250.Sherpa_222_NNPDF30NNLO_llll.deriv.DAOD_HIGG8D1.e5894_s3126_r9364_r9315_p4133
mc16_13TeV.364254.Sherpa_222_NNPDF30NNLO_llvv.deriv.DAOD_HIGG8D1.e5916_s3126_r9364_r9315_p4133

mc16_13TeV.364255.Sherpa_222_NNPDF30NNLO_lvvv.deriv.DAOD_HIGG8D1.e5916_s3126_r9364_r9315_p4133
mc16_13TeV.410155.aMcAtNloPythia8EvtGen_MEN30NLO_A14N23LO_ttW.deriv.DAOD_HIGG8D1.e5070_s3126_r9364_r9315_p4133
mc16_13TeV.410156.aMcAtNloPythia8EvtGen_MEN30NLO_A14N23LO_ttZnunu.deriv.DAOD_HIGG8D1.e5070_s3126_r9364_r9315_p4133
mc16_13TeV.410157.aMcAtNloPythia8EvtGen_MEN30NLO_A14N23LO_ttZqq.deriv.DAOD_HIGG8D1.e5070_s3126_r9364_r9315_p4133
mc16_13TeV.410218.aMcAtNloPythia8EvtGen_MEN30NLO_A14N23LO_ttee.deriv.DAOD_HIGG8D1.e5070_s3126_r9364_r9315_p4133
mc16_13TeV.410219.aMcAtNloPythia8EvtGen_MEN30NLO_A14N23LO_ttmumu.deriv.DAOD_HIGG8D1.e5070_s3126_r9364_r9315_p4133
mc16_13TeV.410220.aMcAtNloPythia8EvtGen_MEN30NLO_A14N23LO_tttautau.deriv.DAOD_HIGG8D1.e5070_s3126_r9364_r9315_p4133
mc16_13TeV.412063.aMcAtNloPythia8EvtGen_tllq_NNPDF30_nf4_A14.deriv.DAOD_TOPQ1.e7054_e5984_s3126_r9364_r9315_p4174
mc16_13TeV.410276.aMcAtNloPythia8EvtGen_MEN30NLO_A14N23LO_ttee_mll_1_5.deriv.DAOD_HIGG8D1.e6087_e5984_s3126_r9364_r9315_p4133
mc16_13TeV.410277.aMcAtNloPythia8EvtGen_MEN30NLO_A14N23LO_ttmumu_mll_1_5.deriv.DAOD_HIGG8D1.e6087_e5984_s3126_r9364_r9315_p4133
mc16_13TeV.410278.aMcAtNloPythia8EvtGen_MEN30NLO_A14N23LO_tttautau_mll_1_5.deriv.DAOD_HIGG8D1.e6087_e5984_s3126_r9364_r9315_p4133
mc16_13TeV.410397.MadGraphPythia8EvtGen_ttbar_wbee_MEN30LO_A14N23LO.deriv.DAOD_HIGG8D1.e6086_e5984_s3126_r9364_r9315_p4133
mc16_13TeV.410398.MadGraphPythia8EvtGen_ttbar_wbmumu_MEN30LO_A14N23LO.deriv.DAOD_HIGG8D1.e6086_e5984_s3126_r9364_r9315_p4133
mc16_13TeV.410399.MadGraphPythia8EvtGen_ttbar_wbtautau_MEN30LO_A14N23LO.deriv.DAOD_HIGG8D1.e6086_e5984_s3126_r9364_r9315_p4133
mc16_13TeV.410658.PhPy8EG_A14_tchan_BW50_lept_top.deriv.DAOD_HIGG8D1.e6671_e5984_s3126_r9364_r9315_p4133
mc16_13TeV.410659.PhPy8EG_A14_tchan_BW50_lept_antitop.deriv.DAOD_HIGG8D1.e6671_e5984_s3126_r9364_r9315_p4133
mc16_13TeV.410644.PowhegPythia8EvtGen_A14_singletop_schan_lept_top.deriv.DAOD_HIGG8D1.e6527_e5984_s3126_r9364_r9315_p4133
mc16_13TeV.410645.PowhegPythia8EvtGen_A14_singletop_schan_lept_antitop.deriv.DAOD_HIGG8D1.e6527_e5984_s3126_r9364_r9315_p4133
mc16_13TeV.304014.MadGraphPythia8EvtGen_A14NNPDF23_3top_SM.deriv.DAOD_HIGG8D1.e4324_s3126_r9364_r9315_p4133
mc16_13TeV.410080.MadGraphPythia8EvtGen_A14NNPDF23_4topSM.deriv.DAOD_HIGG8D1.e4111_s3126_r9364_r9315_p4133
mc16_13TeV.410081.MadGraphPythia8EvtGen_A14NNPDF23_ttbarWW.deriv.DAOD_HIGG8D1.e4111_s3126_r9364_r9315_p4133
mc16_13TeV.364100.Sherpa_221_NNPDF30NNLO_Zmumu_MAXHTPTV0_70_CVetoBVeto.deriv.DAOD_HIGG8D1.e5271_s3126_r9364_r9315_p4133
mc16_13TeV.364101.Sherpa_221_NNPDF30NNLO_Zmumu_MAXHTPTV0_70_CFilterBVeto.deriv.DAOD_HIGG8D1.e5271_s3126_r9364_r9315_p4133
mc16_13TeV.364102.Sherpa_221_NNPDF30NNLO_Zmumu_MAXHTPTV0_70_BFilter.deriv.DAOD_HIGG8D1.e5271_s3126_r9364_r9315_p4133
mc16_13TeV.364103.Sherpa_221_NNPDF30NNLO_Zmumu_MAXHTPTV70_140_CVetoBVeto.deriv.DAOD_HIGG8D1.e5271_s3126_r9364_r9315_p4133
mc16_13TeV.364104.Sherpa_221_NNPDF30NNLO_Zmumu_MAXHTPTV70_140_CFilterBVeto.deriv.DAOD_HIGG8D1.e5271_s3126_r9364_r9315_p4133
mc16_13TeV.364106.Sherpa_221_NNPDF30NNLO_Zmumu_MAXHTPTV140_280_CVetoBVeto.deriv.DAOD_HIGG8D1.e5271_s3126_r9364_r9315_p4133
mc16_13TeV.364107.Sherpa_221_NNPDF30NNLO_Zmumu_MAXHTPTV140_280_CFilterBVeto.deriv.DAOD_HIGG8D1.e5271_s3126_r9364_r9315_p4133
mc16_13TeV.364108.Sherpa_221_NNPDF30NNLO_Zmumu_MAXHTPTV140_280_BFilter.deriv.DAOD_HIGG8D1.e5271_s3126_r9364_r9315_p4133
mc16_13TeV.364109.Sherpa_221_NNPDF30NNLO_Zmumu_MAXHTPTV280_500_CVetoBVeto.deriv.DAOD_HIGG8D1.e5271_s3126_r9364_r9315_p4133
mc16_13TeV.364110.Sherpa_221_NNPDF30NNLO_Zmumu_MAXHTPTV280_500_CFilterBVeto.deriv.DAOD_HIGG8D1.e5271_s3126_r9364_r9315_p4133
mc16_13TeV.364111.Sherpa_221_NNPDF30NNLO_Zmumu_MAXHTPTV280_500_BFilter.deriv.DAOD_HIGG8D1.e5271_e5984_s3126_r9364_r9315_p4133
mc16_13TeV.364111.Sherpa_221_NNPDF30NNLO_Zmumu_MAXHTPTV280_500_BFilter.deriv.DAOD_HIGG8D1.e5271_s3126_r9364_r9315_p4133
mc16_13TeV.364112.Sherpa_221_NNPDF30NNLO_Zmumu_MAXHTPTV500_1000.deriv.DAOD_HIGG8D1.e5271_s3126_r9364_r9315_p4133
mc16_13TeV.364113.Sherpa_221_NNPDF30NNLO_Zmumu_MAXHTPTV1000_E_CMS.deriv.DAOD_HIGG8D1.e5271_s3126_r9364_r9315_p4133
mc16_13TeV.364114.Sherpa_221_NNPDF30NNLO_Zee_MAXHTPTV0_70_CVetoBVeto.deriv.DAOD_HIGG8D1.e5299_s3126_r9364_r9315_p4133
mc16_13TeV.364115.Sherpa_221_NNPDF30NNLO_Zee_MAXHTPTV0_70_CFilterBVeto.deriv.DAOD_HIGG8D1.e5299_s3126_r9364_r9315_p4133
mc16_13TeV.364116.Sherpa_221_NNPDF30NNLO_Zee_MAXHTPTV0_70_BFilter.deriv.DAOD_HIGG8D1.e5299_s3126_r9364_r9315_p4133
mc16_13TeV.364117.Sherpa_221_NNPDF30NNLO_Zee_MAXHTPTV70_140_CVetoBVeto.deriv.DAOD_HIGG8D1.e5299_s3126_r9364_r9315_p4133
mc16_13TeV.364118.Sherpa_221_NNPDF30NNLO_Zee_MAXHTPTV70_140_CFilterBVeto.deriv.DAOD_HIGG8D1.e5299_s3126_r9364_r9315_p4133
mc16_13TeV.364119.Sherpa_221_NNPDF30NNLO_Zee_MAXHTPTV70_140_BFilter.deriv.DAOD_HIGG8D1.e5299_s3126_r9364_r9315_p4133
mc16_13TeV.364120.Sherpa_221_NNPDF30NNLO_Zee_MAXHTPTV140_280_CVetoBVeto.deriv.DAOD_HIGG8D1.e5299_s3126_r9364_r9315_p4133
mc16_13TeV.364121.Sherpa_221_NNPDF30NNLO_Zee_MAXHTPTV140_280_CFilterBVeto.deriv.DAOD_HIGG8D1.e5299_s3126_r9364_r9315_p4133
mc16_13TeV.364122.Sherpa_221_NNPDF30NNLO_Zee_MAXHTPTV140_280_BFilter.deriv.DAOD_HIGG8D1.e5299_s3126_r9364_r9315_p4133
mc16_13TeV.364123.Sherpa_221_NNPDF30NNLO_Zee_MAXHTPTV280_500_CVetoBVeto.deriv.DAOD_HIGG8D1.e5299_s3126_r9364_r9315_p4133
mc16_13TeV.364124.Sherpa_221_NNPDF30NNLO_Zee_MAXHTPTV280_500_CFilterBVeto.deriv.DAOD_HIGG8D1.e5299_s3126_r9364_r9315_p4133
mc16_13TeV.364125.Sherpa_221_NNPDF30NNLO_Zee_MAXHTPTV280_500_BFilter.deriv.DAOD_HIGG8D1.e5299_s3126_r9364_r9315_p4133
mc16_13TeV.364125.Sherpa_221_NNPDF30NNLO_Zee_MAXHTPTV280_500_BFilter.deriv.DAOD_HIGG8D1.e5299_e5984_s3126_r9364_r9315_p4133
mc16_13TeV.364126.Sherpa_221_NNPDF30NNLO_Zee_MAXHTPTV500_1000.deriv.DAOD_HIGG8D1.e5299_s3126_r9364_r9315_p4133
mc16_13TeV.364127.Sherpa_221_NNPDF30NNLO_Zee_MAXHTPTV1000_E_CMS.deriv.DAOD_HIGG8D1.e5299_s3126_r9364_r9315_p4133
mc16_13TeV.364128.Sherpa_221_NNPDF30NNLO_Ztautau_MAXHTPTV0_70_CVetoBVeto.deriv.DAOD_HIGG8D1.e5307_s3126_r9364_r9315_p4133
mc16_13TeV.364129.Sherpa_221_NNPDF30NNLO_Ztautau_MAXHTPTV0_70_CFilterBVeto.deriv.DAOD_HIGG8D1.e5307_s3126_r9364_r9315_p4133
mc16_13TeV.364130.Sherpa_221_NNPDF30NNLO_Ztautau_MAXHTPTV0_70_BFilter.deriv.DAOD_HIGG8D1.e5307_s3126_r9364_r9315_p4133
mc16_13TeV.364131.Sherpa_221_NNPDF30NNLO_Ztautau_MAXHTPTV70_140_CVetoBVeto.deriv.DAOD_HIGG8D1.e5307_s3126_r9364_r9315_p4133
mc16_13TeV.364132.Sherpa_221_NNPDF30NNLO_Ztautau_MAXHTPTV70_140_CFilterBVeto.deriv.DAOD_HIGG8D1.e5307_s3126_r9364_r9315_p4133
mc16_13TeV.364133.Sherpa_221_NNPDF30NNLO_Ztautau_MAXHTPTV70_140_BFilter.deriv.DAOD_HIGG8D1.e5307_s3126_r9364_r9315_p4133
mc16_13TeV.364134.Sherpa_221_NNPDF30NNLO_Ztautau_MAXHTPTV140_280_CVetoBVeto.deriv.DAOD_HIGG8D1.e5307_s3126_r9364_r9315_p4133
mc16_13TeV.364135.Sherpa_221_NNPDF30NNLO_Ztautau_MAXHTPTV140_280_CFilterBVeto.deriv.DAOD_HIGG8D1.e5307_s3126_r9364_r9315_p4133
mc16_13TeV.364136.Sherpa_221_NNPDF30NNLO_Ztautau_MAXHTPTV140_280_BFilter.deriv.DAOD_HIGG8D1.e5307_s3126_r9364_r9315_p4133
mc16_13TeV.364137.Sherpa_221_NNPDF30NNLO_Ztautau_MAXHTPTV280_500_CVetoBVeto.deriv.DAOD_HIGG8D1.e5307_e5984_s3126_r9364_r9315_p4133
mc16_13TeV.364137.Sherpa_221_NNPDF30NNLO_Ztautau_MAXHTPTV280_500_CVetoBVeto.deriv.DAOD_HIGG8D1.e5307_s3126_r9364_r9315_p4133
mc16_13TeV.364138.Sherpa_221_NNPDF30NNLO_Ztautau_MAXHTPTV280_500_CFilterBVeto.deriv.DAOD_HIGG8D1.e5313_s3126_r9364_r9315_p4133

mc16_13TeV.364139.Sherpa_221_NNPDF30NNLO_Ztautau_MAXHTPTV280_500_BFilter.deriv.DAOD_HIGG8D1.e5313_s3126_r9364_r9315_p4133
mc16_13TeV.364140.Sherpa_221_NNPDF30NNLO_Ztautau_MAXHTPTV500_1000.deriv.DAOD_HIGG8D1.e5307_s3126_r9364_r9315_p4133
mc16_13TeV.364141.Sherpa_221_NNPDF30NNLO_Ztautau_MAXHTPTV1000_E_CMS.deriv.DAOD_HIGG8D1.e5307_s3126_r9364_r9315_p4133
mc16_13TeV.364198.Sherpa_221_NN30NNLO_Zmm_Mll10_40_MAXHTPTV0_70_BVeto.deriv.DAOD_HIGG8D1.e5421_s3126_r9364_r9315_p4133
mc16_13TeV.364199.Sherpa_221_NN30NNLO_Zmm_Mll10_40_MAXHTPTV0_70_BFilter.deriv.DAOD_HIGG8D1.e5421_s3126_r9364_r9315_p4133
mc16_13TeV.364200.Sherpa_221_NN30NNLO_Zmm_Mll10_40_MAXHTPTV70_280_BVeto.deriv.DAOD_HIGG8D1.e5421_s3126_r9364_r9315_p4133
mc16_13TeV.364201.Sherpa_221_NN30NNLO_Zmm_Mll10_40_MAXHTPTV70_280_BFilter.deriv.DAOD_HIGG8D1.e5421_s3126_r9364_r9315_p4133
mc16_13TeV.364202.Sherpa_221_NN30NNLO_Zmm_Mll10_40_MAXHTPTV280_E_CMS_BVeto.deriv.DAOD_HIGG8D1.e5421_s3126_r9364_r9315_p4133
mc16_13TeV.364203.Sherpa_221_NN30NNLO_Zmm_Mll10_40_MAXHTPTV280_E_CMS_BFilter.deriv.DAOD_HIGG8D1.e5421_s3126_r9364_r9315_p4133
mc16_13TeV.364204.Sherpa_221_NN30NNLO_Zee_Mll10_40_MAXHTPTV0_70_BVeto.deriv.DAOD_HIGG8D1.e5421_s3126_r9364_r9315_p4133
mc16_13TeV.364205.Sherpa_221_NN30NNLO_Zee_Mll10_40_MAXHTPTV0_70_BFilter.deriv.DAOD_HIGG8D1.e5421_s3126_r9364_r9315_p4133
mc16_13TeV.364206.Sherpa_221_NN30NNLO_Zee_Mll10_40_MAXHTPTV70_280_BVeto.deriv.DAOD_HIGG8D1.e5421_s3126_r9364_r9315_p4133
mc16_13TeV.364207.Sherpa_221_NN30NNLO_Zee_Mll10_40_MAXHTPTV70_280_BFilter.deriv.DAOD_HIGG8D1.e5421_s3126_r9364_r9315_p4133
mc16_13TeV.364208.Sherpa_221_NN30NNLO_Zee_Mll10_40_MAXHTPTV280_E_CMS_BVeto.deriv.DAOD_HIGG8D1.e5421_s3126_r9364_r9315_p4133
mc16_13TeV.364209.Sherpa_221_NN30NNLO_Zee_Mll10_40_MAXHTPTV280_E_CMS_BFilter.deriv.DAOD_HIGG8D1.e5421_s3126_r9364_r9315_p4133
mc16_13TeV.364210.Sherpa_221_NN30NNLO_Ztt_Mll10_40_MAXHTPTV0_70_BVeto.deriv.DAOD_HIGG8D1.e5421_s3126_r9364_r9315_p4133
mc16_13TeV.364211.Sherpa_221_NN30NNLO_Ztt_Mll10_40_MAXHTPTV0_70_BFilter.deriv.DAOD_HIGG8D1.e5421_s3126_r9364_r9315_p4133
mc16_13TeV.364212.Sherpa_221_NN30NNLO_Ztt_Mll10_40_MAXHTPTV70_280_BVeto.deriv.DAOD_HIGG8D1.e5421_s3126_r9364_r9315_p4133
mc16_13TeV.364213.Sherpa_221_NN30NNLO_Ztt_Mll10_40_MAXHTPTV70_280_BFilter.deriv.DAOD_HIGG8D1.e5421_s3126_r9364_r9315_p4133
mc16_13TeV.364214.Sherpa_221_NN30NNLO_Ztt_Mll10_40_MAXHTPTV280_E_CMS_BVeto.deriv.DAOD_HIGG8D1.e5421_s3126_r9364_r9315_p4133
mc16_13TeV.364215.Sherpa_221_NN30NNLO_Ztt_Mll10_40_MAXHTPTV280_E_CMS_BFilter.deriv.DAOD_HIGG8D1.e5421_s3126_r9364_r9315_p4133
mc16_13TeV.364156.Sherpa_221_NNPDF30NNLO_Wmunu_MAXHTPTV0_70_CVetoBVeto.deriv.DAOD_HIGG8D1.e5340_s3126_r9364_r9315_p4133
mc16_13TeV.364157.Sherpa_221_NNPDF30NNLO_Wmunu_MAXHTPTV0_70_CFilterBVeto.deriv.DAOD_HIGG8D1.e5340_s3126_r9364_r9315_p4133
mc16_13TeV.364157.Sherpa_221_NNPDF30NNLO_Wmunu_MAXHTPTV0_70_CFilterBVeto.deriv.DAOD_HIGG8D1.e5340_e5984_s3126_r9364_r9315_p4133
mc16_13TeV.364158.Sherpa_221_NNPDF30NNLO_Wmunu_MAXHTPTV0_70_BFilter.deriv.DAOD_HIGG8D1.e5340_s3126_r9364_r9315_p4133
mc16_13TeV.364159.Sherpa_221_NNPDF30NNLO_Wmunu_MAXHTPTV70_140_CVetoBVeto.deriv.DAOD_HIGG8D1.e5340_s3126_r9364_r9315_p4133
mc16_13TeV.364160.Sherpa_221_NNPDF30NNLO_Wmunu_MAXHTPTV70_140_CFilterBVeto.deriv.DAOD_HIGG8D1.e5340_s3126_r9364_r9315_p4133
mc16_13TeV.364161.Sherpa_221_NNPDF30NNLO_Wmunu_MAXHTPTV70_140_BFilter.deriv.DAOD_HIGG8D1.e5340_s3126_r9364_r9315_p4133
mc16_13TeV.364162.Sherpa_221_NNPDF30NNLO_Wmunu_MAXHTPTV140_280_CVetoBVeto.deriv.DAOD_HIGG8D1.e5340_s3126_r9364_r9315_p4133
mc16_13TeV.364163.Sherpa_221_NNPDF30NNLO_Wmunu_MAXHTPTV140_280_CFilterBVeto.deriv.DAOD_HIGG8D1.e5340_s3126_r9364_r9315_p4133
mc16_13TeV.364163.Sherpa_221_NNPDF30NNLO_Wmunu_MAXHTPTV140_280_CFilterBVeto.deriv.DAOD_HIGG8D1.e5340_e5984_s3126_s3136_r9364_r9315_p4133
mc16_13TeV.364164.Sherpa_221_NNPDF30NNLO_Wmunu_MAXHTPTV140_280_BFilter.deriv.DAOD_HIGG8D1.e5340_s3126_r9364_r9315_p4133
mc16_13TeV.364165.Sherpa_221_NNPDF30NNLO_Wmunu_MAXHTPTV280_500_CVetoBVeto.deriv.DAOD_HIGG8D1.e5340_s3126_r9364_r9315_p4133
mc16_13TeV.364166.Sherpa_221_NNPDF30NNLO_Wmunu_MAXHTPTV280_500_CFilterBVeto.deriv.DAOD_HIGG8D1.e5340_s3126_r9364_r9315_p4133
mc16_13TeV.364167.Sherpa_221_NNPDF30NNLO_Wmunu_MAXHTPTV280_500_BFilter.deriv.DAOD_HIGG8D1.e5340_e5984_s3126_r9364_r9315_p4133
mc16_13TeV.364167.Sherpa_221_NNPDF30NNLO_Wmunu_MAXHTPTV280_500_BFilter.deriv.DAOD_HIGG8D1.e5340_s3126_r9364_r9315_p4133
mc16_13TeV.364168.Sherpa_221_NNPDF30NNLO_Wmunu_MAXHTPTV500_1000.deriv.DAOD_HIGG8D1.e5340_s3126_r9364_r9315_p4133
mc16_13TeV.364169.Sherpa_221_NNPDF30NNLO_Wmunu_MAXHTPTV1000_E_CMS.deriv.DAOD_HIGG8D1.e5340_s3126_r9364_r9315_p4133
mc16_13TeV.364170.Sherpa_221_NNPDF30NNLO_Wenu_MAXHTPTV0_70_CVetoBVeto.deriv.DAOD_HIGG8D1.e5340_s3126_r9364_r9315_p4133
mc16_13TeV.364171.Sherpa_221_NNPDF30NNLO_Wenu_MAXHTPTV0_70_CFilterBVeto.deriv.DAOD_HIGG8D1.e5340_e5984_s3126_r9364_r9315_p4133
mc16_13TeV.364171.Sherpa_221_NNPDF30NNLO_Wenu_MAXHTPTV0_70_CFilterBVeto.deriv.DAOD_HIGG8D1.e5340_s3126_r9364_r9315_p4133
mc16_13TeV.364172.Sherpa_221_NNPDF30NNLO_Wenu_MAXHTPTV0_70_BFilter.deriv.DAOD_HIGG8D1.e5340_s3126_r9364_r9315_p4133
mc16_13TeV.364173.Sherpa_221_NNPDF30NNLO_Wenu_MAXHTPTV70_140_CVetoBVeto.deriv.DAOD_HIGG8D1.e5340_s3126_r9364_r9315_p4133
mc16_13TeV.364174.Sherpa_221_NNPDF30NNLO_Wenu_MAXHTPTV70_140_CFilterBVeto.deriv.DAOD_HIGG8D1.e5340_s3126_r9364_r9315_p4133
mc16_13TeV.364175.Sherpa_221_NNPDF30NNLO_Wenu_MAXHTPTV70_140_BFilter.deriv.DAOD_HIGG8D1.e5340_e5984_s3126_s3136_r9364_r9315_p4133
mc16_13TeV.364175.Sherpa_221_NNPDF30NNLO_Wenu_MAXHTPTV70_140_BFilter.deriv.DAOD_HIGG8D1.e5340_s3126_r9364_r9315_p4133
mc16_13TeV.364176.Sherpa_221_NNPDF30NNLO_Wenu_MAXHTPTV140_280_CVetoBVeto.deriv.DAOD_HIGG8D1.e5340_s3126_r9364_r9315_p4133
mc16_13TeV.364177.Sherpa_221_NNPDF30NNLO_Wenu_MAXHTPTV140_280_CFilterBVeto.deriv.DAOD_HIGG8D1.e5340_s3126_r9364_r9315_p4133
mc16_13TeV.364177.Sherpa_221_NNPDF30NNLO_Wenu_MAXHTPTV140_280_CFilterBVeto.deriv.DAOD_HIGG8D1.e5340_e5984_s3126_s3136_r9364_r9315_p4133
mc16_13TeV.364178.Sherpa_221_NNPDF30NNLO_Wenu_MAXHTPTV140_280_BFilter.deriv.DAOD_HIGG8D1.e5340_s3126_r9364_r9315_p4133
mc16_13TeV.364179.Sherpa_221_NNPDF30NNLO_Wenu_MAXHTPTV280_500_CVetoBVeto.deriv.DAOD_HIGG8D1.e5340_s3126_r9364_r9315_p4133
mc16_13TeV.364180.Sherpa_221_NNPDF30NNLO_Wenu_MAXHTPTV280_500_CFilterBVeto.deriv.DAOD_HIGG8D1.e5340_s3126_r9364_r9315_p4133
mc16_13TeV.364181.Sherpa_221_NNPDF30NNLO_Wenu_MAXHTPTV280_500_BFilter.deriv.DAOD_HIGG8D1.e5340_e5984_s3126_r9364_r9315_p4133
mc16_13TeV.364181.Sherpa_221_NNPDF30NNLO_Wenu_MAXHTPTV280_500_BFilter.deriv.DAOD_HIGG8D1.e5340_s3126_r9364_r9315_p4133
mc16_13TeV.364182.Sherpa_221_NNPDF30NNLO_Wenu_MAXHTPTV500_1000.deriv.DAOD_HIGG8D1.e5340_s3126_r9364_r9315_p4133
mc16_13TeV.364183.Sherpa_221_NNPDF30NNLO_Wenu_MAXHTPTV1000_E_CMS.deriv.DAOD_HIGG8D1.e5340_s3126_r9364_r9315_p4133
mc16_13TeV.364184.Sherpa_221_NNPDF30NNLO_Wtaunu_MAXHTPTV0_70_CVetoBVeto.deriv.DAOD_HIGG8D1.e5340_s3126_r9364_r9315_p4133
mc16_13TeV.364185.Sherpa_221_NNPDF30NNLO_Wtaunu_MAXHTPTV0_70_CFilterBVeto.deriv.DAOD_HIGG8D1.e5340_e5984_s3126_r9364_r9315_p4133
mc16_13TeV.364185.Sherpa_221_NNPDF30NNLO_Wtaunu_MAXHTPTV0_70_CFilterBVeto.deriv.DAOD_HIGG8D1.e5340_s3126_r9364_r9315_p4133
mc16_13TeV.364186.Sherpa_221_NNPDF30NNLO_Wtaunu_MAXHTPTV0_70_BFilter.deriv.DAOD_HIGG8D1.e5340_s3126_r9364_r9315_p4133
mc16_13TeV.364187.Sherpa_221_NNPDF30NNLO_Wtaunu_MAXHTPTV70_140_CVetoBVeto.deriv.DAOD_HIGG8D1.e5340_s3126_r9364_r9315_p4133
mc16_13TeV.364188.Sherpa_221_NNPDF30NNLO_Wtaunu_MAXHTPTV70_140_CFilterBVeto.deriv.DAOD_HIGG8D1.e5340_s3126_r9364_r9315_p4133

mc16_13TeV.364189.Sherpa_221_NNPDF30NNLO_Wtaunu_MAXHTPTV70_140_BFilter.deriv.DAOD_HIGG8D1.e5340_s3126_r9364_r9315_p4133
mc16_13TeV.364190.Sherpa_221_NNPDF30NNLO_Wtaunu_MAXHTPTV140_280_CVetoBVeto.deriv.DAOD_HIGG8D1.e5340_e5984_s3126_r9364_r9315_p4133
mc16_13TeV.364190.Sherpa_221_NNPDF30NNLO_Wtaunu_MAXHTPTV140_280_CVetoBVeto.deriv.DAOD_HIGG8D1.e5340_s3126_r9364_r9315_p4133
mc16_13TeV.364191.Sherpa_221_NNPDF30NNLO_Wtaunu_MAXHTPTV140_280_CFilterBVeto.deriv.DAOD_HIGG8D1.e5340_s3126_r9364_r9315_p4133
mc16_13TeV.364191.Sherpa_221_NNPDF30NNLO_Wtaunu_MAXHTPTV140_280_CFilterBVeto.deriv.DAOD_HIGG8D1.e5340_e5984_s3126_s3136_r9364_r9315_p4133
mc16_13TeV.364192.Sherpa_221_NNPDF30NNLO_Wtaunu_MAXHTPTV140_280_BFilter.deriv.DAOD_HIGG8D1.e5340_s3126_r9364_r9315_p4133
mc16_13TeV.364193.Sherpa_221_NNPDF30NNLO_Wtaunu_MAXHTPTV280_500_CVetoBVeto.deriv.DAOD_HIGG8D1.e5340_s3126_r9364_r9315_p4133
mc16_13TeV.364193.Sherpa_221_NNPDF30NNLO_Wtaunu_MAXHTPTV280_500_CVetoBVeto.deriv.DAOD_HIGG8D1.e5340_e5984_s3126_s3136_r9364_r9315_p4133
mc16_13TeV.364194.Sherpa_221_NNPDF30NNLO_Wtaunu_MAXHTPTV280_500_CFilterBVeto.deriv.DAOD_HIGG8D1.e5340_s3126_r9364_r9315_p4133
mc16_13TeV.364194.Sherpa_221_NNPDF30NNLO_Wtaunu_MAXHTPTV280_500_CFilterBVeto.deriv.DAOD_HIGG8D1.e5340_e5984_s3126_s3136_r9364_r9315_p4133
mc16_13TeV.364195.Sherpa_221_NNPDF30NNLO_Wtaunu_MAXHTPTV280_500_BFilter.deriv.DAOD_HIGG8D1.e5340_s3126_r9364_r9315_p4133
mc16_13TeV.364196.Sherpa_221_NNPDF30NNLO_Wtaunu_MAXHTPTV500_1000.deriv.DAOD_HIGG8D1.e5340_s3126_r9364_r9315_p4133
mc16_13TeV.364197.Sherpa_221_NNPDF30NNLO_Wtaunu_MAXHTPTV1000_E_CMS.deriv.DAOD_HIGG8D1.e5340_s3126_r9364_r9315_p4133
mc16_13TeV.364500.Sherpa_222_NNPDF30NNLO_eegamma_pty_7_15.deriv.DAOD_HIGG8D1.e5928_e5984_s3126_r9364_r9315_p4133
mc16_13TeV.364501.Sherpa_222_NNPDF30NNLO_eegamma_pty_15_35.deriv.DAOD_HIGG8D1.e5928_e5984_s3126_r9364_r9315_p4133
mc16_13TeV.364502.Sherpa_222_NNPDF30NNLO_eegamma_pty_35_70.deriv.DAOD_HIGG8D1.e5928_e5984_s3126_r9364_r9315_p4133
mc16_13TeV.364503.Sherpa_222_NNPDF30NNLO_eegamma_pty_70_140.deriv.DAOD_HIGG8D1.e5928_e5984_s3126_r9364_r9315_p4133
mc16_13TeV.364504.Sherpa_222_NNPDF30NNLO_eegamma_pty_140_E_CMS.deriv.DAOD_HIGG8D1.e5928_e5984_s3126_r9364_r9315_p4133
mc16_13TeV.364505.Sherpa_222_NNPDF30NNLO_mumugamma_pty_7_15.deriv.DAOD_HIGG8D1.e5928_e5984_s3126_r9364_r9315_p4133
mc16_13TeV.364506.Sherpa_222_NNPDF30NNLO_mumugamma_pty_15_35.deriv.DAOD_HIGG8D1.e5988_e5984_s3126_r9364_r9315_p4133
mc16_13TeV.364507.Sherpa_222_NNPDF30NNLO_mumugamma_pty_35_70.deriv.DAOD_HIGG8D1.e5928_e5984_s3126_r9364_r9315_p4133
mc16_13TeV.364508.Sherpa_222_NNPDF30NNLO_mumugamma_pty_70_140.deriv.DAOD_HIGG8D1.e5928_e5984_s3126_r9364_r9315_p4133
mc16_13TeV.364509.Sherpa_222_NNPDF30NNLO_mumugamma_pty_140_E_CMS.deriv.DAOD_HIGG8D1.e5928_e5984_s3126_r9364_r9315_p4133
mc16_13TeV.364510.Sherpa_222_NNPDF30NNLO_tautaugamma_pty_7_15.deriv.DAOD_HIGG8D1.e5928_s3126_r9364_r9315_p4133
mc16_13TeV.364511.Sherpa_222_NNPDF30NNLO_tautaugamma_pty_15_35.deriv.DAOD_HIGG8D1.e5928_s3126_r9364_r9315_p4133
mc16_13TeV.364512.Sherpa_222_NNPDF30NNLO_tautaugamma_pty_35_70.deriv.DAOD_HIGG8D1.e5928_s3126_r9364_r9315_p4133
mc16_13TeV.364513.Sherpa_222_NNPDF30NNLO_tautaugamma_pty_70_140.deriv.DAOD_HIGG8D1.e5982_s3126_r9364_r9315_p4133
mc16_13TeV.364514.Sherpa_222_NNPDF30NNLO_tautaugamma_pty_140_E_CMS.deriv.DAOD_HIGG8D1.e5928_s3126_r9364_r9315_p4133
mc16_13TeV.364521.Sherpa_222_NNPDF30NNLO_enugamma_pty_7_15.deriv.DAOD_HIGG8D1.e5928_s3126_r9364_r9315_p4133
mc16_13TeV.364522.Sherpa_222_NNPDF30NNLO_enugamma_pty_15_35.deriv.DAOD_HIGG8D1.e5928_s3126_r9364_r9315_p4133
mc16_13TeV.364523.Sherpa_222_NNPDF30NNLO_enugamma_pty_35_70.deriv.DAOD_HIGG8D1.e5928_s3126_r9364_r9315_p4133
mc16_13TeV.364524.Sherpa_222_NNPDF30NNLO_enugamma_pty_70_140.deriv.DAOD_HIGG8D1.e5928_s3126_r9364_r9315_p4133
mc16_13TeV.364525.Sherpa_222_NNPDF30NNLO_enugamma_pty_140_E_CMS.deriv.DAOD_HIGG8D1.e5928_s3126_r9364_r9315_p4133
mc16_13TeV.364525.Sherpa_222_NNPDF30NNLO_enugamma_pty_140_E_CMS.deriv.DAOD_HIGG8D1.e5928_e5984_s3126_r9364_r9315_p4133
mc16_13TeV.364526.Sherpa_222_NNPDF30NNLO_munugamma_pty_7_15.deriv.DAOD_HIGG8D1.e5928_s3126_r9364_r9315_p4133
mc16_13TeV.364527.Sherpa_222_NNPDF30NNLO_munugamma_pty_15_35.deriv.DAOD_HIGG8D1.e5928_s3126_r9364_r9315_p4133
mc16_13TeV.364528.Sherpa_222_NNPDF30NNLO_munugamma_pty_35_70.deriv.DAOD_HIGG8D1.e5928_s3126_r9364_r9315_p4133
mc16_13TeV.364529.Sherpa_222_NNPDF30NNLO_munugamma_pty_70_140.deriv.DAOD_HIGG8D1.e5928_s3126_r9364_r9315_p4133
mc16_13TeV.364530.Sherpa_222_NNPDF30NNLO_munugamma_pty_140_E_CMS.deriv.DAOD_HIGG8D1.e5928_s3126_r9364_r9315_p4133
mc16_13TeV.364530.Sherpa_222_NNPDF30NNLO_munugamma_pty_140_E_CMS.deriv.DAOD_HIGG8D1.e5928_e5984_s3126_r9364_r9315_p4133
mc16_13TeV.364531.Sherpa_222_NNPDF30NNLO_taunugamma_pty_7_15.deriv.DAOD_HIGG8D1.e5928_s3126_r9364_r9315_p4133
mc16_13TeV.364532.Sherpa_222_NNPDF30NNLO_taunugamma_pty_15_35.deriv.DAOD_HIGG8D1.e5928_s3126_r9364_r9315_p4133
mc16_13TeV.364533.Sherpa_222_NNPDF30NNLO_taunugamma_pty_35_70.deriv.DAOD_HIGG8D1.e5928_s3126_r9364_r9315_p4133
mc16_13TeV.364534.Sherpa_222_NNPDF30NNLO_taunugamma_pty_70_140.deriv.DAOD_HIGG8D1.e5928_s3126_r9364_r9315_p4133
mc16_13TeV.364535.Sherpa_222_NNPDF30NNLO_taunugamma_pty_140_E_CMS.deriv.DAOD_HIGG8D1.e5928_s3126_r9364_r9315_p4133
mc16_13TeV.364535.Sherpa_222_NNPDF30NNLO_taunugamma_pty_140_E_CMS.deriv.DAOD_HIGG8D1.e5928_e5984_s3126_r9364_r9315_p4133
mc16_13TeV.410560.MadGraphPythia8EvtGen_A14_tZ_4fl_tchan_noAllHad.deriv.DAOD_HIGG8D1.e5803_s3126_r9364_r9315_p4133
mc16_13TeV.410013.PowhegPythiaEvtGen_P2012_Wt_inclusive_top.deriv.DAOD_HIGG8D1.e3753_s3126_r9364_r9315_p4133
mc16_13TeV.410014.PowhegPythiaEvtGen_P2012_Wt_inclusive_antitop.deriv.DAOD_HIGG8D1.e3753_s3126_r9364_r9315_p4133
mc16_13TeV.410408.aMcAtNloPythia8EvtGen_tWZ_Ztoll_minDR1.deriv.DAOD_HIGG8D1.e6423_e5984_s3126_r9364_r9315_p4133
mc16_13TeV.364242.Sherpa_222_NNPDF30NNLO_WWW_3l3v_EW6.deriv.DAOD_HIGG8D1.e5887_s3126_r9364_r9315_p4133
mc16_13TeV.364243.Sherpa_222_NNPDF30NNLO_WWZ_4l2v_EW6.deriv.DAOD_HIGG8D1.e5887_s3126_r9364_r9315_p4133
mc16_13TeV.364244.Sherpa_222_NNPDF30NNLO_WWZ_2l4v_EW6.deriv.DAOD_HIGG8D1.e5887_s3126_r9364_r9315_p4133
mc16_13TeV.364245.Sherpa_222_NNPDF30NNLO_WZZ_5l1v_EW6.deriv.DAOD_HIGG8D1.e5887_s3126_r9364_r9315_p4133
mc16_13TeV.364246.Sherpa_222_NNPDF30NNLO_WZZ_3l3v_EW6.deriv.DAOD_HIGG8D1.e5887_s3126_r9364_r9315_p4133
mc16_13TeV.364247.Sherpa_222_NNPDF30NNLO_ZZZ_6l0v_EW6.deriv.DAOD_HIGG8D1.e5887_s3126_r9364_r9315_p4133
mc16_13TeV.364248.Sherpa_222_NNPDF30NNLO_ZZZ_4l2v_EW6.deriv.DAOD_HIGG8D1.e5887_s3126_r9364_r9315_p4133
mc16_13TeV.364249.Sherpa_222_NNPDF30NNLO_ZZZ_2l4v_EW6.deriv.DAOD_HIGG8D1.e5887_s3126_r9364_r9315_p4133
mc16_13TeV.342284.Pythia8EvtGen_A14NNPDF23LO_WH125_inc.deriv.DAOD_HIGG8D1.e4246_s3126_r9364_r9315_p4133
mc16_13TeV.342285.Pythia8EvtGen_A14NNPDF23LO_ZH125_inc.deriv.DAOD_HIGG8D1.e4246_s3126_r9364_r9315_p4133
mc16_13TeV.341998.aMcAtNloHppEG_UEEE5_CTEQ6L1_CT10ME_tWH125_gamgam_yt_plus1.deriv.DAOD_HIGG8D1.e4394_e5984_s3126_r9364_r9315_p4133
mc16_13TeV.410389.MadGraphPythia8EvtGen_A14NNPDF23_ttgamma_nonallhadronic.deriv.DAOD_HIGG8D1.e6155_e5984_s3126_r9364_r9315_p4133

mc16_13TeV.410470.PhPy8EG_A14_ttbar_hdamp258p75_nonallhad.deriv.DAOD_HIGG8D1.e6337_e5984_s3126_r9364_r9315_p4133
mc16_13TeV.410472.PhPy8EG_A14_ttbar_hdamp258p75_dil.deriv.DAOD_HIGG8D1.e6348_e5984_s3126_r9364_r9315_p4133
mc16_13TeV.346343.PhPy8EG_A14NNPDF23_NNPDF30ME_ttH125_allhad.deriv.DAOD_HIGG8D1.e7148_e5984_s3126_r9364_r9315_p4133
mc16_13TeV.346344.PhPy8EG_A14NNPDF23_NNPDF30ME_ttH125_semilep.deriv.DAOD_HIGG8D1.e7148_e5984_s3126_r9364_r9315_p4133
mc16_13TeV.346345.PhPy8EG_A14NNPDF23_NNPDF30ME_ttH125_dilep.deriv.DAOD_HIGG8D1.e7148_e5984_s3126_r9364_r9315_p4133

mc16d:
mc16_13TeV.364253.Sherpa_222_NNPDF30NNLO_lllv.deriv.DAOD_HIGG8D1.e5916_e5984_s3126_r10201_r10210_p4133
mc16_13TeV.364250.Sherpa_222_NNPDF30NNLO_llll.deriv.DAOD_HIGG8D1.e5894_e5984_s3126_r10201_r10210_p4133
mc16_13TeV.364254.Sherpa_222_NNPDF30NNLO_llvv.deriv.DAOD_HIGG8D1.e5916_e5984_s3126_r10201_r10210_p4133
mc16_13TeV.364255.Sherpa_222_NNPDF30NNLO_lvvv.deriv.DAOD_HIGG8D1.e5916_e5984_s3126_r10201_r10210_p4133
mc16_13TeV.410155.aMcAtNloPythia8EvtGen_MEN30NLO_A14N23LO_ttW.deriv.DAOD_HIGG8D1.e5070_e5984_s3126_r10201_r10210_p4133
mc16_13TeV.410156.aMcAtNloPythia8EvtGen_MEN30NLO_A14N23LO_ttZnunu.deriv.DAOD_HIGG8D1.e5070_e5984_s3126_r10201_r10210_p4133
mc16_13TeV.410157.aMcAtNloPythia8EvtGen_MEN30NLO_A14N23LO_ttZqq.deriv.DAOD_HIGG8D1.e5070_e5984_s3126_r10201_r10210_p4133
mc16_13TeV.410218.aMcAtNloPythia8EvtGen_MEN30NLO_A14N23LO_ttee.deriv.DAOD_HIGG8D1.e5070_e5984_s3126_r10201_r10210_p4133
mc16_13TeV.410219.aMcAtNloPythia8EvtGen_MEN30NLO_A14N23LO_ttmumu.deriv.DAOD_HIGG8D1.e5070_e5984_s3126_r10201_r10210_p4133
mc16_13TeV.410220.aMcAtNloPythia8EvtGen_MEN30NLO_A14N23LO_tttautau.deriv.DAOD_HIGG8D1.e5070_e5984_s3126_r10201_r10210_p4133
mc16_13TeV.410276.aMcAtNloPythia8EvtGen_MEN30NLO_A14N23LO_ttee_mll_1_5.deriv.DAOD_HIGG8D1.e6087_e5984_s3126_r10201_r10210_p4133
mc16_13TeV.410277.aMcAtNloPythia8EvtGen_MEN30NLO_A14N23LO_ttmumu_mll_1_5.deriv.DAOD_HIGG8D1.e6087_e5984_s3126_r10201_r10210_p4133
mc16_13TeV.410278.aMcAtNloPythia8EvtGen_MEN30NLO_A14N23LO_tttautau_mll_1_5.deriv.DAOD_HIGG8D1.e6087_e5984_s3126_r10201_r10210_p4133
mc16_13TeV.410397.MadGraphPythia8EvtGen_ttbar_wbee_MEN30LO_A14N23LO.deriv.DAOD_HIGG8D1.e6086_e5984_s3126_r10201_r10210_p4133
mc16_13TeV.410398.MadGraphPythia8EvtGen_ttbar_wbmumu_MEN30LO_A14N23LO.deriv.DAOD_HIGG8D1.e6086_e5984_s3126_r10201_r10210_p4133
mc16_13TeV.410399.MadGraphPythia8EvtGen_ttbar_wbtautau_MEN30LO_A14N23LO.deriv.DAOD_HIGG8D1.e6086_e5984_s3126_r10201_r10210_p4133
mc16_13TeV.410658.PhPy8EG_A14_tchan_BW50_lept_top.deriv.DAOD_HIGG8D1.e6671_e5984_s3126_r10201_r10210_p4133
mc16_13TeV.410659.PhPy8EG_A14_tchan_BW50_lept_antitop.deriv.DAOD_HIGG8D1.e6671_e5984_s3126_r10201_r10210_p4133
mc16_13TeV.410644.PowhegPythia8EvtGen_A14_singletop_schan_lept_top.deriv.DAOD_HIGG8D1.e6527_e5984_s3126_r10201_r10210_p4133
mc16_13TeV.410645.PowhegPythia8EvtGen_A14_singletop_schan_lept_antitop.deriv.DAOD_HIGG8D1.e6527_s3126_r10201_r10210_p4133
mc16_13TeV.412063.aMcAtNloPythia8EvtGen_tllq_NNPDF30_nf4_A14.deriv.DAOD_TOPQ1.e7054_e5984_s3126_r10201_r10210_p4174
mc16_13TeV.304014.MadGraphPythia8EvtGen_A14NNPDF23_3top_SM.deriv.DAOD_HIGG8D1.e4324_e5984_s3126_r10201_r10210_p4133
mc16_13TeV.410080.MadGraphPythia8EvtGen_A14NNPDF23_4topSM.deriv.DAOD_HIGG8D1.e4111_e5984_s3126_r10201_r10210_p4133
mc16_13TeV.410081.MadGraphPythia8EvtGen_A14NNPDF23_ttbarWW.deriv.DAOD_HIGG8D1.e4111_e5984_s3126_r10201_r10210_p4133
mc16_13TeV.364100.Sherpa_221_NNPDF30NNLO_Zmumu_MAXHTPTV0_70_CVetoBVeto.deriv.DAOD_HIGG8D1.e5271_s3126_r10201_r10210_p4133
mc16_13TeV.364101.Sherpa_221_NNPDF30NNLO_Zmumu_MAXHTPTV0_70_CFilterBVeto.deriv.DAOD_HIGG8D1.e5271_s3126_r10201_r10210_p4133
mc16_13TeV.364101.Sherpa_221_NNPDF30NNLO_Zmumu_MAXHTPTV0_70_CFilterBVeto.deriv.DAOD_HIGG8D1.e5271_e5984_s3126_r10201_r10210_p4133
mc16_13TeV.364102.Sherpa_221_NNPDF30NNLO_Zmumu_MAXHTPTV0_70_BFilter.deriv.DAOD_HIGG8D1.e5271_s3126_r10201_r10210_p4133
mc16_13TeV.364103.Sherpa_221_NNPDF30NNLO_Zmumu_MAXHTPTV70_140_CVetoBVeto.deriv.DAOD_HIGG8D1.e5271_s3126_r10201_r10210_p4133
mc16_13TeV.364104.Sherpa_221_NNPDF30NNLO_Zmumu_MAXHTPTV70_140_CFilterBVeto.deriv.DAOD_HIGG8D1.e5271_s3126_r10201_r10210_p4133
mc16_13TeV.364106.Sherpa_221_NNPDF30NNLO_Zmumu_MAXHTPTV140_280_CVetoBVeto.deriv.DAOD_HIGG8D1.e5271_s3126_r10201_r10210_p4133
mc16_13TeV.364107.Sherpa_221_NNPDF30NNLO_Zmumu_MAXHTPTV140_280_CFilterBVeto.deriv.DAOD_HIGG8D1.e5271_s3126_r10201_r10210_p4133
mc16_13TeV.364108.Sherpa_221_NNPDF30NNLO_Zmumu_MAXHTPTV140_280_BFilter.deriv.DAOD_HIGG8D1.e5271_e5984_s3126_r10201_r10210_p4133
mc16_13TeV.364108.Sherpa_221_NNPDF30NNLO_Zmumu_MAXHTPTV140_280_BFilter.deriv.DAOD_HIGG8D1.e5271_s3126_r10201_r10210_p4133
mc16_13TeV.364109.Sherpa_221_NNPDF30NNLO_Zmumu_MAXHTPTV280_500_CVetoBVeto.deriv.DAOD_HIGG8D1.e5271_e5984_s3126_r10201_r10210_p4133
mc16_13TeV.364109.Sherpa_221_NNPDF30NNLO_Zmumu_MAXHTPTV280_500_CVetoBVeto.deriv.DAOD_HIGG8D1.e5271_s3126_r10201_r10210_p4133
mc16_13TeV.364110.Sherpa_221_NNPDF30NNLO_Zmumu_MAXHTPTV280_500_CFilterBVeto.deriv.DAOD_HIGG8D1.e5271_s3126_r10201_r10210_p4133
mc16_13TeV.364111.Sherpa_221_NNPDF30NNLO_Zmumu_MAXHTPTV280_500_BFilter.deriv.DAOD_HIGG8D1.e5271_e5984_s3126_r10201_r10210_p4133
mc16_13TeV.364111.Sherpa_221_NNPDF30NNLO_Zmumu_MAXHTPTV280_500_BFilter.deriv.DAOD_HIGG8D1.e5271_s3126_r10201_r10210_p4133
mc16_13TeV.364112.Sherpa_221_NNPDF30NNLO_Zmumu_MAXHTPTV500_1000.deriv.DAOD_HIGG8D1.e5271_e5984_s3126_r10201_r10210_p4133
mc16_13TeV.364112.Sherpa_221_NNPDF30NNLO_Zmumu_MAXHTPTV500_1000.deriv.DAOD_HIGG8D1.e5271_s3126_r10201_r10210_p4133
mc16_13TeV.364113.Sherpa_221_NNPDF30NNLO_Zmumu_MAXHTPTV1000_E_CMS.deriv.DAOD_HIGG8D1.e5271_s3126_r10201_r10210_p4133
mc16_13TeV.364114.Sherpa_221_NNPDF30NNLO_Zee_MAXHTPTV0_70_CVetoBVeto.deriv.DAOD_HIGG8D1.e5299_s3126_r10201_r10210_p4133
mc16_13TeV.364115.Sherpa_221_NNPDF30NNLO_Zee_MAXHTPTV0_70_CFilterBVeto.deriv.DAOD_HIGG8D1.e5299_e5984_s3126_r10201_r10210_p4133
mc16_13TeV.364116.Sherpa_221_NNPDF30NNLO_Zee_MAXHTPTV0_70_BFilter.deriv.DAOD_HIGG8D1.e5299_e5984_s3126_r10201_r10210_p4133
mc16_13TeV.364117.Sherpa_221_NNPDF30NNLO_Zee_MAXHTPTV70_140_CVetoBVeto.deriv.DAOD_HIGG8D1.e5299_e5984_s3126_r10201_r10210_p4133
mc16_13TeV.364118.Sherpa_221_NNPDF30NNLO_Zee_MAXHTPTV70_140_CFilterBVeto.deriv.DAOD_HIGG8D1.e5299_e5984_s3126_r10201_r10210_p4133
mc16_13TeV.364119.Sherpa_221_NNPDF30NNLO_Zee_MAXHTPTV70_140_BFilter.deriv.DAOD_HIGG8D1.e5299_e5984_s3126_r10201_r10210_p4133
mc16_13TeV.364120.Sherpa_221_NNPDF30NNLO_Zee_MAXHTPTV140_280_CVetoBVeto.deriv.DAOD_HIGG8D1.e5299_e5984_s3126_r10201_r10210_p4133
mc16_13TeV.364121.Sherpa_221_NNPDF30NNLO_Zee_MAXHTPTV140_280_CFilterBVeto.deriv.DAOD_HIGG8D1.e5299_e5984_s3126_r10201_r10210_p4133
mc16_13TeV.364122.Sherpa_221_NNPDF30NNLO_Zee_MAXHTPTV140_280_BFilter.deriv.DAOD_HIGG8D1.e5299_e5984_s3126_r10201_r10210_p4133
mc16_13TeV.364123.Sherpa_221_NNPDF30NNLO_Zee_MAXHTPTV280_500_CVetoBVeto.deriv.DAOD_HIGG8D1.e5299_e5984_s3126_r10201_r10210_p4133
mc16_13TeV.364124.Sherpa_221_NNPDF30NNLO_Zee_MAXHTPTV280_500_CFilterBVeto.deriv.DAOD_HIGG8D1.e5299_e5984_s3126_r10201_r10210_p4133
mc16_13TeV.364125.Sherpa_221_NNPDF30NNLO_Zee_MAXHTPTV280_500_BFilter.deriv.DAOD_HIGG8D1.e5299_e5984_s3126_r10201_r10210_p4133
mc16_13TeV.364126.Sherpa_221_NNPDF30NNLO_Zee_MAXHTPTV500_1000.deriv.DAOD_HIGG8D1.e5299_e5984_s3126_r10201_r10210_p4133

mc16_13TeV.364127.Sherpa_221_NNPDF30NNLO_Zee_MAXHTPTV1000_E_CMS.deriv.DAOD_HIGG8D1.e5299_e5984_s3126_r10201_r10210_p4133
mc16_13TeV.364128.Sherpa_221_NNPDF30NNLO_Ztautau_MAXHTPTV0_70_CVetoBVeto.deriv.DAOD_HIGG8D1.e5307_e5984_s3126_r10201_r10210_p4133
mc16_13TeV.364129.Sherpa_221_NNPDF30NNLO_Ztautau_MAXHTPTV0_70_CFilterBVeto.deriv.DAOD_HIGG8D1.e5307_e5984_s3126_r10201_r10210_p4133
mc16_13TeV.364130.Sherpa_221_NNPDF30NNLO_Ztautau_MAXHTPTV0_70_BFilter.deriv.DAOD_HIGG8D1.e5307_e5984_s3126_r10201_r10210_p4133
mc16_13TeV.364131.Sherpa_221_NNPDF30NNLO_Ztautau_MAXHTPTV70_140_CVetoBVeto.deriv.DAOD_HIGG8D1.e5307_e5984_s3126_r10201_r10210_p4133
mc16_13TeV.364132.Sherpa_221_NNPDF30NNLO_Ztautau_MAXHTPTV70_140_CFilterBVeto.deriv.DAOD_HIGG8D1.e5307_e5984_s3126_r10201_r10210_p4133
mc16_13TeV.364133.Sherpa_221_NNPDF30NNLO_Ztautau_MAXHTPTV70_140_BFilter.deriv.DAOD_HIGG8D1.e5307_e5984_s3126_r10201_r10210_p4133
mc16_13TeV.364134.Sherpa_221_NNPDF30NNLO_Ztautau_MAXHTPTV140_280_CVetoBVeto.deriv.DAOD_HIGG8D1.e5307_e5984_s3126_r10201_r10210_p4133
mc16_13TeV.364135.Sherpa_221_NNPDF30NNLO_Ztautau_MAXHTPTV140_280_CFilterBVeto.deriv.DAOD_HIGG8D1.e5307_e5984_s3126_r10201_r10210_p4133
mc16_13TeV.364136.Sherpa_221_NNPDF30NNLO_Ztautau_MAXHTPTV140_280_BFilter.deriv.DAOD_HIGG8D1.e5307_e5984_s3126_r10201_r10210_p4133
mc16_13TeV.364137.Sherpa_221_NNPDF30NNLO_Ztautau_MAXHTPTV280_500_CVetoBVeto.deriv.DAOD_HIGG8D1.e5307_e5984_s3126_r10201_r10210_p4133
mc16_13TeV.364138.Sherpa_221_NNPDF30NNLO_Ztautau_MAXHTPTV280_500_CFilterBVeto.deriv.DAOD_HIGG8D1.e5313_e5984_s3126_r10201_r10210_p4133
mc16_13TeV.364139.Sherpa_221_NNPDF30NNLO_Ztautau_MAXHTPTV280_500_BFilter.deriv.DAOD_HIGG8D1.e5313_e5984_s3126_r10201_r10210_p4133
mc16_13TeV.364140.Sherpa_221_NNPDF30NNLO_Ztautau_MAXHTPTV500_1000.deriv.DAOD_HIGG8D1.e5307_e5984_s3126_r10201_r10210_p4133
mc16_13TeV.364141.Sherpa_221_NNPDF30NNLO_Ztautau_MAXHTPTV1000_E_CMS.deriv.DAOD_HIGG8D1.e5307_e5984_s3126_r10201_r10210_p4133
mc16_13TeV.364198.Sherpa_221_NN30NNLO_Zmm_Mll10_40_MAXHTPTV0_70_BVeto.deriv.DAOD_HIGG8D1.e5421_e5984_s3126_r10201_r10210_p4133
mc16_13TeV.364199.Sherpa_221_NN30NNLO_Zmm_Mll10_40_MAXHTPTV0_70_BFilter.deriv.DAOD_HIGG8D1.e5421_e5984_s3126_r10201_r10210_p4133
mc16_13TeV.364200.Sherpa_221_NN30NNLO_Zmm_Mll10_40_MAXHTPTV70_280_BVeto.deriv.DAOD_HIGG8D1.e5421_e5984_s3126_r10201_r10210_p4133
mc16_13TeV.364201.Sherpa_221_NN30NNLO_Zmm_Mll10_40_MAXHTPTV70_280_BFilter.deriv.DAOD_HIGG8D1.e5421_e5984_s3126_r10201_r10210_p4133
mc16_13TeV.364202.Sherpa_221_NN30NNLO_Zmm_Mll10_40_MAXHTPTV280_E_CMS_BVeto.deriv.DAOD_HIGG8D1.e5421_e5984_s3126_r10201_r10210_p4133
mc16_13TeV.364203.Sherpa_221_NN30NNLO_Zmm_Mll10_40_MAXHTPTV280_E_CMS_BFilter.deriv.DAOD_HIGG8D1.e5421_e5984_s3126_r10201_r10210_p4133
mc16_13TeV.364204.Sherpa_221_NN30NNLO_Zee_Mll10_40_MAXHTPTV0_70_BVeto.deriv.DAOD_HIGG8D1.e5421_e5984_s3126_r10201_r10210_p4133
mc16_13TeV.364205.Sherpa_221_NN30NNLO_Zee_Mll10_40_MAXHTPTV0_70_BFilter.deriv.DAOD_HIGG8D1.e5421_e5984_s3126_r10201_r10210_p4133
mc16_13TeV.364206.Sherpa_221_NN30NNLO_Zee_Mll10_40_MAXHTPTV70_280_BVeto.deriv.DAOD_HIGG8D1.e5421_e5984_s3126_r10201_r10210_p4133
mc16_13TeV.364207.Sherpa_221_NN30NNLO_Zee_Mll10_40_MAXHTPTV70_280_BFilter.deriv.DAOD_HIGG8D1.e5421_e5984_s3126_r10201_r10210_p4133
mc16_13TeV.364208.Sherpa_221_NN30NNLO_Zee_Mll10_40_MAXHTPTV280_E_CMS_BVeto.deriv.DAOD_HIGG8D1.e5421_e5984_s3126_r10201_r10210_p4133
mc16_13TeV.364209.Sherpa_221_NN30NNLO_Zee_Mll10_40_MAXHTPTV280_E_CMS_BFilter.deriv.DAOD_HIGG8D1.e5421_e5984_s3126_r10201_r10210_p4133
mc16_13TeV.364210.Sherpa_221_NN30NNLO_Ztt_Mll10_40_MAXHTPTV0_70_BVeto.deriv.DAOD_HIGG8D1.e5421_e5984_s3126_r10201_r10210_p4133
mc16_13TeV.364211.Sherpa_221_NN30NNLO_Ztt_Mll10_40_MAXHTPTV0_70_BFilter.deriv.DAOD_HIGG8D1.e5421_e5984_s3126_r10201_r10210_p4133
mc16_13TeV.364212.Sherpa_221_NN30NNLO_Ztt_Mll10_40_MAXHTPTV70_280_BVeto.deriv.DAOD_HIGG8D1.e5421_e5984_s3126_r10201_r10210_p4133
mc16_13TeV.364213.Sherpa_221_NN30NNLO_Ztt_Mll10_40_MAXHTPTV70_280_BFilter.deriv.DAOD_HIGG8D1.e5421_e5984_s3126_r10201_r10210_p4133
mc16_13TeV.364214.Sherpa_221_NN30NNLO_Ztt_Mll10_40_MAXHTPTV280_E_CMS_BVeto.deriv.DAOD_HIGG8D1.e5421_e5984_s3126_r10201_r10210_p4133
mc16_13TeV.364215.Sherpa_221_NN30NNLO_Ztt_Mll10_40_MAXHTPTV280_E_CMS_BFilter.deriv.DAOD_HIGG8D1.e5421_e5984_s3126_r10201_r10210_p4133
mc16_13TeV.364156.Sherpa_221_NNPDF30NNLO_Wmunu_MAXHTPTV0_70_CVetoBVeto.deriv.DAOD_HIGG8D1.e5340_s3126_r10201_r10210_p4133
mc16_13TeV.364156.Sherpa_221_NNPDF30NNLO_Wmunu_MAXHTPTV0_70_CVetoBVeto.deriv.DAOD_HIGG8D1.e5340_e5984_s3126_s3136_r10201_r10210_p4133
mc16_13TeV.364157.Sherpa_221_NNPDF30NNLO_Wmunu_MAXHTPTV0_70_CFilterBVeto.deriv.DAOD_HIGG8D1.e5340_e5984_s3126_s3136_r10201_r10210_p4133
mc16_13TeV.364157.Sherpa_221_NNPDF30NNLO_Wmunu_MAXHTPTV0_70_CFilterBVeto.deriv.DAOD_HIGG8D1.e5340_s3126_r10201_r10210_p4133
mc16_13TeV.364157.Sherpa_221_NNPDF30NNLO_Wmunu_MAXHTPTV0_70_CFilterBVeto.deriv.DAOD_HIGG8D1.e5340_e5984_s3126_r10201_r10210_p4133
mc16_13TeV.364158.Sherpa_221_NNPDF30NNLO_Wmunu_MAXHTPTV0_70_BFilter.deriv.DAOD_HIGG8D1.e5340_e5984_s3126_s3136_r10201_r10210_p4133
mc16_13TeV.364158.Sherpa_221_NNPDF30NNLO_Wmunu_MAXHTPTV0_70_BFilter.deriv.DAOD_HIGG8D1.e5340_s3126_r10201_r10210_p4133
mc16_13TeV.364159.Sherpa_221_NNPDF30NNLO_Wmunu_MAXHTPTV70_140_CVetoBVeto.deriv.DAOD_HIGG8D1.e5340_s3126_r10201_r10210_p4133
mc16_13TeV.364159.Sherpa_221_NNPDF30NNLO_Wmunu_MAXHTPTV70_140_CVetoBVeto.deriv.DAOD_HIGG8D1.e5340_e5984_s3126_r10201_r10210_p4133
mc16_13TeV.364159.Sherpa_221_NNPDF30NNLO_Wmunu_MAXHTPTV70_140_CVetoBVeto.deriv.DAOD_HIGG8D1.e5340_e5984_s3126_s3136_r10201_r10210_p4133
mc16_13TeV.364160.Sherpa_221_NNPDF30NNLO_Wmunu_MAXHTPTV70_140_CFilterBVeto.deriv.DAOD_HIGG8D1.e5340_e5984_s3126_r10201_r10210_p4133
mc16_13TeV.364160.Sherpa_221_NNPDF30NNLO_Wmunu_MAXHTPTV70_140_CFilterBVeto.deriv.DAOD_HIGG8D1.e5340_s3126_r10201_r10210_p4133
mc16_13TeV.364161.Sherpa_221_NNPDF30NNLO_Wmunu_MAXHTPTV70_140_BFilter.deriv.DAOD_HIGG8D1.e5340_s3126_r10201_r10210_p4133
mc16_13TeV.364161.Sherpa_221_NNPDF30NNLO_Wmunu_MAXHTPTV70_140_BFilter.deriv.DAOD_HIGG8D1.e5340_e5984_s3126_s3136_r10201_r10210_p4133
mc16_13TeV.364162.Sherpa_221_NNPDF30NNLO_Wmunu_MAXHTPTV140_280_CVetoBVeto.deriv.DAOD_HIGG8D1.e5340_s3126_r10201_r10210_p4133
mc16_13TeV.364162.Sherpa_221_NNPDF30NNLO_Wmunu_MAXHTPTV140_280_CVetoBVeto.deriv.DAOD_HIGG8D1.e5340_e5984_s3126_s3136_r10201_r10210_p4133
mc16_13TeV.364163.Sherpa_221_NNPDF30NNLO_Wmunu_MAXHTPTV140_280_CFilterBVeto.deriv.DAOD_HIGG8D1.e5340_s3126_r10201_r10210_p4133
mc16_13TeV.364163.Sherpa_221_NNPDF30NNLO_Wmunu_MAXHTPTV140_280_CFilterBVeto.deriv.DAOD_HIGG8D1.e5340_e5984_s3126_s3136_r10201_r10210_p4133
mc16_13TeV.364163.Sherpa_221_NNPDF30NNLO_Wmunu_MAXHTPTV140_280_CFilterBVeto.deriv.DAOD_HIGG8D1.e5340_e5984_s3126_r10201_r10210_p4133
mc16_13TeV.364164.Sherpa_221_NNPDF30NNLO_Wmunu_MAXHTPTV140_280_BFilter.deriv.DAOD_HIGG8D1.e5340_s3126_r10201_r10210_p4133
mc16_13TeV.364164.Sherpa_221_NNPDF30NNLO_Wmunu_MAXHTPTV140_280_BFilter.deriv.DAOD_HIGG8D1.e5340_e5984_s3126_s3136_r10201_r10210_p4133
mc16_13TeV.364165.Sherpa_221_NNPDF30NNLO_Wmunu_MAXHTPTV280_500_CVetoBVeto.deriv.DAOD_HIGG8D1.e5340_e5984_s3126_s3136_r10201_r10210_p4133
mc16_13TeV.364165.Sherpa_221_NNPDF30NNLO_Wmunu_MAXHTPTV280_500_CVetoBVeto.deriv.DAOD_HIGG8D1.e5340_s3126_r10201_r10210_p4133
mc16_13TeV.364166.Sherpa_221_NNPDF30NNLO_Wmunu_MAXHTPTV280_500_CFilterBVeto.deriv.DAOD_HIGG8D1.e5340_s3126_r10201_r10210_p4133
mc16_13TeV.364166.Sherpa_221_NNPDF30NNLO_Wmunu_MAXHTPTV280_500_CFilterBVeto.deriv.DAOD_HIGG8D1.e5340_e5984_s3126_s3136_r10201_r10210_p4133
mc16_13TeV.364167.Sherpa_221_NNPDF30NNLO_Wmunu_MAXHTPTV280_500_BFilter.deriv.DAOD_HIGG8D1.e5340_e5984_s3126_r10201_r10210_p4133
mc16_13TeV.364167.Sherpa_221_NNPDF30NNLO_Wmunu_MAXHTPTV280_500_BFilter.deriv.DAOD_HIGG8D1.e5340_s3126_r10201_r10210_p4133
mc16_13TeV.364168.Sherpa_221_NNPDF30NNLO_Wmunu_MAXHTPTV500_1000.deriv.DAOD_HIGG8D1.e5340_s3126_r10201_r10210_p4133
mc16_13TeV.364168.Sherpa_221_NNPDF30NNLO_Wmunu_MAXHTPTV500_1000.deriv.DAOD_HIGG8D1.e5340_e5984_s3126_s3136_r10201_r10210_p4133

mc16_13TeV.364169.Sherpa_221_NNPDF30NNLO_Wmunu_MAXHTPTV1000_E_CMS.deriv.DAOD_HIGG8D1.e5340_s3126_r10201_r10210_p4133
mc16_13TeV.364169.Sherpa_221_NNPDF30NNLO_Wmunu_MAXHTPTV1000_E_CMS.deriv.DAOD_HIGG8D1.e5340_e5984_s3126_s3136_r10201_r10210_p4133
mc16_13TeV.364170.Sherpa_221_NNPDF30NNLO_Wenu_MAXHTPTV0_70_CVetoBVeto.deriv.DAOD_HIGG8D1.e5340_e5984_s3126_s3136_r10201_r10210_p4133
mc16_13TeV.364170.Sherpa_221_NNPDF30NNLO_Wenu_MAXHTPTV0_70_CVetoBVeto.deriv.DAOD_HIGG8D1.e5340_s3126_r10201_r10210_p4133
mc16_13TeV.364171.Sherpa_221_NNPDF30NNLO_Wenu_MAXHTPTV0_70_CFilterBVeto.deriv.DAOD_HIGG8D1.e5340_e5984_s3126_r10201_r10210_p4133
mc16_13TeV.364171.Sherpa_221_NNPDF30NNLO_Wenu_MAXHTPTV0_70_CFilterBVeto.deriv.DAOD_HIGG8D1.e5340_s3126_r10201_r10210_p4133
mc16_13TeV.364171.Sherpa_221_NNPDF30NNLO_Wenu_MAXHTPTV0_70_CFilterBVeto.deriv.DAOD_HIGG8D1.e5340_e5984_s3126_s3136_r10201_r10210_p4133
mc16_13TeV.364172.Sherpa_221_NNPDF30NNLO_Wenu_MAXHTPTV0_70_BFilter.deriv.DAOD_HIGG8D1.e5340_e5984_s3126_s3136_r10201_r10210_p4133
mc16_13TeV.364172.Sherpa_221_NNPDF30NNLO_Wenu_MAXHTPTV0_70_BFilter.deriv.DAOD_HIGG8D1.e5340_e5984_s3126_r10201_r10210_p4133
mc16_13TeV.364172.Sherpa_221_NNPDF30NNLO_Wenu_MAXHTPTV0_70_BFilter.deriv.DAOD_HIGG8D1.e5340_s3126_r10201_r10210_p4133
mc16_13TeV.364173.Sherpa_221_NNPDF30NNLO_Wenu_MAXHTPTV70_140_CVetoBVeto.deriv.DAOD_HIGG8D1.e5340_s3126_r10201_r10210_p4133
mc16_13TeV.364173.Sherpa_221_NNPDF30NNLO_Wenu_MAXHTPTV70_140_CVetoBVeto.deriv.DAOD_HIGG8D1.e5340_e5984_s3126_r10201_r10210_p4133
mc16_13TeV.364174.Sherpa_221_NNPDF30NNLO_Wenu_MAXHTPTV70_140_CFilterBVeto.deriv.DAOD_HIGG8D1.e5340_s3126_r10201_r10210_p4133
mc16_13TeV.364174.Sherpa_221_NNPDF30NNLO_Wenu_MAXHTPTV70_140_CFilterBVeto.deriv.DAOD_HIGG8D1.e5340_e5984_s3126_r10201_r10210_p4133
mc16_13TeV.364175.Sherpa_221_NNPDF30NNLO_Wenu_MAXHTPTV70_140_BFilter.deriv.DAOD_HIGG8D1.e5340_e5984_s3126_r10201_r10210_p4133
mc16_13TeV.364175.Sherpa_221_NNPDF30NNLO_Wenu_MAXHTPTV70_140_BFilter.deriv.DAOD_HIGG8D1.e5340_e5984_s3126_s3136_r10201_r10210_p4133
mc16_13TeV.364175.Sherpa_221_NNPDF30NNLO_Wenu_MAXHTPTV70_140_BFilter.deriv.DAOD_HIGG8D1.e5340_s3126_r10201_r10210_p4133
mc16_13TeV.364176.Sherpa_221_NNPDF30NNLO_Wenu_MAXHTPTV140_280_CVetoBVeto.deriv.DAOD_HIGG8D1.e5340_e5984_s3126_s3136_r10201_r10210_p4133
mc16_13TeV.364176.Sherpa_221_NNPDF30NNLO_Wenu_MAXHTPTV140_280_CVetoBVeto.deriv.DAOD_HIGG8D1.e5340_s3126_r10201_r10210_p4133
mc16_13TeV.364177.Sherpa_221_NNPDF30NNLO_Wenu_MAXHTPTV140_280_CFilterBVeto.deriv.DAOD_HIGG8D1.e5340_s3126_r10201_r10210_p4133
mc16_13TeV.364177.Sherpa_221_NNPDF30NNLO_Wenu_MAXHTPTV140_280_CFilterBVeto.deriv.DAOD_HIGG8D1.e5340_e5984_s3126_s3136_r10201_r10210_p4133
mc16_13TeV.364177.Sherpa_221_NNPDF30NNLO_Wenu_MAXHTPTV140_280_CFilterBVeto.deriv.DAOD_HIGG8D1.e5340_e5984_s3126_r10201_r10210_p4133
mc16_13TeV.364178.Sherpa_221_NNPDF30NNLO_Wenu_MAXHTPTV140_280_BFilter.deriv.DAOD_HIGG8D1.e5340_e5984_s3126_r10201_r10210_p4133
mc16_13TeV.364178.Sherpa_221_NNPDF30NNLO_Wenu_MAXHTPTV140_280_BFilter.deriv.DAOD_HIGG8D1.e5340_s3126_r10201_r10210_p4133
mc16_13TeV.364179.Sherpa_221_NNPDF30NNLO_Wenu_MAXHTPTV280_500_CVetoBVeto.deriv.DAOD_HIGG8D1.e5340_s3126_r10201_r10210_p4133
mc16_13TeV.364179.Sherpa_221_NNPDF30NNLO_Wenu_MAXHTPTV280_500_CVetoBVeto.deriv.DAOD_HIGG8D1.e5340_e5984_s3126_r10201_r10210_p4133
mc16_13TeV.364180.Sherpa_221_NNPDF30NNLO_Wenu_MAXHTPTV280_500_CFilterBVeto.deriv.DAOD_HIGG8D1.e5340_e5984_s3126_s3136_r10201_r10210_p4133
mc16_13TeV.364180.Sherpa_221_NNPDF30NNLO_Wenu_MAXHTPTV280_500_CFilterBVeto.deriv.DAOD_HIGG8D1.e5340_s3126_r10201_r10210_p4133
mc16_13TeV.364181.Sherpa_221_NNPDF30NNLO_Wenu_MAXHTPTV280_500_BFilter.deriv.DAOD_HIGG8D1.e5340_e5984_s3126_r10201_r10210_p4133
mc16_13TeV.364181.Sherpa_221_NNPDF30NNLO_Wenu_MAXHTPTV280_500_BFilter.deriv.DAOD_HIGG8D1.e5340_s3126_r10201_r10210_p4133
mc16_13TeV.364182.Sherpa_221_NNPDF30NNLO_Wenu_MAXHTPTV500_1000.deriv.DAOD_HIGG8D1.e5340_s3126_r10201_r10210_p4133
mc16_13TeV.364182.Sherpa_221_NNPDF30NNLO_Wenu_MAXHTPTV500_1000.deriv.DAOD_HIGG8D1.e5340_e5984_s3126_s3136_r10201_r10210_p4133
mc16_13TeV.364183.Sherpa_221_NNPDF30NNLO_Wenu_MAXHTPTV1000_E_CMS.deriv.DAOD_HIGG8D1.e5340_e5984_s3126_r10201_r10210_p4133
mc16_13TeV.364184.Sherpa_221_NNPDF30NNLO_Wtaunu_MAXHTPTV0_70_CVetoBVeto.deriv.DAOD_HIGG8D1.e5340_e5984_s3126_r10201_r10210_p4133
mc16_13TeV.364184.Sherpa_221_NNPDF30NNLO_Wtaunu_MAXHTPTV0_70_CVetoBVeto.deriv.DAOD_HIGG8D1.e5340_s3126_r10201_r10210_p4133
mc16_13TeV.364185.Sherpa_221_NNPDF30NNLO_Wtaunu_MAXHTPTV0_70_CFilterBVeto.deriv.DAOD_HIGG8D1.e5340_e5984_s3126_r10201_r10210_p4133
mc16_13TeV.364186.Sherpa_221_NNPDF30NNLO_Wtaunu_MAXHTPTV0_70_BFilter.deriv.DAOD_HIGG8D1.e5340_e5984_s3126_r10201_r10210_p4133
mc16_13TeV.364187.Sherpa_221_NNPDF30NNLO_Wtaunu_MAXHTPTV70_140_CVetoBVeto.deriv.DAOD_HIGG8D1.e5340_e5984_s3126_r10201_r10210_p4133
mc16_13TeV.364188.Sherpa_221_NNPDF30NNLO_Wtaunu_MAXHTPTV70_140_CFilterBVeto.deriv.DAOD_HIGG8D1.e5340_e5984_s3126_r10201_r10210_p4133
mc16_13TeV.364189.Sherpa_221_NNPDF30NNLO_Wtaunu_MAXHTPTV70_140_BFilter.deriv.DAOD_HIGG8D1.e5340_s3126_r10201_r10210_p4133
mc16_13TeV.364189.Sherpa_221_NNPDF30NNLO_Wtaunu_MAXHTPTV70_140_BFilter.deriv.DAOD_HIGG8D1.e5340_e5984_s3126_r10201_r10210_p4133
mc16_13TeV.364190.Sherpa_221_NNPDF30NNLO_Wtaunu_MAXHTPTV140_280_CVetoBVeto.deriv.DAOD_HIGG8D1.e5340_s3126_r10201_r10210_p4133
mc16_13TeV.364190.Sherpa_221_NNPDF30NNLO_Wtaunu_MAXHTPTV140_280_CVetoBVeto.deriv.DAOD_HIGG8D1.e5340_e5984_s3126_s3136_r10201_r10210_p4133
mc16_13TeV.364191.Sherpa_221_NNPDF30NNLO_Wtaunu_MAXHTPTV140_280_CFilterBVeto.deriv.DAOD_HIGG8D1.e5340_e5984_s3126_s3136_r10201_r10210_p4133
mc16_13TeV.364191.Sherpa_221_NNPDF30NNLO_Wtaunu_MAXHTPTV140_280_CFilterBVeto.deriv.DAOD_HIGG8D1.e5340_s3126_r10201_r10210_p4133
mc16_13TeV.364192.Sherpa_221_NNPDF30NNLO_Wtaunu_MAXHTPTV140_280_BFilter.deriv.DAOD_HIGG8D1.e5340_e5984_s3126_r10201_r10210_p4133
mc16_13TeV.364193.Sherpa_221_NNPDF30NNLO_Wtaunu_MAXHTPTV280_500_CVetoBVeto.deriv.DAOD_HIGG8D1.e5340_e5984_s3126_r10201_r10210_p4133
mc16_13TeV.364193.Sherpa_221_NNPDF30NNLO_Wtaunu_MAXHTPTV280_500_CVetoBVeto.deriv.DAOD_HIGG8D1.e5340_e5984_s3126_s3136_r10201_r10210_p4133
mc16_13TeV.364194.Sherpa_221_NNPDF30NNLO_Wtaunu_MAXHTPTV280_500_CFilterBVeto.deriv.DAOD_HIGG8D1.e5340_e5984_s3126_r10201_r10210_p4133
mc16_13TeV.364194.Sherpa_221_NNPDF30NNLO_Wtaunu_MAXHTPTV280_500_CFilterBVeto.deriv.DAOD_HIGG8D1.e5340_s3126_r10201_r10210_p4133
mc16_13TeV.364194.Sherpa_221_NNPDF30NNLO_Wtaunu_MAXHTPTV280_500_CFilterBVeto.deriv.DAOD_HIGG8D1.e5340_e5984_s3126_s3136_r10201_r10210_p4133
mc16_13TeV.364195.Sherpa_221_NNPDF30NNLO_Wtaunu_MAXHTPTV280_500_BFilter.deriv.DAOD_HIGG8D1.e5340_e5984_s3126_r10201_r10210_p4133
mc16_13TeV.364195.Sherpa_221_NNPDF30NNLO_Wtaunu_MAXHTPTV280_500_BFilter.deriv.DAOD_HIGG8D1.e5340_s3126_r10201_r10210_p4133
mc16_13TeV.364196.Sherpa_221_NNPDF30NNLO_Wtaunu_MAXHTPTV500_1000.deriv.DAOD_HIGG8D1.e5340_e5984_s3126_s3136_r10201_r10210_p4133
mc16_13TeV.364196.Sherpa_221_NNPDF30NNLO_Wtaunu_MAXHTPTV500_1000.deriv.DAOD_HIGG8D1.e5340_s3126_r10201_r10210_p4133
mc16_13TeV.364197.Sherpa_221_NNPDF30NNLO_Wtaunu_MAXHTPTV1000_E_CMS.deriv.DAOD_HIGG8D1.e5340_e5984_s3126_r10201_r10210_p4133
mc16_13TeV.364500.Sherpa_222_NNPDF30NNLO_eegamma_pty_7_15.deriv.DAOD_HIGG8D1.e5928_e5984_s3126_r10201_r10210_p4133
mc16_13TeV.364501.Sherpa_222_NNPDF30NNLO_eegamma_pty_15_35.deriv.DAOD_HIGG8D1.e5928_e5984_s3126_r10201_r10210_p4133
mc16_13TeV.364502.Sherpa_222_NNPDF30NNLO_eegamma_pty_35_70.deriv.DAOD_HIGG8D1.e5928_e5984_s3126_r10201_r10210_p4133
mc16_13TeV.364503.Sherpa_222_NNPDF30NNLO_eegamma_pty_70_140.deriv.DAOD_HIGG8D1.e5928_e5984_s3126_r10201_r10210_p4133
mc16_13TeV.364504.Sherpa_222_NNPDF30NNLO_eegamma_pty_140_E_CMS.deriv.DAOD_HIGG8D1.e5928_e5984_s3126_r10201_r10210_p4133
mc16_13TeV.364505.Sherpa_222_NNPDF30NNLO_mumugamma_pty_7_15.deriv.DAOD_HIGG8D1.e5928_e5984_s3126_r10201_r10210_p4133

mc16_13TeV.364506.Sherpa_222_NNPDF30NNLO_mumugamma_pty_15_35.deriv.DAOD_HIGG8D1.e5928_e5984_s3126_r10201_r10210_p4133
mc16_13TeV.364507.Sherpa_222_NNPDF30NNLO_mumugamma_pty_35_70.deriv.DAOD_HIGG8D1.e5928_e5984_s3126_r10201_r10210_p4133
mc16_13TeV.364508.Sherpa_222_NNPDF30NNLO_mumugamma_pty_70_140.deriv.DAOD_HIGG8D1.e5928_e5984_s3126_r10201_r10210_p4133
mc16_13TeV.364509.Sherpa_222_NNPDF30NNLO_mumugamma_pty_140_E_CMS.deriv.DAOD_HIGG8D1.e5928_e5984_s3126_r10201_r10210_p4133
mc16_13TeV.364510.Sherpa_222_NNPDF30NNLO_tautaugamma_pty_7_15.deriv.DAOD_HIGG8D1.e5928_e5984_s3126_r10201_r10210_p4133
mc16_13TeV.364511.Sherpa_222_NNPDF30NNLO_tautaugamma_pty_15_35.deriv.DAOD_HIGG8D1.e5928_e5984_s3126_r10201_r10210_p4133
mc16_13TeV.364512.Sherpa_222_NNPDF30NNLO_tautaugamma_pty_35_70.deriv.DAOD_HIGG8D1.e5928_e5984_s3126_r10201_r10210_p4133
mc16_13TeV.364513.Sherpa_222_NNPDF30NNLO_tautaugamma_pty_70_140.deriv.DAOD_HIGG8D1.e5982_e5984_s3126_r10201_r10210_p4133
mc16_13TeV.364513.Sherpa_222_NNPDF30NNLO_tautaugamma_pty_70_140.deriv.DAOD_HIGG8D1.e5928_e5984_s3126_r10201_r10210_p4133
mc16_13TeV.364514.Sherpa_222_NNPDF30NNLO_tautaugamma_pty_140_E_CMS.deriv.DAOD_HIGG8D1.e5928_e5984_s3126_r10201_r10210_p4133
mc16_13TeV.364521.Sherpa_222_NNPDF30NNLO_enugamma_pty_7_15.deriv.DAOD_HIGG8D1.e5928_e5984_s3126_r10201_r10210_p4133
mc16_13TeV.364522.Sherpa_222_NNPDF30NNLO_enugamma_pty_15_35.deriv.DAOD_HIGG8D1.e5928_e5984_s3126_r10201_r10210_p4133
mc16_13TeV.364523.Sherpa_222_NNPDF30NNLO_enugamma_pty_35_70.deriv.DAOD_HIGG8D1.e5928_e5984_s3126_r10201_r10210_p4133
mc16_13TeV.364524.Sherpa_222_NNPDF30NNLO_enugamma_pty_70_140.deriv.DAOD_HIGG8D1.e5928_e5984_s3126_r10201_r10210_p4133
mc16_13TeV.364525.Sherpa_222_NNPDF30NNLO_enugamma_pty_140_E_CMS.deriv.DAOD_HIGG8D1.e5928_e5984_s3126_r10201_r10210_p4133
mc16_13TeV.364526.Sherpa_222_NNPDF30NNLO_munugamma_pty_7_15.deriv.DAOD_HIGG8D1.e5928_e5984_s3126_r10201_r10210_p4133
mc16_13TeV.364527.Sherpa_222_NNPDF30NNLO_munugamma_pty_15_35.deriv.DAOD_HIGG8D1.e5928_e5984_s3126_r10201_r10210_p4133
mc16_13TeV.364528.Sherpa_222_NNPDF30NNLO_munugamma_pty_35_70.deriv.DAOD_HIGG8D1.e5928_e5984_s3126_r10201_r10210_p4133
mc16_13TeV.364529.Sherpa_222_NNPDF30NNLO_munugamma_pty_70_140.deriv.DAOD_HIGG8D1.e5928_e5984_s3126_r10201_r10210_p4133
mc16_13TeV.364530.Sherpa_222_NNPDF30NNLO_munugamma_pty_140_E_CMS.deriv.DAOD_HIGG8D1.e5928_e5984_s3126_r10201_r10210_p4133
mc16_13TeV.364531.Sherpa_222_NNPDF30NNLO_taunugamma_pty_7_15.deriv.DAOD_HIGG8D1.e5928_e5984_s3126_r10201_r10210_p4133
mc16_13TeV.364532.Sherpa_222_NNPDF30NNLO_taunugamma_pty_15_35.deriv.DAOD_HIGG8D1.e5928_e5984_s3126_r10201_r10210_p4133
mc16_13TeV.364533.Sherpa_222_NNPDF30NNLO_taunugamma_pty_35_70.deriv.DAOD_HIGG8D1.e5928_e5984_s3126_r10201_r10210_p4133
mc16_13TeV.364534.Sherpa_222_NNPDF30NNLO_taunugamma_pty_70_140.deriv.DAOD_HIGG8D1.e5928_e5984_s3126_r10201_r10210_p4133
mc16_13TeV.364535.Sherpa_222_NNPDF30NNLO_taunugamma_pty_140_E_CMS.deriv.DAOD_HIGG8D1.e5928_e5984_s3126_r10201_r10210_p4133
mc16_13TeV.410560.MadGraphPythia8EvtGen_A14_tZ_4fl_tchan_noAllHad.deriv.DAOD_HIGG8D1.e5803_e5984_s3126_r10201_r10210_p4133
mc16_13TeV.410013.PowhegPythiaEvtGen_P2012_Wt_inclusive_top.deriv.DAOD_HIGG8D1.e3753_s3126_r10201_r10210_p4133
mc16_13TeV.410014.PowhegPythiaEvtGen_P2012_Wt_inclusive_antitop.deriv.DAOD_HIGG8D1.e3753_s3126_r10201_r10210_p4133
mc16_13TeV.410408.aMcAtNloPythia8EvtGen_tWZ_Ztoll_minDR1.deriv.DAOD_HIGG8D1.e6423_e5984_s3126_r10201_r10210_p4133
mc16_13TeV.364242.Sherpa_222_NNPDF30NNLO_WWW_3l3v_EW6.deriv.DAOD_HIGG8D1.e5887_e5984_s3126_r10201_r10210_p4133
mc16_13TeV.364243.Sherpa_222_NNPDF30NNLO_WWZ_4l2v_EW6.deriv.DAOD_HIGG8D1.e5887_e5984_s3126_r10201_r10210_p4133
mc16_13TeV.364244.Sherpa_222_NNPDF30NNLO_WWZ_2l4v_EW6.deriv.DAOD_HIGG8D1.e5887_e5984_s3126_r10201_r10210_p4133
mc16_13TeV.364245.Sherpa_222_NNPDF30NNLO_WZZ_5l1v_EW6.deriv.DAOD_HIGG8D1.e5887_e5984_s3126_r10201_r10210_p4133
mc16_13TeV.364246.Sherpa_222_NNPDF30NNLO_WZZ_3l3v_EW6.deriv.DAOD_HIGG8D1.e5887_e5984_s3126_r10201_r10210_p4133
mc16_13TeV.364247.Sherpa_222_NNPDF30NNLO_ZZZ_6l0v_EW6.deriv.DAOD_HIGG8D1.e5887_e5984_s3126_r10201_r10210_p4133
mc16_13TeV.364248.Sherpa_222_NNPDF30NNLO_ZZZ_4l2v_EW6.deriv.DAOD_HIGG8D1.e5887_e5984_s3126_r10201_r10210_p4133
mc16_13TeV.364249.Sherpa_222_NNPDF30NNLO_ZZZ_2l4v_EW6.deriv.DAOD_HIGG8D1.e5887_e5984_s3126_r10201_r10210_p4133
mc16_13TeV.342284.Pythia8EvtGen_A14NNPDF23LO_WH125_inc.deriv.DAOD_HIGG8D1.e4246_e5984_s3126_r10201_r10210_p4133
mc16_13TeV.342285.Pythia8EvtGen_A14NNPDF23LO_ZH125_inc.deriv.DAOD_HIGG8D1.e4246_e5984_s3126_r10201_r10210_p4133
mc16_13TeV.341998.aMcAtNloHppEG_UEEE5_CTEQ6L1_CT10ME_tWH125_gamgam_yt_plus1.deriv.DAOD_HIGG8D1.e4394_e5984_s3126_r10201_r10210_p4133
mc16_13TeV.410470.PhPy8EG_A14_ttbar_hdamp258p75_nonallhad.deriv.DAOD_HIGG8D1.e6337_e5984_s3126_r10201_r10210_p4133
mc16_13TeV.410472.PhPy8EG_A14_ttbar_hdamp258p75_dil.deriv.DAOD_HIGG8D1.e6348_e5984_s3126_r10201_r10210_p4133
mc16_13TeV.346343.PhPy8EG_A14NNPDF23_NNPDF30ME_ttH125_allhad.deriv.DAOD_HIGG8D1.e7148_e5984_s3126_r10201_r10210_p4133
mc16_13TeV.346344.PhPy8EG_A14NNPDF23_NNPDF30ME_ttH125_semilep.deriv.DAOD_HIGG8D1.e7148_e5984_a875_r10201_r10210_p4133
mc16_13TeV.346345.PhPy8EG_A14NNPDF23_NNPDF30ME_ttH125_dilep.deriv.DAOD_HIGG8D1.e7148_e5984_a875_r10201_r10210_p4133

mc16e:
mc16_13TeV.361605.PowhegPy8EG_CT10nloME_AZNLOCTEQ6L1_ZZvvvv_mll4.deriv.DAOD_HIGG8D1.e4054_e5984_s3126_r10724_r10726_p4133
mc16_13TeV.361602.PowhegPy8EG_CT10nloME_AZNLOCTEQ6L1_WZlvvv_mll4.deriv.DAOD_HIGG8D1.e4054_e5984_s3126_r10724_r10726_p4133
mc16_13TeV.361601.PowhegPy8EG_CT10nloME_AZNLOCTEQ6L1_WZlvll_mll4.deriv.DAOD_HIGG8D1.e4475_e5984_s3126_r10724_r10726_p4133
mc16_13TeV.361600.PowhegPy8EG_CT10nloME_AZNLOCTEQ6L1_WWlvlv.deriv.DAOD_HIGG8D1.e4616_e5984_s3126_r10724_r10726_p4133
mc16_13TeV.361603.PowhegPy8EG_CT10nloME_AZNLOCTEQ6L1_ZZllll_mll4.deriv.DAOD_HIGG8D1.e4475_e5984_s3126_r10724_r10726_p4133
mc16_13TeV.361604.PowhegPy8EG_CT10nloME_AZNLOCTEQ6L1_ZZvvll_mll4.deriv.DAOD_HIGG8D1.e4475_e5984_s3126_r10724_r10726_p4133
mc16_13TeV.364288.Sherpa_222_NNPDF30NNLO_llll_lowMllPtComplement.deriv.DAOD_HIGG8D1.e6096_s3126_r10724_p3983 mc16_13TeV.364287.Sherpa_222_NNPDF3
mc16_13TeV.364285.Sherpa_222_NNPDF30NNLO_llvvjj_EW6.deriv.DAOD_HIGG8D1.e6055_e5984_s3126_r10724_r10726_p3983
mc16_13TeV.364284.Sherpa_222_NNPDF30NNLO_lllvjj_EW6.deriv.DAOD_HIGG8D1.e6055_s3126_r10724_p3983
mc16_13TeV.364283.Sherpa_222_NNPDF30NNLO_lllljj_EW6.deriv.DAOD_HIGG8D1.e6055_s3126_r10724_p3983
mc16_13TeV.364739.MGPy8EG_NNPDF30NLO_A14NNPDF23LO_lvlljjEW6_OFMinus.deriv.DAOD_HIGG8D1.e7421_e5984_s3126_r10724_r10726_p4133
mc16_13TeV.364742.MGPy8EG_NNPDF30NLO_A14NNPDF23LO_lvlljjEW6_SFPlus.deriv.DAOD_HIGG8D1.e7421_e5984_s3126_r10724_r10726_p4133
mc16_13TeV.364740.MGPy8EG_NNPDF30NLO_A14NNPDF23LO_lvlljjEW6_OFPlus.deriv.DAOD_HIGG8D1.e7421_e5984_s3126_r10724_r10726_p4133
mc16_13TeV.364741.MGPy8EG_NNPDF30NLO_A14NNPDF23LO_lvlljjEW6_SFMinus.deriv.DAOD_HIGG8D1.e7421_e5984_s3126_r10724_r10726_p4133
mc16_13TeV.364253.Sherpa_222_NNPDF30NNLO_lllv.deriv.DAOD_HIGG8D1.e5916_e5984_s3126_r10724_r10726_p4133

mc16_13TeV.364250.Sherpa_222_NNPDF30NNLO_llll.deriv.DAOD_HIGG8D1.e5894_e5984_s3126_r10724_r10726_p4133
mc16_13TeV.364254.Sherpa_222_NNPDF30NNLO_llvv.deriv.DAOD_HIGG8D1.e5916_e5984_s3126_r10724_r10726_p4133
mc16_13TeV.364255.Sherpa_222_NNPDF30NNLO_lvvv.deriv.DAOD_HIGG8D1.e5916_e5984_s3126_r10724_r10726_p4133
mc16_13TeV.410155.aMcAtNloPythia8EvtGen_MEN30NLO_A14N23LO_ttW.deriv.DAOD_HIGG8D1.e5070_e5984_s3126_r10724_r10726_p4133
mc16_13TeV.410156.aMcAtNloPythia8EvtGen_MEN30NLO_A14N23LO_ttZnunu.deriv.DAOD_HIGG8D1.e5070_e5984_s3126_r10724_r10726_p4133
mc16_13TeV.410157.aMcAtNloPythia8EvtGen_MEN30NLO_A14N23LO_ttZqq.deriv.DAOD_HIGG8D1.e5070_e5984_s3126_r10724_r10726_p4133
mc16_13TeV.410218.aMcAtNloPythia8EvtGen_MEN30NLO_A14N23LO_ttee.deriv.DAOD_HIGG8D1.e5070_e5984_s3126_r10724_r10726_p4133
mc16_13TeV.410219.aMcAtNloPythia8EvtGen_MEN30NLO_A14N23LO_ttmumu.deriv.DAOD_HIGG8D1.e5070_e5984_s3126_r10724_r10726_p4133
mc16_13TeV.410220.aMcAtNloPythia8EvtGen_MEN30NLO_A14N23LO_tttautau.deriv.DAOD_HIGG8D1.e5070_e5984_s3126_r10724_r10726_p4133
mc16_13TeV.410276.aMcAtNloPythia8EvtGen_MEN30NLO_A14N23LO_ttee_mll_1_5.deriv.DAOD_HIGG8D1.e6087_e5984_s3126_r10724_r10726_p4133
mc16_13TeV.410277.aMcAtNloPythia8EvtGen_MEN30NLO_A14N23LO_ttmumu_mll_1_5.deriv.DAOD_HIGG8D1.e6087_e5984_s3126_r10724_r10726_p4133
mc16_13TeV.410278.aMcAtNloPythia8EvtGen_MEN30NLO_A14N23LO_tttautau_mll_1_5.deriv.DAOD_HIGG8D1.e6087_e5984_s3126_r10724_r10726_p4133
mc16_13TeV.410397.MadGraphPythia8EvtGen_ttbar_wbee_MEN30LO_A14N23LO.deriv.DAOD_HIGG8D1.e6086_e5984_s3126_r10724_r10726_p4133
mc16_13TeV.410398.MadGraphPythia8EvtGen_ttbar_wbmumu_MEN30LO_A14N23LO.deriv.DAOD_HIGG8D1.e6086_e5984_s3126_r10724_r10726_p4133
mc16_13TeV.410399.MadGraphPythia8EvtGen_ttbar_wbtautau_MEN30LO_A14N23LO.deriv.DAOD_HIGG8D1.e6086_e5984_s3126_r10724_r10726_p4133
mc16_13TeV.410658.PhPy8EG_A14_tchan_BW50_lept_top.deriv.DAOD_HIGG8D1.e6671_e5984_s3126_s3136_r10724_r10726_p4133
mc16_13TeV.410659.PhPy8EG_A14_tchan_BW50_lept_antitop.deriv.DAOD_HIGG8D1.e6671_e5984_s3126_s3136_r10724_r10726_p4133
mc16_13TeV.410644.PowhegPythia8EvtGen_A14_singletop_schan_lept_top.deriv.DAOD_HIGG8D1.e6527_e5984_s3126_r10724_r10726_p4133
mc16_13TeV.410645.PowhegPythia8EvtGen_A14_singletop_schan_lept_antitop.deriv.DAOD_HIGG8D1.e6527_e5984_s3126_r10724_r10726_p4133
mc16_13TeV.412063.aMcAtNloPythia8EvtGen_tllq_NNPDF30_nf4_A14.deriv.DAOD_TOPQ1.e7054_e5984_s3126_r10724_r10726_p4174
mc16_13TeV.304014.MadGraphPythia8EvtGen_A14NNPDF23_3top_SM.deriv.DAOD_HIGG8D1.e4324_e5984_s3126_r10724_r10726_p4133
mc16_13TeV.410080.MadGraphPythia8EvtGen_A14NNPDF23_4topSM.deriv.DAOD_HIGG8D1.e4111_e5984_s3126_r10724_r10726_p4133
mc16_13TeV.410081.MadGraphPythia8EvtGen_A14NNPDF23_ttbarWW.deriv.DAOD_HIGG8D1.e4111_e5984_s3126_r10724_r10726_p4133
mc16_13TeV.364100.Sherpa_221_NNPDF30NNLO_Zmumu_MAXHTPTV0_70_CVetoBVeto.deriv.DAOD_HIGG8D1.e5271_e5984_s3126_s3136_r10724_r10726_p4133
mc16_13TeV.364100.Sherpa_221_NNPDF30NNLO_Zmumu_MAXHTPTV0_70_CVetoBVeto.deriv.DAOD_HIGG8D1.e5271_e5984_s3126_r10724_r10726_p4133
mc16_13TeV.364101.Sherpa_221_NNPDF30NNLO_Zmumu_MAXHTPTV0_70_CFilterBVeto.deriv.DAOD_HIGG8D1.e5271_e5984_s3126_r10724_r10726_p4133
mc16_13TeV.364102.Sherpa_221_NNPDF30NNLO_Zmumu_MAXHTPTV0_70_BFilter.deriv.DAOD_HIGG8D1.e5271_e5984_s3126_s3136_r10724_r10726_p4133
mc16_13TeV.364102.Sherpa_221_NNPDF30NNLO_Zmumu_MAXHTPTV0_70_BFilter.deriv.DAOD_HIGG8D1.e5271_e5984_s3126_r10724_r10726_p4133
mc16_13TeV.364103.Sherpa_221_NNPDF30NNLO_Zmumu_MAXHTPTV70_140_CVetoBVeto.deriv.DAOD_HIGG8D1.e5271_e5984_s3126_r10724_r10726_p4133
mc16_13TeV.364103.Sherpa_221_NNPDF30NNLO_Zmumu_MAXHTPTV70_140_CVetoBVeto.deriv.DAOD_HIGG8D1.e5271_e5984_s3126_s3136_r10724_r10726_p4133
mc16_13TeV.364104.Sherpa_221_NNPDF30NNLO_Zmumu_MAXHTPTV70_140_CFilterBVeto.deriv.DAOD_HIGG8D1.e5271_e5984_s3126_r10724_r10726_p4133
mc16_13TeV.364104.Sherpa_221_NNPDF30NNLO_Zmumu_MAXHTPTV70_140_CFilterBVeto.deriv.DAOD_HIGG8D1.e5271_e5984_s3126_s3136_r10724_r10726_p4133
mc16_13TeV.364106.Sherpa_221_NNPDF30NNLO_Zmumu_MAXHTPTV140_280_CVetoBVeto.deriv.DAOD_HIGG8D1.e5271_e5984_s3126_s3136_r10724_r10726_p4133
mc16_13TeV.364106.Sherpa_221_NNPDF30NNLO_Zmumu_MAXHTPTV140_280_CVetoBVeto.deriv.DAOD_HIGG8D1.e5271_e5984_s3126_r10724_r10726_p4133
mc16_13TeV.364107.Sherpa_221_NNPDF30NNLO_Zmumu_MAXHTPTV140_280_CFilterBVeto.deriv.DAOD_HIGG8D1.e5271_e5984_s3126_r10724_r10726_p4133
mc16_13TeV.364107.Sherpa_221_NNPDF30NNLO_Zmumu_MAXHTPTV140_280_CFilterBVeto.deriv.DAOD_HIGG8D1.e5271_e5984_s3126_s3136_r10724_r10726_p4133
mc16_13TeV.364108.Sherpa_221_NNPDF30NNLO_Zmumu_MAXHTPTV140_280_BFilter.deriv.DAOD_HIGG8D1.e5271_e5984_s3126_r10724_r10726_p4133
mc16_13TeV.364109.Sherpa_221_NNPDF30NNLO_Zmumu_MAXHTPTV280_500_CVetoBVeto.deriv.DAOD_HIGG8D1.e5271_e5984_s3126_r10724_r10726_p4133
mc16_13TeV.364110.Sherpa_221_NNPDF30NNLO_Zmumu_MAXHTPTV280_500_CFilterBVeto.deriv.DAOD_HIGG8D1.e5271_e5984_s3126_r10724_r10726_p4133
mc16_13TeV.364110.Sherpa_221_NNPDF30NNLO_Zmumu_MAXHTPTV280_500_CFilterBVeto.deriv.DAOD_HIGG8D1.e5271_e5984_s3126_s3136_r10724_r10726_p4133
mc16_13TeV.364111.Sherpa_221_NNPDF30NNLO_Zmumu_MAXHTPTV280_500_BFilter.deriv.DAOD_HIGG8D1.e5271_e5984_s3126_s3136_r10724_r10726_p4133
mc16_13TeV.364111.Sherpa_221_NNPDF30NNLO_Zmumu_MAXHTPTV280_500_BFilter.deriv.DAOD_HIGG8D1.e5271_e5984_s3126_r10724_r10726_p4133
mc16_13TeV.364112.Sherpa_221_NNPDF30NNLO_Zmumu_MAXHTPTV500_1000.deriv.DAOD_HIGG8D1.e5271_e5984_s3126_r10724_r10726_p4133
mc16_13TeV.364113.Sherpa_221_NNPDF30NNLO_Zmumu_MAXHTPTV1000_E_CMS.deriv.DAOD_HIGG8D1.e5271_e5984_s3126_r10724_r10726_p4133
mc16_13TeV.364113.Sherpa_221_NNPDF30NNLO_Zmumu_MAXHTPTV1000_E_CMS.deriv.DAOD_HIGG8D1.e5271_e5984_s3126_s3136_r10724_r10726_p4133
mc16_13TeV.364114.Sherpa_221_NNPDF30NNLO_Zee_MAXHTPTV0_70_CVetoBVeto.deriv.DAOD_HIGG8D1.e5299_e5984_s3126_s3136_r10724_r10726_p4133
mc16_13TeV.364114.Sherpa_221_NNPDF30NNLO_Zee_MAXHTPTV0_70_CVetoBVeto.deriv.DAOD_HIGG8D1.e5299_e5984_s3126_r10724_r10726_p4133
mc16_13TeV.364115.Sherpa_221_NNPDF30NNLO_Zee_MAXHTPTV0_70_CFilterBVeto.deriv.DAOD_HIGG8D1.e5299_e5984_s3126_s3136_r10724_r10726_p4133
mc16_13TeV.364115.Sherpa_221_NNPDF30NNLO_Zee_MAXHTPTV0_70_CFilterBVeto.deriv.DAOD_HIGG8D1.e5299_e5984_s3126_r10724_r10726_p4133
mc16_13TeV.364116.Sherpa_221_NNPDF30NNLO_Zee_MAXHTPTV0_70_BFilter.deriv.DAOD_HIGG8D1.e5299_e5984_s3126_r10724_r10726_p4133
mc16_13TeV.364117.Sherpa_221_NNPDF30NNLO_Zee_MAXHTPTV70_140_CVetoBVeto.deriv.DAOD_HIGG8D1.e5299_e5984_s3126_s3136_r10724_r10726_p4133
mc16_13TeV.364117.Sherpa_221_NNPDF30NNLO_Zee_MAXHTPTV70_140_CVetoBVeto.deriv.DAOD_HIGG8D1.e5299_e5984_s3126_r10724_r10726_p4133
mc16_13TeV.364118.Sherpa_221_NNPDF30NNLO_Zee_MAXHTPTV70_140_CFilterBVeto.deriv.DAOD_HIGG8D1.e5299_e5984_s3126_s3136_r10724_r10726_p4133
mc16_13TeV.364118.Sherpa_221_NNPDF30NNLO_Zee_MAXHTPTV70_140_CFilterBVeto.deriv.DAOD_HIGG8D1.e5299_e5984_s3126_r10724_r10726_p4133
mc16_13TeV.364119.Sherpa_221_NNPDF30NNLO_Zee_MAXHTPTV70_140_BFilter.deriv.DAOD_HIGG8D1.e5299_e5984_s3126_r10724_r10726_p4133
mc16_13TeV.364120.Sherpa_221_NNPDF30NNLO_Zee_MAXHTPTV140_280_CVetoBVeto.deriv.DAOD_HIGG8D1.e5299_e5984_s3126_r10724_r10726_p4133
mc16_13TeV.364121.Sherpa_221_NNPDF30NNLO_Zee_MAXHTPTV140_280_CFilterBVeto.deriv.DAOD_HIGG8D1.e5299_e5984_s3126_r10724_r10726_p4133
mc16_13TeV.364122.Sherpa_221_NNPDF30NNLO_Zee_MAXHTPTV140_280_BFilter.deriv.DAOD_HIGG8D1.e5299_e5984_s3126_s3136_r10724_r10726_p4133
mc16_13TeV.364122.Sherpa_221_NNPDF30NNLO_Zee_MAXHTPTV140_280_BFilter.deriv.DAOD_HIGG8D1.e5299_e5984_s3126_r10724_r10726_p4133
mc16_13TeV.364123.Sherpa_221_NNPDF30NNLO_Zee_MAXHTPTV280_500_CVetoBVeto.deriv.DAOD_HIGG8D1.e5299_e5984_s3126_r10724_r10726_p4133
mc16_13TeV.364124.Sherpa_221_NNPDF30NNLO_Zee_MAXHTPTV280_500_CFilterBVeto.deriv.DAOD_HIGG8D1.e5299_e5984_s3126_r10724_r10726_p4133
mc16_13TeV.364125.Sherpa_221_NNPDF30NNLO_Zee_MAXHTPTV280_500_BFilter.deriv.DAOD_HIGG8D1.e5299_e5984_s3126_s3136_r10724_r10726_p4133

mc16_13TeV.364125.Sherpa_221_NNPDF30NNLO_Zee_MAXHTPTV280_500_BFilter.deriv.DAOD_HIGG8D1.e5299_e5984_s3126_r10724_r10726_p4133
mc16_13TeV.364126.Sherpa_221_NNPDF30NNLO_Zee_MAXHTPTV500_1000.deriv.DAOD_HIGG8D1.e5299_e5984_s3126_r10724_r10726_p4133
mc16_13TeV.364126.Sherpa_221_NNPDF30NNLO_Zee_MAXHTPTV500_1000.deriv.DAOD_HIGG8D1.e5299_e5984_s3126_s3136_r10724_r10726_p4133
mc16_13TeV.364127.Sherpa_221_NNPDF30NNLO_Zee_MAXHTPTV1000_E_CMS.deriv.DAOD_HIGG8D1.e5299_e5984_s3126_s3136_r10724_r10726_p4133
mc16_13TeV.364127.Sherpa_221_NNPDF30NNLO_Zee_MAXHTPTV1000_E_CMS.deriv.DAOD_HIGG8D1.e5299_e5984_s3126_r10724_r10726_p4133
mc16_13TeV.364128.Sherpa_221_NNPDF30NNLO_Ztautau_MAXHTPTV0_70_CVetoBVeto.deriv.DAOD_HIGG8D1.e5307_e5984_s3126_s3136_r10724_r10726_p4133
mc16_13TeV.364128.Sherpa_221_NNPDF30NNLO_Ztautau_MAXHTPTV0_70_CVetoBVeto.deriv.DAOD_HIGG8D1.e5307_e5984_s3126_r10724_r10726_p4133
mc16_13TeV.364129.Sherpa_221_NNPDF30NNLO_Ztautau_MAXHTPTV0_70_CFilterBVeto.deriv.DAOD_HIGG8D1.e5307_e5984_s3126_r10724_r10726_p4133
mc16_13TeV.364129.Sherpa_221_NNPDF30NNLO_Ztautau_MAXHTPTV0_70_CFilterBVeto.deriv.DAOD_HIGG8D1.e5307_e5984_s3126_s3136_r10724_r10726_p4133
mc16_13TeV.364130.Sherpa_221_NNPDF30NNLO_Ztautau_MAXHTPTV0_70_BFilter.deriv.DAOD_HIGG8D1.e5307_e5984_s3126_s3136_r10724_r10726_p4133
mc16_13TeV.364130.Sherpa_221_NNPDF30NNLO_Ztautau_MAXHTPTV0_70_BFilter.deriv.DAOD_HIGG8D1.e5307_e5984_s3126_r10724_r10726_p4133
mc16_13TeV.364131.Sherpa_221_NNPDF30NNLO_Ztautau_MAXHTPTV70_140_CVetoBVeto.deriv.DAOD_HIGG8D1.e5307_e5984_s3126_r10724_r10726_p4133
mc16_13TeV.364132.Sherpa_221_NNPDF30NNLO_Ztautau_MAXHTPTV70_140_CFilterBVeto.deriv.DAOD_HIGG8D1.e5307_e5984_s3126_r10724_r10726_p4133
mc16_13TeV.364132.Sherpa_221_NNPDF30NNLO_Ztautau_MAXHTPTV70_140_CFilterBVeto.deriv.DAOD_HIGG8D1.e5307_e5984_s3126_s3136_r10724_r10726_p4133
mc16_13TeV.364133.Sherpa_221_NNPDF30NNLO_Ztautau_MAXHTPTV70_140_BFilter.deriv.DAOD_HIGG8D1.e5307_e5984_s3126_r10724_r10726_p4133
mc16_13TeV.364134.Sherpa_221_NNPDF30NNLO_Ztautau_MAXHTPTV140_280_CVetoBVeto.deriv.DAOD_HIGG8D1.e5307_e5984_s3126_r10724_r10726_p4133
mc16_13TeV.364135.Sherpa_221_NNPDF30NNLO_Ztautau_MAXHTPTV140_280_CFilterBVeto.deriv.DAOD_HIGG8D1.e5307_e5984_s3126_r10724_r10726_p4133
mc16_13TeV.364135.Sherpa_221_NNPDF30NNLO_Ztautau_MAXHTPTV140_280_CFilterBVeto.deriv.DAOD_HIGG8D1.e5307_e5984_s3126_s3136_r10724_r10726_p4133
mc16_13TeV.364136.Sherpa_221_NNPDF30NNLO_Ztautau_MAXHTPTV140_280_BFilter.deriv.DAOD_HIGG8D1.e5307_e5984_s3126_r10724_r10726_p4133
mc16_13TeV.364137.Sherpa_221_NNPDF30NNLO_Ztautau_MAXHTPTV280_500_CVetoBVeto.deriv.DAOD_HIGG8D1.e5307_e5984_s3126_r10724_r10726_p4133
mc16_13TeV.364138.Sherpa_221_NNPDF30NNLO_Ztautau_MAXHTPTV280_500_CFilterBVeto.deriv.DAOD_HIGG8D1.e5313_e5984_s3126_s3136_r10724_r10726_p4133
mc16_13TeV.364138.Sherpa_221_NNPDF30NNLO_Ztautau_MAXHTPTV280_500_CFilterBVeto.deriv.DAOD_HIGG8D1.e5313_e5984_s3126_r10724_r10726_p4133
mc16_13TeV.364139.Sherpa_221_NNPDF30NNLO_Ztautau_MAXHTPTV280_500_BFilter.deriv.DAOD_HIGG8D1.e5313_e5984_s3126_r10724_r10726_p4133
mc16_13TeV.364139.Sherpa_221_NNPDF30NNLO_Ztautau_MAXHTPTV280_500_BFilter.deriv.DAOD_HIGG8D1.e5313_e5984_s3126_s3136_r10724_r10726_p4133
mc16_13TeV.364140.Sherpa_221_NNPDF30NNLO_Ztautau_MAXHTPTV500_1000.deriv.DAOD_HIGG8D1.e5307_e5984_s3126_r10724_r10726_p4133
mc16_13TeV.364140.Sherpa_221_NNPDF30NNLO_Ztautau_MAXHTPTV500_1000.deriv.DAOD_HIGG8D1.e5307_e5984_s3126_s3136_r10724_r10726_p4133
mc16_13TeV.364141.Sherpa_221_NNPDF30NNLO_Ztautau_MAXHTPTV1000_E_CMS.deriv.DAOD_HIGG8D1.e5307_e5984_s3126_s3136_r10724_r10726_p4133
mc16_13TeV.364141.Sherpa_221_NNPDF30NNLO_Ztautau_MAXHTPTV1000_E_CMS.deriv.DAOD_HIGG8D1.e5307_e5984_s3126_r10724_r10726_p4133
mc16_13TeV.364198.Sherpa_221_NN30NNLO_Zmm_Mll10_40_MAXHTPTV0_70_BVeto.deriv.DAOD_HIGG8D1.e5421_e5984_s3126_r10724_r10726_p4133
mc16_13TeV.364199.Sherpa_221_NN30NNLO_Zmm_Mll10_40_MAXHTPTV0_70_BFilter.deriv.DAOD_HIGG8D1.e5421_e5984_s3126_r10724_r10726_p4133
mc16_13TeV.364200.Sherpa_221_NN30NNLO_Zmm_Mll10_40_MAXHTPTV70_280_BVeto.deriv.DAOD_HIGG8D1.e5421_e5984_s3126_r10724_r10726_p4133
mc16_13TeV.364201.Sherpa_221_NN30NNLO_Zmm_Mll10_40_MAXHTPTV70_280_BFilter.deriv.DAOD_HIGG8D1.e5421_e5984_s3126_r10724_r10726_p4133
mc16_13TeV.364202.Sherpa_221_NN30NNLO_Zmm_Mll10_40_MAXHTPTV280_E_CMS_BVeto.deriv.DAOD_HIGG8D1.e5421_e5984_s3126_r10724_r10726_p4133
mc16_13TeV.364203.Sherpa_221_NN30NNLO_Zmm_Mll10_40_MAXHTPTV280_E_CMS_BFilter.deriv.DAOD_HIGG8D1.e5421_e5984_s3126_r10724_r10726_p4133
mc16_13TeV.364204.Sherpa_221_NN30NNLO_Zee_Mll10_40_MAXHTPTV0_70_BVeto.deriv.DAOD_HIGG8D1.e5421_e5984_s3126_r10724_r10726_p4133
mc16_13TeV.364205.Sherpa_221_NN30NNLO_Zee_Mll10_40_MAXHTPTV0_70_BFilter.deriv.DAOD_HIGG8D1.e5421_e5984_s3126_r10724_r10726_p4133
mc16_13TeV.364206.Sherpa_221_NN30NNLO_Zee_Mll10_40_MAXHTPTV70_280_BVeto.deriv.DAOD_HIGG8D1.e5421_e5984_s3126_r10724_r10726_p4133
mc16_13TeV.364207.Sherpa_221_NN30NNLO_Zee_Mll10_40_MAXHTPTV70_280_BFilter.deriv.DAOD_HIGG8D1.e5421_e5984_s3126_r10724_r10726_p4133
mc16_13TeV.364208.Sherpa_221_NN30NNLO_Zee_Mll10_40_MAXHTPTV280_E_CMS_BVeto.deriv.DAOD_HIGG8D1.e5421_e5984_s3126_r10724_r10726_p4133
mc16_13TeV.364209.Sherpa_221_NN30NNLO_Zee_Mll10_40_MAXHTPTV280_E_CMS_BFilter.deriv.DAOD_HIGG8D1.e5421_e5984_s3126_r10724_r10726_p4133
mc16_13TeV.364210.Sherpa_221_NN30NNLO_Ztt_Mll10_40_MAXHTPTV0_70_BVeto.deriv.DAOD_HIGG8D1.e5421_e5984_s3126_r10724_r10726_p4133
mc16_13TeV.364211.Sherpa_221_NN30NNLO_Ztt_Mll10_40_MAXHTPTV0_70_BFilter.deriv.DAOD_HIGG8D1.e5421_e5984_s3126_r10724_r10726_p4133
mc16_13TeV.364212.Sherpa_221_NN30NNLO_Ztt_Mll10_40_MAXHTPTV70_280_BVeto.deriv.DAOD_HIGG8D1.e5421_e5984_s3126_r10724_r10726_p4133
mc16_13TeV.364213.Sherpa_221_NN30NNLO_Ztt_Mll10_40_MAXHTPTV70_280_BFilter.deriv.DAOD_HIGG8D1.e5421_e5984_s3126_r10724_r10726_p4133
mc16_13TeV.364214.Sherpa_221_NN30NNLO_Ztt_Mll10_40_MAXHTPTV280_E_CMS_BVeto.deriv.DAOD_HIGG8D1.e5421_e5984_s3126_r10724_r10726_p4133
mc16_13TeV.364215.Sherpa_221_NN30NNLO_Ztt_Mll10_40_MAXHTPTV280_E_CMS_BFilter.deriv.DAOD_HIGG8D1.e5421_e5984_s3126_r10724_r10726_p4133
mc16_13TeV.364156.Sherpa_221_NNPDF30NNLO_Wmunu_MAXHTPTV0_70_CVetoBVeto.deriv.DAOD_HIGG8D1.e5340_e5984_s3126_r10724_r10726_p4133
mc16_13TeV.364157.Sherpa_221_NNPDF30NNLO_Wmunu_MAXHTPTV0_70_CFilterBVeto.deriv.DAOD_HIGG8D1.e5340_e5984_s3126_r10724_r10726_p4133
mc16_13TeV.364158.Sherpa_221_NNPDF30NNLO_Wmunu_MAXHTPTV0_70_BFilter.deriv.DAOD_HIGG8D1.e5340_e5984_s3126_s3136_r10724_r10726_p4133
mc16_13TeV.364158.Sherpa_221_NNPDF30NNLO_Wmunu_MAXHTPTV0_70_BFilter.deriv.DAOD_HIGG8D1.e5340_e5984_s3126_r10724_r10726_p4133
mc16_13TeV.364159.Sherpa_221_NNPDF30NNLO_Wmunu_MAXHTPTV70_140_CVetoBVeto.deriv.DAOD_HIGG8D1.e5340_e5984_s3126_s3136_r10724_r10726_p4133
mc16_13TeV.364160.Sherpa_221_NNPDF30NNLO_Wmunu_MAXHTPTV70_140_CFilterBVeto.deriv.DAOD_HIGG8D1.e5340_e5984_s3126_s3136_r10724_r10726_p4133
mc16_13TeV.364160.Sherpa_221_NNPDF30NNLO_Wmunu_MAXHTPTV70_140_CFilterBVeto.deriv.DAOD_HIGG8D1.e5340_e5984_s3126_r10724_r10726_p4133
mc16_13TeV.364161.Sherpa_221_NNPDF30NNLO_Wmunu_MAXHTPTV70_140_BFilter.deriv.DAOD_HIGG8D1.e5340_e5984_s3126_r10724_r10726_p4133
mc16_13TeV.364162.Sherpa_221_NNPDF30NNLO_Wmunu_MAXHTPTV140_280_CVetoBVeto.deriv.DAOD_HIGG8D1.e5340_e5984_s3126_r10724_r10726_p4133
mc16_13TeV.364163.Sherpa_221_NNPDF30NNLO_Wmunu_MAXHTPTV140_280_CFilterBVeto.deriv.DAOD_HIGG8D1.e5340_e5984_s3126_s3136_r10724_r10726_p4133
mc16_13TeV.364163.Sherpa_221_NNPDF30NNLO_Wmunu_MAXHTPTV140_280_CFilterBVeto.deriv.DAOD_HIGG8D1.e5340_e5984_s3126_r10724_r10726_p4133
mc16_13TeV.364164.Sherpa_221_NNPDF30NNLO_Wmunu_MAXHTPTV140_280_BFilter.deriv.DAOD_HIGG8D1.e5340_e5984_s3126_r10724_r10726_p4133
mc16_13TeV.364165.Sherpa_221_NNPDF30NNLO_Wmunu_MAXHTPTV280_500_CVetoBVeto.deriv.DAOD_HIGG8D1.e5340_e5984_s3126_r10724_r10726_p4133
mc16_13TeV.364165.Sherpa_221_NNPDF30NNLO_Wmunu_MAXHTPTV280_500_CVetoBVeto.deriv.DAOD_HIGG8D1.e5340_e5984_s3126_s3136_r10724_r10726_p4133
mc16_13TeV.364166.Sherpa_221_NNPDF30NNLO_Wmunu_MAXHTPTV280_500_CFilterBVeto.deriv.DAOD_HIGG8D1.e5340_e5984_s3126_s3136_r10724_r10726_p4133
mc16_13TeV.364166.Sherpa_221_NNPDF30NNLO_Wmunu_MAXHTPTV280_500_CFilterBVeto.deriv.DAOD_HIGG8D1.e5340_e5984_s3126_r10724_r10726_p4133

mc16_13TeV.364167.Sherpa_221_NNPDF30NNLO_Wmunu_MAXHTPTV280_500_BFilter.deriv.DAOD_HIGG8D1.e5340_e5984_s3126_r10724_r10726_p4133
mc16_13TeV.364167.Sherpa_221_NNPDF30NNLO_Wmunu_MAXHTPTV280_500_BFilter.deriv.DAOD_HIGG8D1.e5340_e5984_s3126_s3136_r10724_r10726_p4133
mc16_13TeV.364168.Sherpa_221_NNPDF30NNLO_Wmunu_MAXHTPTV500_1000.deriv.DAOD_HIGG8D1.e5340_e5984_s3126_r10724_r10726_p4133
mc16_13TeV.364168.Sherpa_221_NNPDF30NNLO_Wmunu_MAXHTPTV500_1000.deriv.DAOD_HIGG8D1.e5340_e5984_s3126_s3136_r10724_r10726_p4133
mc16_13TeV.364169.Sherpa_221_NNPDF30NNLO_Wmunu_MAXHTPTV1000_E_CMS.deriv.DAOD_HIGG8D1.e5340_e5984_s3126_s3136_r10724_r10726_p4133
mc16_13TeV.364169.Sherpa_221_NNPDF30NNLO_Wmunu_MAXHTPTV1000_E_CMS.deriv.DAOD_HIGG8D1.e5340_e5984_s3126_r10724_r10726_p4133
mc16_13TeV.364170.Sherpa_221_NNPDF30NNLO_Wenu_MAXHTPTV0_70_CVetoBVeto.deriv.DAOD_HIGG8D1.e5340_e5984_s3126_r10724_r10726_p4133
mc16_13TeV.364171.Sherpa_221_NNPDF30NNLO_Wenu_MAXHTPTV0_70_CFilterBVeto.deriv.DAOD_HIGG8D1.e5340_e5984_s3126_r10724_r10726_p4133
mc16_13TeV.364172.Sherpa_221_NNPDF30NNLO_Wenu_MAXHTPTV0_70_BFilter.deriv.DAOD_HIGG8D1.e5340_e5984_s3126_r10724_r10726_p4133
mc16_13TeV.364173.Sherpa_221_NNPDF30NNLO_Wenu_MAXHTPTV70_140_CVetoBVeto.deriv.DAOD_HIGG8D1.e5340_e5984_s3126_s3136_r10724_r10726_p4133
mc16_13TeV.364174.Sherpa_221_NNPDF30NNLO_Wenu_MAXHTPTV70_140_CFilterBVeto.deriv.DAOD_HIGG8D1.e5340_e5984_s3126_r10724_r10726_p4133
mc16_13TeV.364175.Sherpa_221_NNPDF30NNLO_Wenu_MAXHTPTV70_140_BFilter.deriv.DAOD_HIGG8D1.e5340_e5984_s3126_s3136_r10724_r10726_p4133
mc16_13TeV.364176.Sherpa_221_NNPDF30NNLO_Wenu_MAXHTPTV140_280_CVetoBVeto.deriv.DAOD_HIGG8D1.e5340_e5984_s3126_r10724_r10726_p4133
mc16_13TeV.364177.Sherpa_221_NNPDF30NNLO_Wenu_MAXHTPTV140_280_CFilterBVeto.deriv.DAOD_HIGG8D1.e5340_e5984_s3126_r10724_r10726_p4133
mc16_13TeV.364177.Sherpa_221_NNPDF30NNLO_Wenu_MAXHTPTV140_280_CFilterBVeto.deriv.DAOD_HIGG8D1.e5340_e5984_s3126_s3136_r10724_r10726_p4133
mc16_13TeV.364178.Sherpa_221_NNPDF30NNLO_Wenu_MAXHTPTV140_280_BFilter.deriv.DAOD_HIGG8D1.e5340_e5984_s3126_r10724_r10726_p4133
mc16_13TeV.364179.Sherpa_221_NNPDF30NNLO_Wenu_MAXHTPTV280_500_CVetoBVeto.deriv.DAOD_HIGG8D1.e5340_e5984_s3126_r10724_r10726_p4133
mc16_13TeV.364179.Sherpa_221_NNPDF30NNLO_Wenu_MAXHTPTV280_500_CVetoBVeto.deriv.DAOD_HIGG8D1.e5340_e5984_s3126_s3136_r10724_r10726_p4133
mc16_13TeV.364180.Sherpa_221_NNPDF30NNLO_Wenu_MAXHTPTV280_500_CFilterBVeto.deriv.DAOD_HIGG8D1.e5340_e5984_s3126_s3136_r10724_r10726_p4133
mc16_13TeV.364180.Sherpa_221_NNPDF30NNLO_Wenu_MAXHTPTV280_500_CFilterBVeto.deriv.DAOD_HIGG8D1.e5340_e5984_s3126_r10724_r10726_p4133
mc16_13TeV.364181.Sherpa_221_NNPDF30NNLO_Wenu_MAXHTPTV280_500_BFilter.deriv.DAOD_HIGG8D1.e5340_e5984_s3126_s3136_r10724_r10726_p4133
mc16_13TeV.364181.Sherpa_221_NNPDF30NNLO_Wenu_MAXHTPTV280_500_BFilter.deriv.DAOD_HIGG8D1.e5340_e5984_s3126_r10724_r10726_p4133
mc16_13TeV.364182.Sherpa_221_NNPDF30NNLO_Wenu_MAXHTPTV500_1000.deriv.DAOD_HIGG8D1.e5340_e5984_s3126_s3136_r10724_r10726_p4133
mc16_13TeV.364182.Sherpa_221_NNPDF30NNLO_Wenu_MAXHTPTV500_1000.deriv.DAOD_HIGG8D1.e5340_e5984_s3126_r10724_r10726_p4133
mc16_13TeV.364183.Sherpa_221_NNPDF30NNLO_Wenu_MAXHTPTV1000_E_CMS.deriv.DAOD_HIGG8D1.e5340_e5984_s3126_r10724_r10726_p4133
mc16_13TeV.364183.Sherpa_221_NNPDF30NNLO_Wenu_MAXHTPTV1000_E_CMS.deriv.DAOD_HIGG8D1.e5340_e5984_s3126_s3136_r10724_r10726_p4133
mc16_13TeV.364184.Sherpa_221_NNPDF30NNLO_Wtaunu_MAXHTPTV0_70_CVetoBVeto.deriv.DAOD_HIGG8D1.e5340_e5984_s3126_r10724_r10726_p4133
mc16_13TeV.364185.Sherpa_221_NNPDF30NNLO_Wtaunu_MAXHTPTV0_70_CFilterBVeto.deriv.DAOD_HIGG8D1.e5340_e5984_s3126_r10724_r10726_p4133
mc16_13TeV.364186.Sherpa_221_NNPDF30NNLO_Wtaunu_MAXHTPTV0_70_BFilter.deriv.DAOD_HIGG8D1.e5340_e5984_s3126_s3136_r10724_r10726_p4133
mc16_13TeV.364186.Sherpa_221_NNPDF30NNLO_Wtaunu_MAXHTPTV0_70_BFilter.deriv.DAOD_HIGG8D1.e5340_e5984_s3126_r10724_r10726_p4133
mc16_13TeV.364187.Sherpa_221_NNPDF30NNLO_Wtaunu_MAXHTPTV70_140_CVetoBVeto.deriv.DAOD_HIGG8D1.e5340_e5984_s3126_r10724_r10726_p4133
mc16_13TeV.364188.Sherpa_221_NNPDF30NNLO_Wtaunu_MAXHTPTV70_140_CFilterBVeto.deriv.DAOD_HIGG8D1.e5340_e5984_s3126_r10724_r10726_p4133
mc16_13TeV.364189.Sherpa_221_NNPDF30NNLO_Wtaunu_MAXHTPTV70_140_BFilter.deriv.DAOD_HIGG8D1.e5340_e5984_s3126_r10724_r10726_p4133
mc16_13TeV.364189.Sherpa_221_NNPDF30NNLO_Wtaunu_MAXHTPTV70_140_BFilter.deriv.DAOD_HIGG8D1.e5340_e5984_s3126_s3136_r10724_r10726_p4133
mc16_13TeV.364190.Sherpa_221_NNPDF30NNLO_Wtaunu_MAXHTPTV140_280_CVetoBVeto.deriv.DAOD_HIGG8D1.e5340_e5984_s3126_r10724_r10726_p4133
mc16_13TeV.364190.Sherpa_221_NNPDF30NNLO_Wtaunu_MAXHTPTV140_280_CVetoBVeto.deriv.DAOD_HIGG8D1.e5340_e5984_s3126_s3136_r10724_r10726_p4133
mc16_13TeV.364191.Sherpa_221_NNPDF30NNLO_Wtaunu_MAXHTPTV140_280_CFilterBVeto.deriv.DAOD_HIGG8D1.e5340_e5984_s3126_r10724_r10726_p4133
mc16_13TeV.364191.Sherpa_221_NNPDF30NNLO_Wtaunu_MAXHTPTV140_280_CFilterBVeto.deriv.DAOD_HIGG8D1.e5340_e5984_s3126_s3136_r10724_r10726_p4133
mc16_13TeV.364192.Sherpa_221_NNPDF30NNLO_Wtaunu_MAXHTPTV140_280_BFilter.deriv.DAOD_HIGG8D1.e5340_e5984_s3126_s3136_r10724_r10726_p4133
mc16_13TeV.364192.Sherpa_221_NNPDF30NNLO_Wtaunu_MAXHTPTV140_280_BFilter.deriv.DAOD_HIGG8D1.e5340_e5984_s3126_r10724_r10726_p4133
mc16_13TeV.364193.Sherpa_221_NNPDF30NNLO_Wtaunu_MAXHTPTV280_500_CVetoBVeto.deriv.DAOD_HIGG8D1.e5340_e5984_s3126_r10724_r10726_p4133
mc16_13TeV.364193.Sherpa_221_NNPDF30NNLO_Wtaunu_MAXHTPTV280_500_CVetoBVeto.deriv.DAOD_HIGG8D1.e5340_e5984_s3126_s3136_r10724_r10726_p4133
mc16_13TeV.364194.Sherpa_221_NNPDF30NNLO_Wtaunu_MAXHTPTV280_500_CFilterBVeto.deriv.DAOD_HIGG8D1.e5340_e5984_s3126_s3136_r10724_r10726_p4133
mc16_13TeV.364194.Sherpa_221_NNPDF30NNLO_Wtaunu_MAXHTPTV280_500_CFilterBVeto.deriv.DAOD_HIGG8D1.e5340_e5984_s3126_r10724_r10726_p4133
mc16_13TeV.364195.Sherpa_221_NNPDF30NNLO_Wtaunu_MAXHTPTV280_500_BFilter.deriv.DAOD_HIGG8D1.e5340_e5984_s3126_s3136_r10724_r10726_p4133
mc16_13TeV.364195.Sherpa_221_NNPDF30NNLO_Wtaunu_MAXHTPTV280_500_BFilter.deriv.DAOD_HIGG8D1.e5340_e5984_s3126_r10724_r10726_p4133
mc16_13TeV.364196.Sherpa_221_NNPDF30NNLO_Wtaunu_MAXHTPTV500_1000.deriv.DAOD_HIGG8D1.e5340_e5984_s3126_s3136_r10724_r10726_p4133
mc16_13TeV.364196.Sherpa_221_NNPDF30NNLO_Wtaunu_MAXHTPTV500_1000.deriv.DAOD_HIGG8D1.e5340_e5984_s3126_r10724_r10726_p4133
mc16_13TeV.364197.Sherpa_221_NNPDF30NNLO_Wtaunu_MAXHTPTV1000_E_CMS.deriv.DAOD_HIGG8D1.e5340_e5984_s3126_s3136_r10724_r10726_p4133
mc16_13TeV.364197.Sherpa_221_NNPDF30NNLO_Wtaunu_MAXHTPTV1000_E_CMS.deriv.DAOD_HIGG8D1.e5340_e5984_s3126_r10724_r10726_p4133
mc16_13TeV.364500.Sherpa_222_NNPDF30NNLO_eegamma_pty_7_15.deriv.DAOD_HIGG8D1.e5928_e5984_s3126_r10724_r10726_p4133
mc16_13TeV.364501.Sherpa_222_NNPDF30NNLO_eegamma_pty_15_35.deriv.DAOD_HIGG8D1.e5928_e5984_s3126_r10724_r10726_p4133
mc16_13TeV.364502.Sherpa_222_NNPDF30NNLO_eegamma_pty_35_70.deriv.DAOD_HIGG8D1.e5928_e5984_s3126_r10724_r10726_p4133
mc16_13TeV.364503.Sherpa_222_NNPDF30NNLO_eegamma_pty_70_140.deriv.DAOD_HIGG8D1.e5928_e5984_s3126_r10724_r10726_p4133
mc16_13TeV.364504.Sherpa_222_NNPDF30NNLO_eegamma_pty_140_E_CMS.deriv.DAOD_HIGG8D1.e5928_e5984_s3126_r10724_r10726_p4133
mc16_13TeV.364505.Sherpa_222_NNPDF30NNLO_mumugamma_pty_7_15.deriv.DAOD_HIGG8D1.e5928_e5984_s3126_r10724_r10726_p4133
mc16_13TeV.364506.Sherpa_222_NNPDF30NNLO_mumugamma_pty_15_35.deriv.DAOD_HIGG8D1.e5928_e5984_s3126_r10724_r10726_p4133
mc16_13TeV.364507.Sherpa_222_NNPDF30NNLO_mumugamma_pty_35_70.deriv.DAOD_HIGG8D1.e5928_e5984_s3126_r10724_r10726_p4133
mc16_13TeV.364508.Sherpa_222_NNPDF30NNLO_mumugamma_pty_70_140.deriv.DAOD_HIGG8D1.e5928_e5984_s3126_r10724_r10726_p4133
mc16_13TeV.364509.Sherpa_222_NNPDF30NNLO_mumugamma_pty_140_E_CMS.deriv.DAOD_HIGG8D1.e5928_e5984_s3126_r10724_r10726_p4133
mc16_13TeV.364511.Sherpa_222_NNPDF30NNLO_tautaugamma_pty_15_35.deriv.DAOD_HIGG8D1.e5928_e5984_s3126_r10724_r10726_p4133
mc16_13TeV.364512.Sherpa_222_NNPDF30NNLO_tautaugamma_pty_35_70.deriv.DAOD_HIGG8D1.e5928_e5984_s3126_r10724_r10726_p4133

mc16_13TeV.364513.Sherpa_222_NNPDF30NNLO_tautaugamma_pty_70_140.deriv.DAOD_HIGG8D1.e5982_e5984_s3126_r10724_r10726_p4133
mc16_13TeV.364514.Sherpa_222_NNPDF30NNLO_tautaugamma_pty_140_E_CMS.deriv.DAOD_HIGG8D1.e5928_e5984_s3126_r10724_r10726_p4133
mc16_13TeV.364522.Sherpa_222_NNPDF30NNLO_enugamma_pty_15_35.deriv.DAOD_HIGG8D1.e5928_e5984_s3126_r10724_r10726_p4133
mc16_13TeV.364523.Sherpa_222_NNPDF30NNLO_enugamma_pty_35_70.deriv.DAOD_HIGG8D1.e5928_e5984_s3126_r10724_r10726_p4133
mc16_13TeV.364524.Sherpa_222_NNPDF30NNLO_enugamma_pty_70_140.deriv.DAOD_HIGG8D1.e5928_e5984_s3126_r10724_r10726_p4133
mc16_13TeV.364525.Sherpa_222_NNPDF30NNLO_enugamma_pty_140_E_CMS.deriv.DAOD_HIGG8D1.e5928_e5984_s3126_r10724_r10726_p4133
mc16_13TeV.364527.Sherpa_222_NNPDF30NNLO_munugamma_pty_15_35.deriv.DAOD_HIGG8D1.e5928_e5984_s3126_r10724_r10726_p4133
mc16_13TeV.364528.Sherpa_222_NNPDF30NNLO_munugamma_pty_35_70.deriv.DAOD_HIGG8D1.e5928_e5984_s3126_r10724_r10726_p4133
mc16_13TeV.364529.Sherpa_222_NNPDF30NNLO_munugamma_pty_70_140.deriv.DAOD_HIGG8D1.e5928_e5984_s3126_r10724_r10726_p4133
mc16_13TeV.364530.Sherpa_222_NNPDF30NNLO_munugamma_pty_140_E_CMS.deriv.DAOD_HIGG8D1.e5928_e5984_s3126_r10724_r10726_p4133
mc16_13TeV.364532.Sherpa_222_NNPDF30NNLO_taunugamma_pty_15_35.deriv.DAOD_HIGG8D1.e5928_e5984_s3126_r10724_r10726_p4133
mc16_13TeV.364533.Sherpa_222_NNPDF30NNLO_taunugamma_pty_35_70.deriv.DAOD_HIGG8D1.e5928_e5984_s3126_r10724_r10726_p4133
mc16_13TeV.364534.Sherpa_222_NNPDF30NNLO_taunugamma_pty_70_140.deriv.DAOD_HIGG8D1.e5928_e5984_s3126_r10724_r10726_p4133
mc16_13TeV.364535.Sherpa_222_NNPDF30NNLO_taunugamma_pty_140_E_CMS.deriv.DAOD_HIGG8D1.e5928_e5984_s3126_r10724_r10726_p4133
mc16_13TeV.410560.MadGraphPythia8EvtGen_A14_tZ_4fl_tchan_noAllHad.deriv.DAOD_HIGG8D1.e5803_e5984_s3126_r10724_r10726_p4133
mc16_13TeV.410408.aMcAtNloPythia8EvtGen_tWZ_Ztoll_minDR1.deriv.DAOD_HIGG8D1.e6423_e5984_s3126_r10724_r10726_p4133
mc16_13TeV.364242.Sherpa_222_NNPDF30NNLO_WWW_3l3v_EW6.deriv.DAOD_HIGG8D1.e5887_e5984_s3126_r10724_r10726_p4133
mc16_13TeV.364243.Sherpa_222_NNPDF30NNLO_WWZ_4l2v_EW6.deriv.DAOD_HIGG8D1.e5887_e5984_s3126_r10724_r10726_p4133
mc16_13TeV.364244.Sherpa_222_NNPDF30NNLO_WWZ_2l4v_EW6.deriv.DAOD_HIGG8D1.e5887_e5984_s3126_r10724_r10726_p4133
mc16_13TeV.364245.Sherpa_222_NNPDF30NNLO_WZZ_5l1v_EW6.deriv.DAOD_HIGG8D1.e5887_e5984_s3126_r10724_r10726_p4133
mc16_13TeV.364246.Sherpa_222_NNPDF30NNLO_WZZ_3l3v_EW6.deriv.DAOD_HIGG8D1.e5887_e5984_s3126_r10724_r10726_p4133
mc16_13TeV.364247.Sherpa_222_NNPDF30NNLO_ZZZ_6l0v_EW6.deriv.DAOD_HIGG8D1.e5887_e5984_s3126_r10724_r10726_p4133
mc16_13TeV.364248.Sherpa_222_NNPDF30NNLO_ZZZ_4l2v_EW6.deriv.DAOD_HIGG8D1.e5887_e5984_s3126_r10724_r10726_p4133
mc16_13TeV.364249.Sherpa_222_NNPDF30NNLO_ZZZ_2l4v_EW6.deriv.DAOD_HIGG8D1.e5887_e5984_s3126_r10724_r10726_p4133
mc16_13TeV.342284.Pythia8EvtGen_A14NNPDF23LO_WH125_inc.deriv.DAOD_HIGG8D1.e4246_e5984_s3126_r10724_r10726_p4133
mc16_13TeV.342285.Pythia8EvtGen_A14NNPDF23LO_ZH125_inc.deriv.DAOD_HIGG8D1.e4246_e5984_s3126_r10724_r10726_p4133
mc16_13TeV.341998.aMcAtNloHppEG_UEEE5_CTEQ6L1_CT10ME_tWH125_gamgam_yt_plus1.deriv.DAOD_HIGG8D1.e4394_e5984_s3126_r10724_r10726_p4133
mc16_13TeV.410389.MadGraphPythia8EvtGen_A14NNPDF23_ttgamma_nonallhadronic.deriv.DAOD_HIGG8D1.e6155_e5984_s3126_r10724_r10726_p4133
mc16_13TeV.410470.PhPy8EG_A14_ttbar_hdamp258p75_nonallhad.deriv.DAOD_HIGG8D1.e6337_e5984_s3126_r10724_r10726_p4133
mc16_13TeV.410472.PhPy8EG_A14_ttbar_hdamp258p75_dil.deriv.DAOD_HIGG8D1.e6348_e5984_s3126_r10724_r10726_p4133
mc16_13TeV.346343.PhPy8EG_A14NNPDF23_NNPDF30ME_ttH125_allhad.deriv.DAOD_HIGG8D1.e7148_e5984_s3126_r10724_r10726_p4133
mc16_13TeV.346343.PhPy8EG_A14NNPDF23_NNPDF30ME_ttH125_allhad.deriv.DAOD_HIGG8D1.e7148_e5984_a875_r10724_r10726_p4133
mc16_13TeV.346344.PhPy8EG_A14NNPDF23_NNPDF30ME_ttH125_semilep.deriv.DAOD_HIGG8D1.e7148_e5984_a875_r10724_r10726_p4133
mc16_13TeV.346344.PhPy8EG_A14NNPDF23_NNPDF30ME_ttH125_semilep.deriv.DAOD_HIGG8D1.e7148_e5984_s3126_r10724_r10726_p4133
mc16_13TeV.346345.PhPy8EG_A14NNPDF23_NNPDF30ME_ttH125_dilep.deriv.DAOD_HIGG8D1.e7148_e5984_a875_r10724_r10726_p4133
mc16_13TeV.346345.PhPy8EG_A14NNPDF23_NNPDF30ME_ttH125_dilep.deriv.DAOD_HIGG8D1.e7148_e5984_s3126_r10724_r10726_p4133